THE DEVELOPMENT OF A MATHEMATICAL MODEL TO PREDICT THE FLEXURAL RESPONSE OF REINFORCED CONCRETE BEAMS TO CYCLIC LOADS, USING SYSTEM IDENTIFICATION

BY

JOHN F. STANTON

and

HUGH D. McNIVEN

REPORT TO THE

NATIONAL SCIENCE FOUNDATION

REPORT NO. UCB/EERC-79/02

EARTHQUAKE ENGINEERING RESEARCH CENTER
COLLEGE OF ENGINEERING
UNIVERSITY OF CALIFORNIA
BERKELEY, CALIFORNIA
JANUARY 1979

BIBLIOGRAPHIC DATA SHEET	1. Report No. NSF/RA-790056	2.	3. Recipient's Accession No.
4. Title and Subtitle "The Development of a Mathematical Model to Predict the Flexural Response of Reinforced Concrete Beams to Cyclic Loads, Using System Identification:			5. Report Date 6.
7. Author(s)			8. Performing Organization Rept. No.
9. Performing Organization Name and Address			10. Project/Task/Work Unit No. 11. Contract/Grant No.
12. Sponsoring Organization Name and Address (CONTINUED FROM PAGE 1)			13. Type of Report & Period Covered 14.

15. Supplementary Notes

16. Abstracts (CONTINUED FROM PAGE 1)

When the steel model was complete, it was incorporated into the global model. The steel parameters were held constant, and the concrete and bond-slip parameters were then identified using the results of tests on laterally loaded reinforced concrete beams.

Comparisons between the predicted and measured response for a number of different beam configurations show that the model is able to reproduce the physical behavior of the beams very well. If the shear span of the beam is short, or if the compression reinforcement buckles, the predictions are inferior, but are still reasonable.

7b. Identifiers/Open-Ended Terms

7c. COSATI Field/Group

18. Availability Statement	19. Security Class (This Report) UNCLASSIFIED	21. No. of Pages
	20. Security Class (This Page UNCLASSIFIED	22. Price

ACKNOWLEDGEMENT

The research described in this report was supported by the National Science Foundation under Grant No. ENV76-04262-A02. This support is gratefully acknowledged.

ABSTRACT

This report describes the development of a mathematical model to predict the flexural response of reinforced concrete beams to cyclic loads. The objective is to take the first step towards the construction of a model which will predict accurately the nonlinear response of reinforced concrete framed structures when they are subjected to dynamic loads such as seismic disturbances. The model is constructed using System Identification. The process consists of selecting a form for the model, and then using suitable mathematical techniques to adjust the numerical coefficients within it so that it reproduces as closely as possible the results of experiments.

The first essential is to understand the physical behavior to be reproduced. The response of reinforced concrete members to large cyclic loads is nonlinear and inelastic and it changes throughout the history of the load. Because it is so complicated, the physical behavior of the material and the mechanics which underlie it are investigated in considerable detail. A model form is then selected which divides the member into hypothetical layers. The material in each layer obeys an appropriate nonlinear constitutive law and the number forces are derived by integration across the cross section. The individual model which describes the steel behavior was developed especially for the purpose and is of particular interest.

The experimental results to which the model was fitted were taken from a previous study in which a number of cantilever beams were subjected to cyclic lateral loads. Beams of several different geometries were tested, allowing the model to be appraised in a variety of configurations.

Besides experimental results and an analytical model form, System Identification requires a minimization procedure to find the optimum parameter values. Many algorithms exist for the purpose, and a number are investigated in order to select one with suitable characteristics.

The identification was carried out in several stages. The first was to construct a model for the response of the steel reinforcement using data from axial tests on steel bars. Even this identification process contained several stages, because the original version of the model had constant parameters and it proved unable to reproduce the measured behavior adequately. The parameters were therefore made strain-dependent, and several cycles of modifying the model and re-identifying the parameters were necessary before a satisfactory match could be achieved.

When the steel model was complete, it was incorporated into the global model. The steel parameters were held constant, and the concrete and bond-slip parameters were then identified using the results of tests on laterally loaded reinforced concrete beams.

Comparisons between the predicted and measured response for a number of different beam configurations show that the model is able to reproduce the physical behavior of the beams very well. If the shear span of the beam is short, or if the compression reinforcement buckles, the predictions are inferior, but are still reasonable.

Preceding page blank

TABLE OF CONTENTS

Table of Contents (Cont'd) Page

Table of Contents (Cont'd)

Chapter 1

INTRODUCTION

Consideration of earthquake forces generally dominates the design of structures built in seismically active regions. Before the advent of the digital computer, these seismic forces had to be accounted for in very simplistic ways, and the resulting designs were relatively uneconomical for the level of safety they provided. More efficient structures, resulting from improved analyses, have recently been made possible by parallel developments in computing capability and dynamic analysis. The advances have in fact been so dramatic that the weakest link in the chain of structural analysis is now the mathematical models which describe material behavior.

In current design philosophy, structures are expected to behave inelastically when subjected to severe earthquake loading, but in most cases linear elastic constitutive models are used to predict the response, which is then modified to allow for the inelastic deformations using approximate techniques.

Analyses which make use of nonlinear constitutive models for the materials offer a more logical approach, but they introduce the added difficulty of selecting a good model. There is by definition only one form for a linear model, whereas there are an infinite number of nonlinear ones, so there is no lack of possibilities. But the choice is restricted by the fact that a useful model should both be reliable under all circumstances and should provide the best possible accuracy for the amount of computational effort required to use it. The development of a model to satisfy these requirements is not a trivial task, and this

research is directed towards the construction of such a model for reinforced concrete beams in flexure.

In the past, nonlinear models have been constructed rather arbitrarily, but recently a procedure known as System Identification has gained considerable popularity. McNiven and Matzen [40] used it with success to develop a nonlinear model for structural steel, and it is discussed in some detail in their report. In their words; "System Identification can be defined as the process of selecting the form of the model, and then, using measured test data, systematically adjusting the parameters until, based on a predefined criterion, the best correlation is achieved between the predicted and measured response." This tuning of the model by adjusting its parameters provides an excellent way of ensuring the best possible performance for a given model form, which is necessary if the model is to be efficient.

Measured response from a number of different experiments can be used, and optimum parameters can be found for each. Unless the model form is perfect, the parameter sets will not be identical, but such an exercise provides an indication of the model's reliability. System Identification is thus seen to offer unique advantages in developing analytical models for physical materials and is used extensively in this research. It is discussed in more detail in Chapter 2.

The flexure response of a member can be defined in a number of ways. Relationships can be established between moment and curvature, end moment and end rotation, or lateral force and lateral deflection. The last two can both be derived from the first by integration, and so the moment-curvature relationship, being the most fundamental, is the one which we choose to model.

The objectives of the study can be stated as follows:

1. To construct a mathematical model which will predict the resisting moment of a reinforced concrete member when it is subjected to a given curvature. The model should be able to reproduce both the nonlinearity and the history-dependence of the relation.
2. To demonstrate the usefulness of System Identification in developing mathematical models of material behavior.

This report of the study is arranged in such a way that each chapter is reasonably autonomous. Chapter 2 describes the process of System Identification and its application to the problem at hand. In Chapter 3, some of the problems involved in modelling the behavior of reinforced concrete members are considered, and an approach is selected for constructing a model. It requires separate consideration of the individual materials in the member, and so in Chapters 4 and 5 individual models are developed for the stress-strain behavior of reinforcing steel and plain concrete. Chapter 6 describes the construction of a bond-slip relation, which is used to define the strain in the reinforcement when the strain in the adjacent concrete is known. In Chapter 7, these three individual models are integrated to form the analytical model for the flexural response of the beam, which is referred to hereafter as the "global model." This completes the description of the development of the material model form. One of the essential parts of the System Identification process is an algorithm which will minimize a function which is only defined numerically. There are many such algorithms available, and they all have slightly different characteristics. Chapter 8 discusses some of the best ones, and gives the reasons why we chose the one we did. It is outlined in the last section of the chapter, and Appendix A presents the mathematical

foundation on which it rests. The results of the study are presented in Chapter 9, and Chapter 10 contains the conclusions and offers suggestions for further research in the area. A digital computer was used extensively, for which a program was written in FORTRAN IV. Appendix B contains an outline of the whole program and details of some of the numerical procedures which might be useful in future work in the area.

Chapter 2

SYSTEM IDENTIFICATION

Most engineering problems are referred to as direct because a prediction of the output of a physical system is sought when the characteristics of the system and the input are known. Recently, more attention has been paid to inverse problems, in which the response of the system to a given input is known from experiments and a mathematical model is to be found which will describe the behavior. Inverse problems are generally much harder to solve than direct ones, and furthermore, exact solutions are seldom available.

For many years electrical engineers have used System Identification to solve inverse problems, but the method has only recently been applied to problems in the field of Civil Engineering. It is a process by which approximate solutions to inverse problems may be obtained, and it consists of three main steps.

1. Select a form for the mathematical model which is to describe the physical behavior, but leave the values of the numerical coefficients (or parameters) within it unspecified.
2. Select a criterion function. This is a precise mathematical definition of how good the match is between the measured physical output and the response predicted by the model.
3. Adjust the values of the parameters in the model until the best possible match is achieved between the known (experimental) output and that predicted by the model.

The quality of the match is judged by using the criterion function.

The form of the model is obviously important and to a large degree controls how well the predictions can be made to fit the experimental data. For example, an exact solution to the inverse problem implies a perfect fit, which in turn requires a perfect model form. These are rare. Normally we have to be content with using engineering judgement and a knowledge of the physical characteristics of the system to produce the best possible approximate model form. In this study the choice of the model form is guided by the experience of previous investigators, and, where necessary, a number of different forms are tried in order to find the one best suited to our purpose.

The criterion function is usually a mathematical definition of the discrepancy between the predicted and measured response quantities. We use the integral squared difference between the measured and calculated moments when both the physical beam and the mathematical model are subjected to the same history of curvatures. The integral is approximated here by a sum of values at discrete points along the curve. This least square definition is a common choice for the criterion function, but many others are possible.

The adjustment of the parameters would be an extremely tedious undertaking if no error function were defined. However, the error function provides an objective test for the quality of the fit between the predicted and measured response, and so the optimum parameters can be established by the simple expedient of minimizing it. There are a variety of algorithms available for performing this task, each of which have their own individual characteristics, and a number of the better ones are discussed in Chapter 8.

If there are N parameters in the model, the error function can be viewed as an N-dimensional surface in N+1 dimensional space. If N is greater than two, this is hard to visualize, but Fig. 2.1 illustrates the case of N equal to 2. The problem is then to find the location of the minimum of the error surface, the coordinates of which will be the desired optimizing parameters. The search process is complicated by the fact that the error function may be undefined for certain values of the parameters, and the sum of all such points is referred to as the infeasible region of the parameter space. Clearly we must prevent the search for the minimum from entering it. Some of the techniques for doing so are discussed in Chapter 4, where the problem was encountered in connection with the mathematical model for steel reinforcing bars. The minimizing parameters must lie within the feasible region, but if they lie close to the edge of it, the minimization problem risks being poorly conditioned, in which case numerical difficulties seriously hinder the algorithm's ability to locate the minimum of the error function. For this reason the model form should be chosen so as to generate an error surface which is as well conditioned as possible. Alternatively, the model form can be chosen arbitrarily, and then the parameters scaled to improve the conditioning. This is discussed in Chapter 8.

System Identification has three main attractions. First, the parameter adjustment can be done automatically, and by computer. For almost any nonlinear model, the task would be impossible by hand. Second, the resulting set of minimizing parameters is unique, provided only that the error function has a unique global minimum. The fulfillment of this condition cannot be guaranteed but experience shows that good models of physical systems almost invariably possess error functions with unique

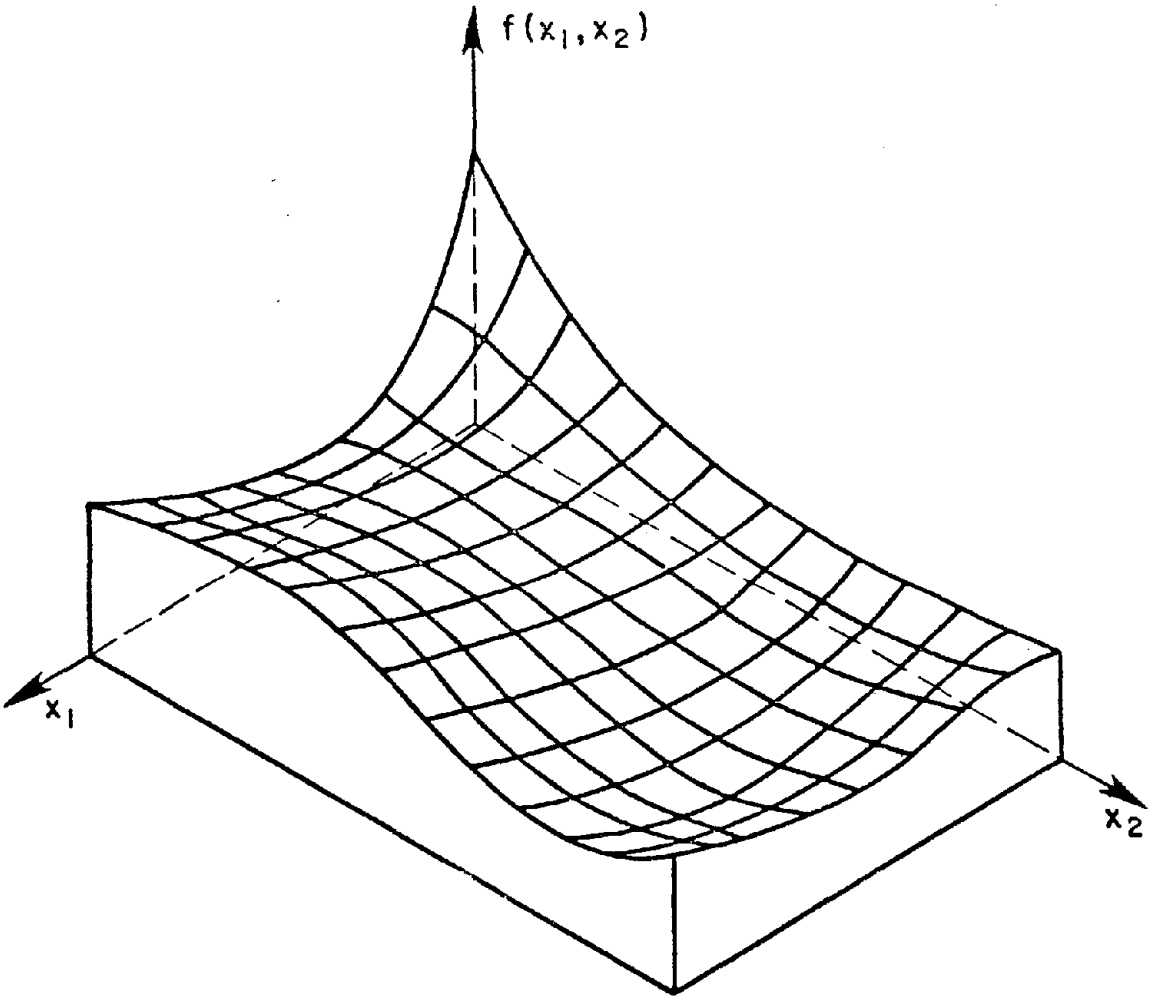

FIG. 2.1 - TWO-DIMENSIONAL SURFACE IN THREE-DIMENSIONAL SPACE

minima. Thus, two computers using the same data and the same model will produce the same optimum parameter set. Perhaps the most important feature of the procedure is that it permits the model form to be appraised. If, when the optimum parameter set is found and used, the predicted response is still not satisfactory, then the fault lies with the form of the model, which must be changed. Without knowing the optimum parameters, there is no way of telling whether the parameter values or the model form should be modified.

This description of System Identification is somewhat idealized in that it suggests that the selection of the model and the minimization of the error function are both self-contained processes each of which happens only once. If the initial choice of the model form is good enough, then this will indeed be the case. However, in this study, the processes are extensively interwoven. The model finally adopted to describe the moment-curvature relation for reinforced concrete is very complicated and is built up of three individual models for steel, concrete and bond-slip. Altogether there are some fifty parameters. To assemble the whole model before identifying any of the parameters seemed unwise, so whenever possible the parameters in the individual models are determined before the assembly process begins. For example, the parameters in the steel model are identified using data from separate tests on steel bars. But even the construction of these individual models is not entirely straightforward. In the case of the steel, a model form was chosen, the optimum parameters were found, and then, because the match was poor, several cycles of modifying the model form and identifying the new parameters were performed until eventually a satisfactory match was obtained. The details are discussed in Chapter 4.

Chapter 3

MODELLING THE BEHAVIOR OF REINFORCED CONCRETE - PROBLEMS and APPROACHES

3.1 Introduction

When reinforced concrete beams are subjected to cyclic loads, their flexural response is complicated and non-linear, and in forming analytical models for them some balance must be struck between the accuracy required and the cost and unwieldiness of the model. Clearly this depends on the use to which the model is to be put.

The sources of nonlinearity are two-fold: geometric and material. Reinforced concrete frame members are seldom sufficiently slender that stability problems dominate their design, and so geometric non-linearities are usually considered only if the structure is subjected to very large deformations such as may occur during a strong motion earthquake. Even then they are frequently neglected in the interests of simplicity.

Material nonlinearities cause the more serious problem, for the response of reinforced concrete is not only nonlinear, but it is also history dependent. This means that, in any member, not only does the moment-curvature relationship vary along the member, but also, at any given cross section, it varies with time throughout the loading history.

If a frame structure is to be analyzed by the displacement method, there are three levels of complication at which we can specify the constitutive law which defines the material behavior:

1. The member is made up of a single element, and member end forces are related directly to member end displacements.
2. The member is divided into elements longitudinally in each of which the local cross-section forces and deformations

are related. These are integrated along the beam to give an end-force to end-displacement relation.

3. The member is divided into elements longitudinally and across the cross section. The constitutive law for each material relates strains to stresses, which are integrated first over the cross section and then along the member, as in 2 above.

Method 1 is clearly the simplest and is used for structures made of straight prismatic linear elastic members. Method 2 is used for curved or nonprismatic members. Method 3 is the most complicated and is justified only for use on nonhomogeneous members (reinforced concrete, sandwich construction, etc.).

Method 3 is the most rational way of dealing with reinforced concrete subjected to cyclic loads because the nonlinear behavior of each material can be specified explicitly. However, it is also the most expensive, because at each level an iterative calculation is needed to provide the relationship at the next higher level, and so for each increment of load at least three nested iterations must be carried out. A time history dynamic analysis could prove very expensive.

The computational effort can be reduced in a number of ways, each of which incurs a subsequent loss of accuracy. For example,

1. Assume the form of the relationship between moment and curvature rather than direct stress and strain. This avoids integration over the cross-section and one level of iteration.
2. Reduce the number of elements. If the longitudinal mesh is made coarser, then the elements should be bunched in those regions where most inelastic action is expected. In the limit, one nonlinear element could be placed at each end of

the member (if that is the critical region) and linear elastic elements used elsewhere.

It is natural to seek improved efficiency by distributing the elements across the cross-section in a similar way. Unfortunately this is not possible, because the location at which most elements are needed varies with time. The best we can do is to use as few elements as are consistent with a unique solution and the desired accuracy. This question is addressed in section 7.3.

3. Use simple material constitutive relations. For example, stresses are in general more easily calculated from a relationship which expresses stress as an explicit function of strain than vice versa.

Many models have been proposed in the literature, which has been well surveyed by Park [1]. Those which make their constitutive assumptions at level 3 as described above are referred to hereafter as layered models, because the cross section is divided into layers parallel to the axis of bending. Those which make the assumption at level 2 are called "homogeneous models" because for such models a composite member is treated as if it were homogeneous. Some of the material behaviors of these homogeneous models are expressed in the form of a moment-curvature relationship, some in the form of a moment-rotation relationship (treating all nonlinearity as if it occurred at a single point and describing it by a nonlinear rotational spring) and some have been used to define a force-deflection relationship, for example for the tip of a laterally loaded cantilever. Within each group (layered or homogeneous) there is a wide variation in the sophistication of the models, but there are two

factors which distinguish one group as a whole from the other. First, the layered models require more computational effort than do the global ones. The second is a difference in approach. Homogeneous models describe the physics of the problem at a less detailed level than do layered models, because they disregard the mechanical behavior of the individual materials and attempt simply to reproduce the overall characteristics of the response in the form of a moment-curvature or force-deflection relationship. Layered models, on the other hand, attempt to reproduce the mechanical behavior of the individual component materials of the reinforced concrete member, and, from a knowledge of their separate response mechanisms, synthesize a mathematical model for the overall behavior.

3.2 Homogeneous Models

3.2.1 General

Some of the recently published homogeneous models are presented and their merits discussed briefly.

3.2.2 Individual Models

Bilinear -- This is the crudest model used to describe any elasto-plastic material, with or without strain-hardening [2, 3, 4]. It neglects both the Bauschinger effect in the steel and any deterioration of stiffness with cycling and so gives poor results.

Bilinear Degrading -- Hidalgo and Clough [5] proposed a bilinear model in which the stiffnesses are history dependent. It predicts response frequency well, but the response amplitude and hysteretic behavior in P-δ space show only moderate agreement with experimental results.

Multi-linear Degrading

Takeda, Sozen and Nielsen [6] accounted for stiffness degradation

by using a multi-linear model in which the stiffnesses vary during the load history and are calculated from a rather complicated set of rules. The model works reasonably well and with some extensions it was incorporated into the general purpose nonlinear analysis program DRAIN 2-D [7]. It is probably the best homogeneous model.

Iwan [8] suggested the use of a combination of elastic and "slip-stick" elements to make up a model for restoring force which is elasto-plastic and includes some degradation. The parameters in the slip-stick elements are ratios of measureable physical quantities (e.g. yield strain). Stiffness degradation (i.e. decreasing stiffness with increasing maximum deformation) can be described, but deterioration (stiffness reduction due to cycling between constant strain limits) cannot.

Atalay and Penzien [9] proposed a nonlinear model defined by a smooth continuous trigonometric function. It is empirical and was obtained by fitting the curve to experimental results. The tests were somewhat restricted in scope and so the model should be verified under a wider range of conditions before it can be used with confidence.

Tani, Nagasaka, Nomura, and Hiramatsu [10] proposed an empirical formulation with ten constants which can describe a range of shapes for hysteresis loops. However, the expressions are cumbersome and no attempt was made to correlate the constants with physical properties of the member, so, as it stands, the model cannot be used to predict response.

3.3 Layered Models

3.3.1 General

Fig. 3.1 shows a typical reinforced concrete beam divided for modeling purposes into layers. Stress is assumed to be constant through the thickness of any layer, but it may have a different value in each.

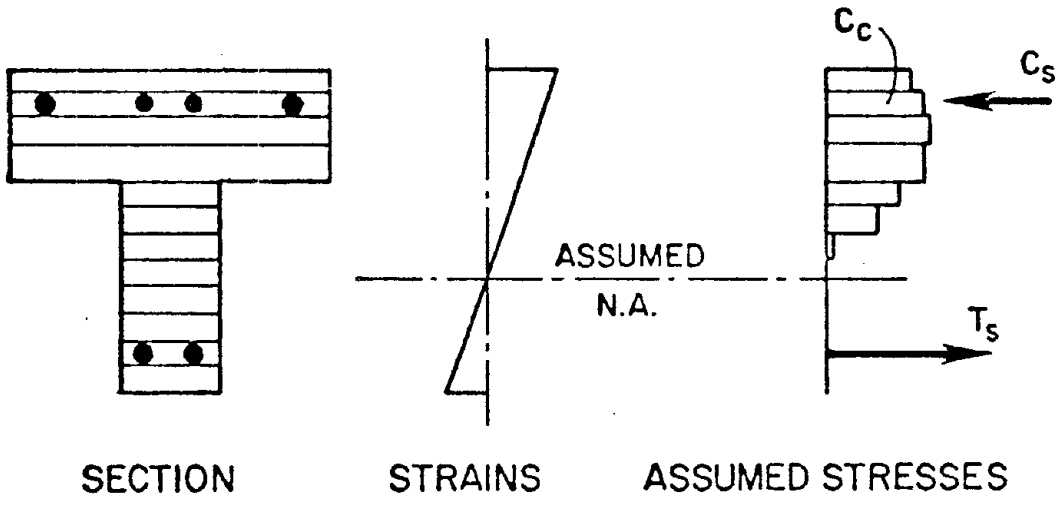

FIG. 3.1 - CROSS SECTION OF LAYERED MODEL

The following ingredients are needed to predict the resisting moment corresponding to a given curvature and a given axial load:

(a) The shape of the concrete strain distribution. For simplicity, it is generally taken to be linear.

(b) A bond relation between steel and concrete. We need to be able to calculate the axial strain in the steel, given the concrete strain at the same depth. The simplest relation assumes perfect bond, in which case the strains in the two materials are identical.

(c) A constitutive relation for direct compression of concrete.

(d) A constitutive relation for steel bars in tension and compression.

The procedure is then to locate the neutral axis of the member by satisfying axial force equilibrium. If the strains vary linearly with depth, the strain field in the concrete is completely defined by its slope (which is the curvature and is known) and an assumed position of the neutral axis. The strains in the steel layers are calculated using the bond relation (b), and then the constitutive relations for the two materials are used to define the stress in each layer. The forces in each layer are then calculated and summed to give a total axial force on the member. This predicted value is compared to the applied axial load, and the calculation is repeated with a different neutral axis position until the two agree within a close enough tolerance. When the neutral axis has been located, the resisting moment is calculated by summing the moments of the forces in each layer.

Having described the general, layered model, it is useful to clarify its limitations. The most serious one is that the concrete is treated

as a continuum across which a strain field of predictable shape exists. This condition is violated by the presence of even the smallest flexural crack. However, if we consider average strain instead of true strain, then the model may still be expected to give reasonable results, despite the cracks. By average strain we mean a change in length per unit length of an element large enough to contain a number of cracks. But if the flexural cracks are wide and the member is also subjected to large shear forces, the reinforcing bars are liable to become kinked by the lateral load on them. Shear will also cause a network of diagonal cracks to form in the concrete, and the displacements associated with both of these actions violate the continuum assumptions. Therefore the model will probably give poor results for members subjected to high shears. The same limitation applies to all of the layered models published to date, so they should be used only on members sufficiently slender that the effects of shear are indeed negligible.

Another restriction is imposed by the constitutive model for the reinforcing steel if it is unable to include the effects of buckling.

We also need an idea of the relative importance of the four ingredients listed above so that each can be modelled with an appropriate degree of sophistication.

The constitutive model for steel appears to have the greatest influence on the accuracy of the overall model. This is particularly true in the prediction of beam behavior [11], because the axial loads are generally very small. Cracks form in the concrete and remain open for most of each load cycle, during which time the steel couple provides the whole resisting moment. The concrete model plays a greater part in predicting column behavior since the axial loads are generally large enough to

prevent cracks.

It is difficult to assess the influence of assuming a linear distribution of the average strain because of the lack of alternatives with which to compare the assumption, and because of the difficulties of making physical measurements which are sufficiently precise to be useful. Ma's results do not indicate that the assumption contributes significantly to the error. Karsan and Jirsa [12] tested unreinforced concrete specimens and loaded them eccentrically but in such a way that the whole section experienced compressive stress. They found that the strains were linearly distributed . Their test results cannot be offered as conclusive proof of a linear strain distribution in a reinforced concrete beam, but they certainly lend support to the assumption. We therefore accept it here.

The importance of the bond relation depends on the behavior to be modelled. In a cantilever test, the reinforcing bars will inevitably pull out of the anchor block to some extent, causing a rotation at the built-in end of the beam. If the measurements of beam curvature are independent of this end rotation, the bond relation may be expected to assume only a modest importance. But if the end rotation has to be predicted analytically, the bond-slip relation becomes an essential component. Bond deterioration is a complicated phenomenon which is by no means fully understood and so there is a temptation to ignore it. The models so far proposed for deterioration have been either very simple or very complex. The few investigators [13, 14] who have included it in a global model of a reinforced concrete member have used a relatively crude approximation, whereas those who have studied bond per se [15, 16] have only been able to mimic the physical behavior satisfactorily by using a

fine mesh (often nonlinear) finite element analysis. In Chapter 6 we attempt to develop a model which lies between these two extremes.

3.3.2 Individual Models

Some of the more important layered models are outlined. Many of them share a common stress-strain relation for either steel or concrete, and these are discussed in detail in Chapters 4 and 5, respectively.

In a thorough research program under the direction of Park in New Zealand [17,18,19,20,21] a single model, with variations, has been used. The steel is described by a Ramberg-Osgood [22] function bounded by the monotonic curve, and the concrete, by Hognestad's [23] formula, extended to include the effects of binders. No allowance is made for bond-slip. Rather low-strength steel with a long yield plateau was used in the experiments, so the model was never really tested in the strain-hardening range. However, Thompson [19] used the Park model to achieve reasonable matching in the region covered by his tests.

Gerstle and Tulin [24,25,26,27] have conducted a pertinent research program at Boulder, Colorado. They used the work of Kriz and Lee [28] to produce a complex expression for the σ-ε curve of plain concrete, neglecting the influence of binders. Later, they found that the member response was insensitive to the exact shape of the concrete σ-ε curve, so they used a simple bilinear expression, which surprisingly gave better results than the more complicated one. Their law for steel contains a linear part and an exponential part. The parameters in it are assumed to be constant, and bond-slip is not taken into account. Agreement between predicted and experimental member response was only moderate.

Brown and Jirsa [13] used a trilinear concrete diagram which

includes the effects of binders in a manner based on Yamishiro's work [29]. Their steel curve consists of linear and exponential parts derived from Gerstle and Tulin's test data. The full test data for the steel were not published so a comparison between analytical and experimental curves could not be made. However, the analytical expression is a poor fit for Aktan, Karlssen and Sozen's data [30]. A simple allowance was made for bond-slip and for the end rotation due to bar pull-out using Burns and Seiss' method [31]. It is hard to judge from the published data how good the predicted response is, but it appears to be at least moderate.

Menegotto and Pinto [32] presented a theoretical model and tested it against experimental results for a monotonically loaded frame. Correlation was good.

For concrete they used Hognestad's parabola and a straight line representing average binding conditions. Branch curves in their steel model were described by a single nonlinear expression which possesses a straight line asymptote. Bond slip was not included. The approach is more elegant and less empirical than most of the others, but experimental evidence is lacking on its performance under cyclic load.

Ma [33] produced what is probably the best model to date. For concrete he used Hognestad's parabola and a linear continuation which includes the effects of binders. The steel was described by a combination of a Ramberg-Osgood function and the monotonic curve. The rules for changing from one curve to another are a little complicated, but the model agrees excellently with the results of axial tests on reinforcing bars. The reinforced concrete response is not quite so good, but is still close. Discrepancies appear attributable to the lack of bond-slip

mechanism and to the effect of rubble in the concrete cracks.

Aoyama [3] modelled the stress-strain behavior of both concrete and steel with bilinear σ-ε relations, and his predicted moment-rotation curves differed significantly from test results. Most of the difference can be attributed to the model's inability to simulate the Bauschinger effect.

Bertero and Bresler [34] discussed the effects which contribute to the flexibility of a reinforced concrete member subjected to cyclic load. They concluded that bond-slip and shear deformation (resisted largely by the reinforcing bars in dowel action) are both important, particularly in causing concrete spalling and thereby initiating failure of the member.

3.4 Choice of Model for Use with System Identification

The objective in using system identification is to produce the best possible predictions for a given model form. It therefore seems logical to start with the model form which has the greatest potential for accuracy, and to abandon it in favor of something simpler only if it proves unacceptably expensive. The work of Ma [33], Menegotto and Pinto [32], and Park et al [17,18,19,20,21] leaves no doubt about the superior potential of the layered approach, but questions remain about the expense of using it in identification. To identify N parameters simultaneously requires approximately $10N^2$ function evaluations, each of which consists of predicting the moment at each strain value of a given deformation history. If N is large (say 10) and the moment is needed at 100 different curvature values, 100,000 moment calculations will be required.

Park, Kent and Sampson [21] analyzed a beam composed of ten elements longitudinally, with ten layers in the cross section. 100 load increments were applied, which took some three hours on an IBM 360/55 computer. This is estimated to be equivalent to about fifteen minutes on the CDC 6400 at

the University of California at Berkeley. Menegotto and Pinto report the analysis of a frame containing 12 longitudinal elements, and a total of 3960 concrete and 264 steel elements. No details are given of the number of load steps or the computer time needed. The problem appears to require about fifty times as much effort as Park's, but was executed all the same. Ma reports that, with his model, a moment curvature analysis of a section with 40 concrete elements over 170 load steps used 7.5 seconds of CP time on the CDC 6400.

What little evidence is available therefore suggests that the layered approach is indeed feasible, and so it was selected for use with system identification. The details of the individual steel, concrete and bond-slip models used are given in Chapters 4, 5, and 6.

3.5 Experimental Set Up and Measurements Taken

Identification of the parameters in a material model requires some reliable experimental data to which the model can be fitted. In this case we need data from a reinforced concrete beam tested in flexure -- specifically, the history of curvatures and corresponding moments at some point or points along the beam where the response is significantly non-linear. Since shear is not accounted for in the model, the beam specimen should be sufficiently slender for shear to have a negligible effect on the experimental results.

A number of experimental studies on cyclic loading of reinforced concrete members have recently been conducted at the University of California at Berkeley, and we are fortunate to have the results available to use, thus avoiding the need to duplicate time-consuming work.

The work of Ma, Bertero, and Popov [33] was chosen as being the most suitable, primarily because, in addition to the flexural beam tests,

separate cyclic axial-load tests were carried out on the reinforcing bars to determine their stress-strain behavior in the nonlinear range. The properties of reinforcing steel vary noticeably from batch to batch (because the manufacturers find it cheaper to use recycled steel, low quality control, and a mean strength well above the guaranteed minimum) and so it is important to test bars from the same batch as those actually used in the reinforced concrete beam. Ma did this. A brief description of the tests is given here; for more details see Ref. [33].

9 cantilever beams were tested, 6 rectangular (beams R1-6), and 3 T-beams (T1-3). The intention was to investigate the effects of varying the slab size, the longitudinal reinforcement, the stirrup ties, the shear-span ratio, and the loading history, and so the individual tests were designed accordingly. Each group (Rectangular and T) contained one control specimen, while in each other beam in the group one variable differed from the control specimen's. Each beam was cast into a large concrete end block, (see Fig. 3.2), and a cyclic lateral load was applied to its tip by a hydraulic actuator. Readings were taken of the lateral load, tip deflection, tip rotation, the rotations at two 7-in. intervals from the fixed end, the steel strains in the same region, and the shear distortion. The rotations were obtained from clip gages connected to yokes which were fixed either to the steel reinforcement or to the concrete, (see Fig. 3.3). The average curvature in a 7-in. beam segment was obtained by dividing the difference in rotation between the two ends of the segment by the gage length. In the later tests, a quantity, paradoxically called the "fixed-end rotation," was also recorded. This was an estimate of the beam rotation at the built-in end caused by the bars pulling out of the end-block. The movements of the top and bottom bars

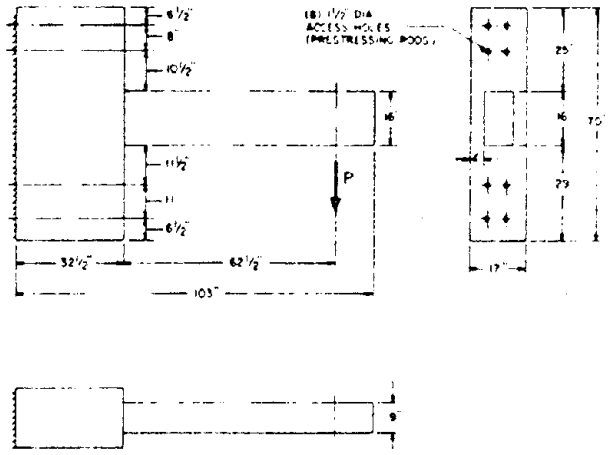

(a) Beams R1, R2, R3, R4, R6

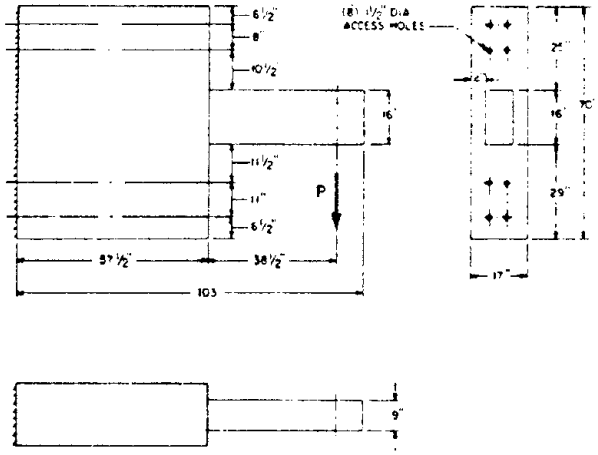

(b) Beam R5

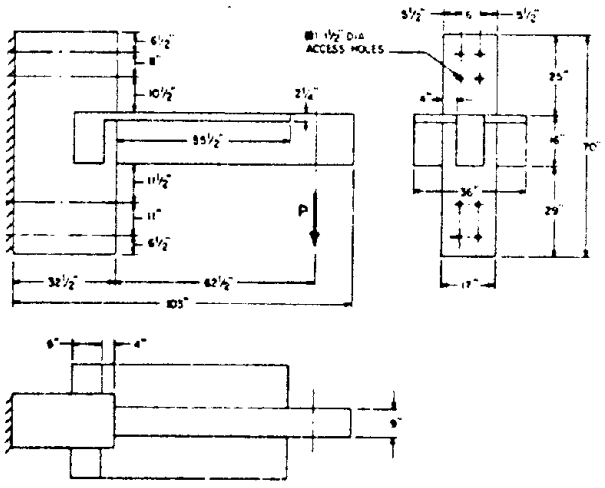

(c) Beams T1 - T3

FIG. 3.2 - SPECIMEN DIMENSIONS

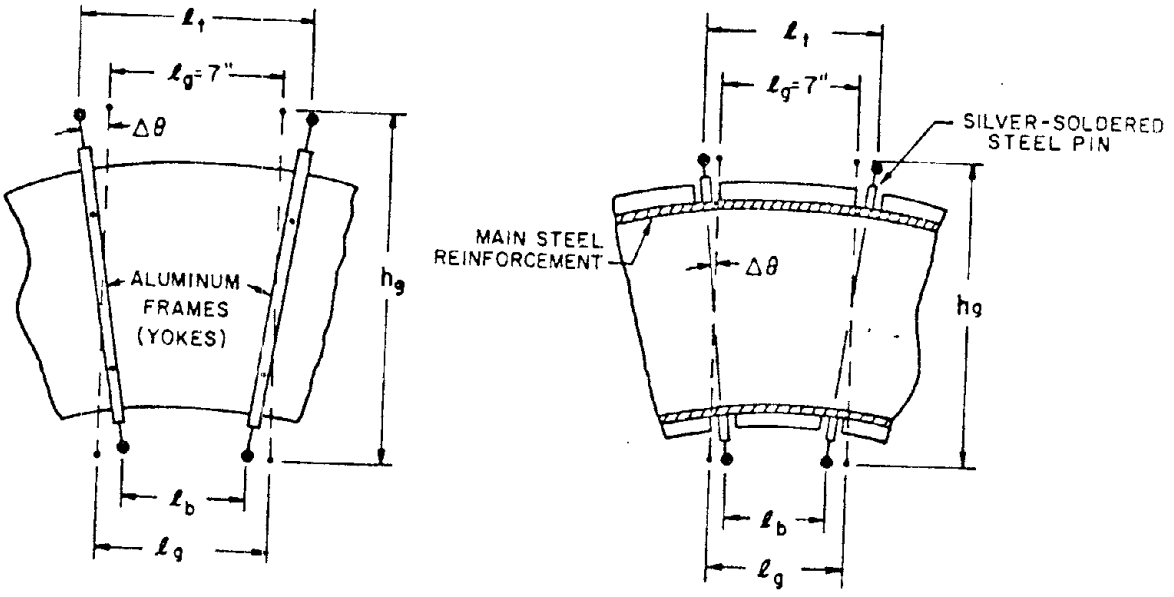

RELATIVE ROTATION $\Delta\theta = \dfrac{\Delta + \bar{\Delta}}{h_g}$

$\Delta = (\ell_t - \ell_g)$
$\bar{\Delta} = (\ell_b - \ell_g)$
} MEASURED BY CLIP GAGES

AVERAGE CURVATURE $\phi_{av} = \Delta\theta / \ell_g$

FIG. 3.3 - METHOD OF MEASURING CURVATURE

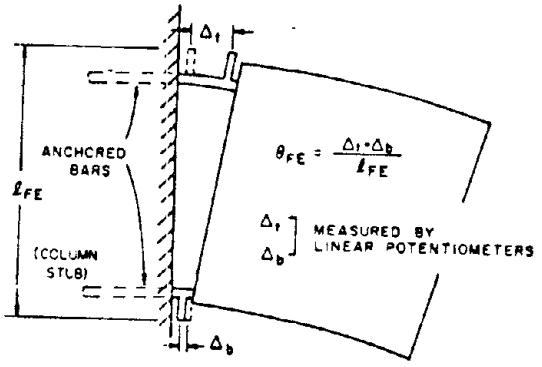

FIXED END ROTATION θ_{FE} MEASUREMENT

FIG. 3.4 - METHOD OF MEASURING END ROTATION

relative to the face of the end block were measured (see Fig. 3.4) and the rotation deduced from them.

Beams T2 and R4 were loaded by imposing on them the maximum possible deflection in alternating directions until they failed (after three-quarters and one and one-quarter complete cycles, respectively). Their moment-curvature histories are shown in Fig. 3.5. The other beams were subjected to a cyclic load of gradually increasing amplitude, such as might be expected during the build-up of a severe earthquake, until they too failed.

Six specimens were machined from the reinforcing steel and were tested axially in a servo-controlled MTS machine. The strain histories were chosen to be similar to those of some of the bars in the reinforced concrete beam tests. The dimensions of the test specimens can be seen in Fig. 3.6, and a typical stress-strain history in Fig. 4.1.

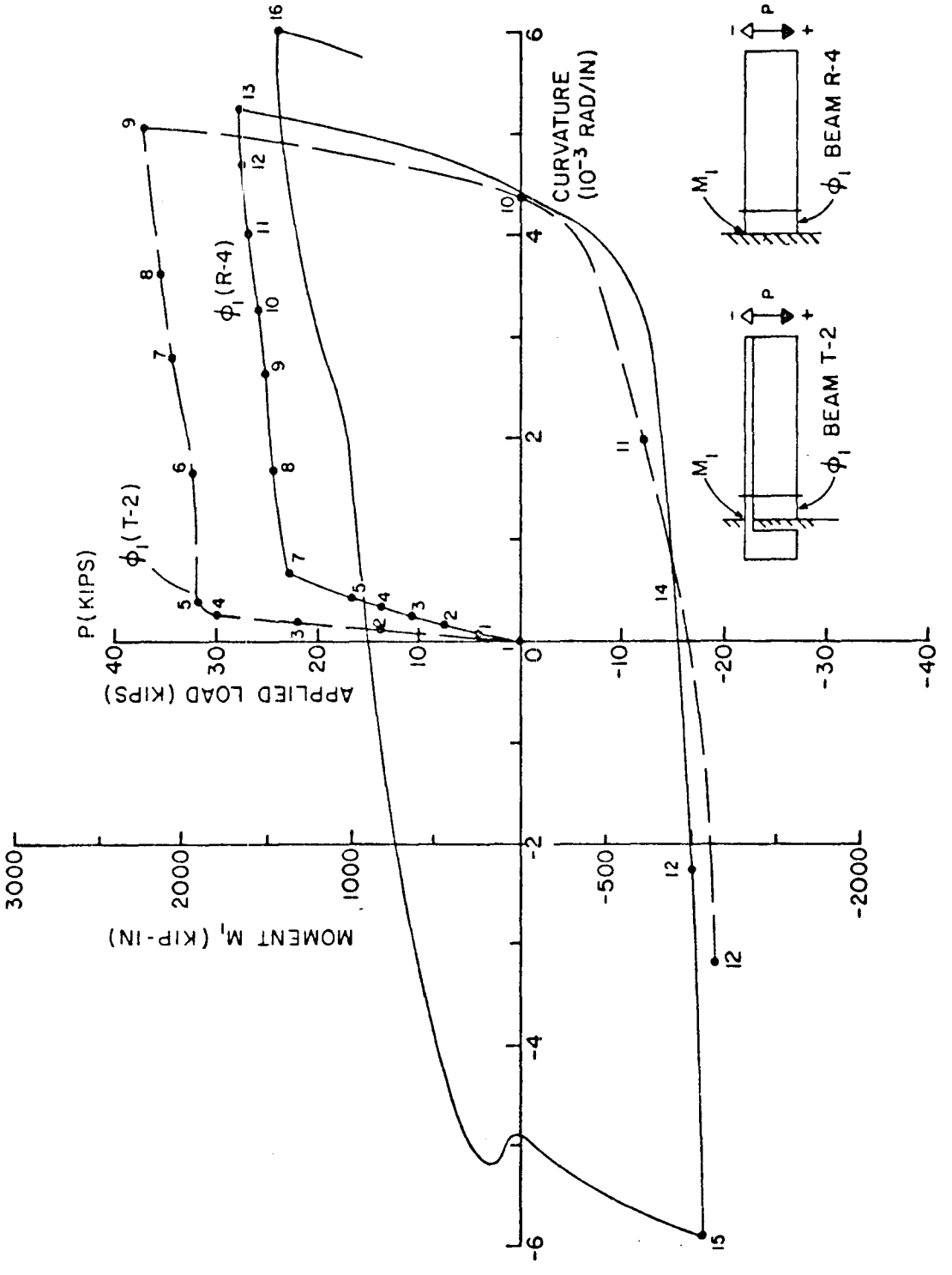

FIG. 3.5 - EXPERIMENTAL MOMENT-CURVATURE RELATION. BEAMS R4 AND T2.

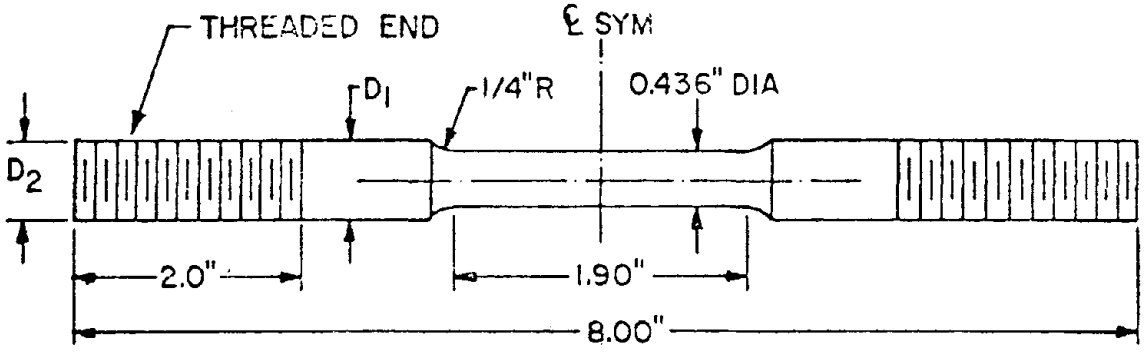

	D_1	D_2
#6 REBAR SPECIMENS	0.625"	0.625"
#5 REBAR SPECIMENS	0.587"	0.500"

FIG. 3.6 - DIMENSIONS OF REINFORCING BAR SPECIMENS

Chapter 4

ANALYTICAL MODEL FOR STEEL

4.1 General

We seek an analytical model which will predict the stress response of steel reinforcing bars to an arbitrary history of strain. Before going into details of the model, we take a closer look at the behavior that we are trying to imitate.

4.2 Experimental Results

A number of investigators have performed cyclic load tests on steel bars [25,30,33] but those of Ma, Bertero and Popov are the most appropriate, and an example of their results can be seen in Fig. 4.1. In tension, the model must cover the whole range of strain from zero to fracture, but in compression, the resistance of the concrete prevents the occurrence of large strains, and so the model only needs to extend to a strain of some ten times the yield strain. Ideally, the model should account for the possible buckling of the compression bars between stirrups, but this would make it too unwieldy to be workable.

4.2.1 Bauschinger Effect

Under monotonic loading, the steel may be expected to display a linear elastic response, a yield plateau, and a curved strain hardening response which flattens out as the maximum stress is approached. Under repeated loading ($P \rightarrow 0 \rightarrow P$) the pattern is similar. Unloading takes place essentially elastically, as does reloading, until it meets the monotonic curve whose path it then resumes.

Under cyclic load, however, the response is quite different, as

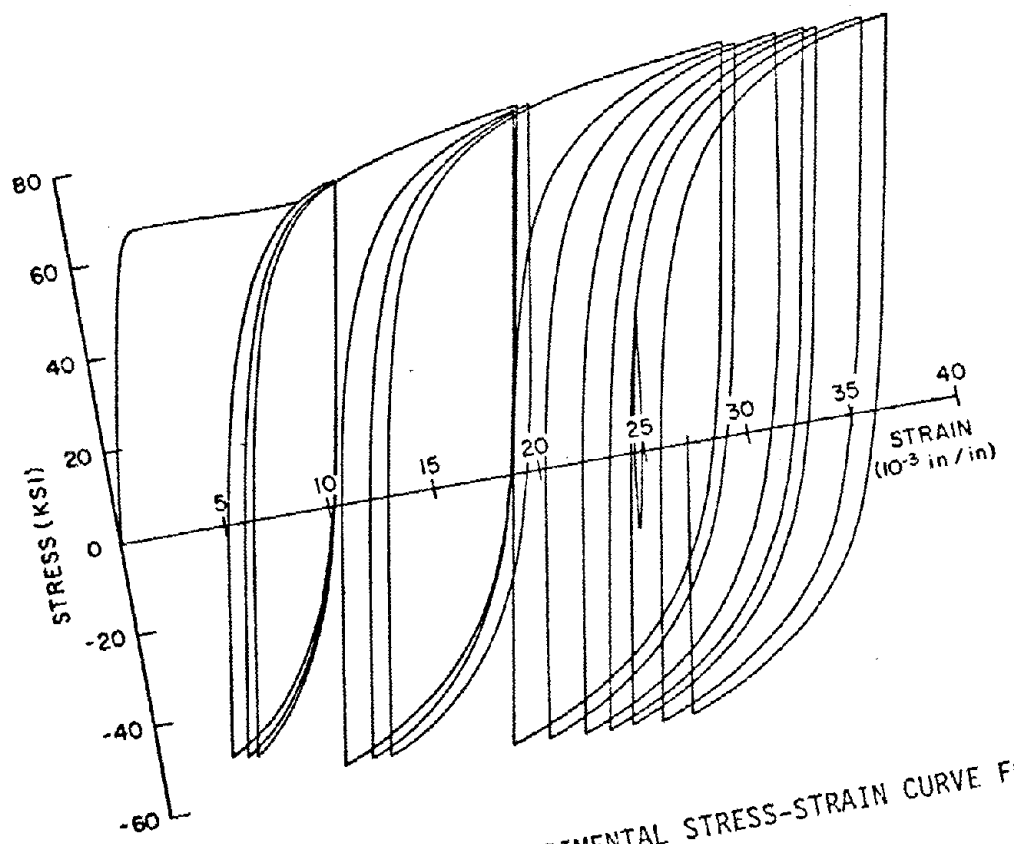

FIG. 4.1 - TYPICAL EXPERIMENTAL STRESS-STRAIN CURVE FOR STEEL

can be seen in Fig. 4.2. Suppose the steel yields first in tension. If the loading direction is then reversed, the subsequent yield in compression follows a rounded path, rather than the sharp one observed with the virgin material.

After the compression yield stress has been reached, the loading path is very similar to the monotonic curve. The rounded yield curve, and the early departure from the linear elastic which it implies, is known as the Bauschinger effect [35,36]. The exact shape of the curve may be expected to depend on:

1. Virgin material properties
2. Entire load (or deformation) history
3. Strain rate
4. Aging effects
5. Temperature effects

Of these, the first two are demonstrably important. Of the others, the strain rates usually experienced in earthquake loading are not high enough to affect the material properties significantly.

Aging causes the material to regain to some extent its virgin properties after they have been erased by cyclic loading. However, the process is gradual and takes months or years to complete, so it is likely to need consideration only in the analysis of structures subjected to a series of earthquakes months apart, and even then, the damage to other elements (concrete, partitions, etc.) is likely to have a greater effect on the structure's dynamic behavior.

Plastic work will cause the bars to heat up, but even with the most conservative assumptions, the temperature rise will not be large enough

to affect the mechanical properties of the steel. Thus, we neglect temperature, strain rate, and aging in formulating the model.

4.2.2 Details of Cyclic Stress-Strain Behavior

The tests show that:

1. Response is linear elastic if the material has never been stressed up to yield.
2. Even a very small excursion beyond the yield strain in one direction causes the immediate loss of sharp yield in the other (Bauschinger effect).
3. Upon reloading in the original direction, the yield may or may not be sharp, but the criteria on which this depends are not entirely clear. (This finding is contrary to Timoshenko's [35] interpretation of Bauschinger's work [36] which suggested that the material need be yielded in only one direction for the sharp yield point to be lost in both.) The test shown in Fig. 4.3 shows that a small initial yield in compression causes a subsequent rounded loop in tension, followed by an almost sharp one in compression. The sharp compression yield only really vanishes either after the addition of a tensile plastic strain increment greater than the original compressive one (resulting in a net plastic strain which is tensile) or after the addition of a tensile plastic strain increment greater than about 3.5×10^{-3} in/in. Presumably, similar behavior would be observed if the loading directions were reversed. Unfortunately, the loading sequences in the other tests are not such that this point can be clarified. The test results shown in Fig. 4.4 might be taken to imply that the second criterion is

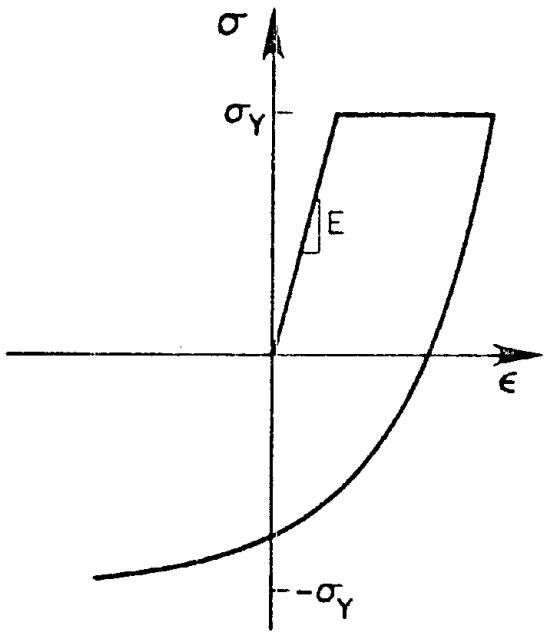

FIG. 4.2 - BAUSCHINGER EFFECT

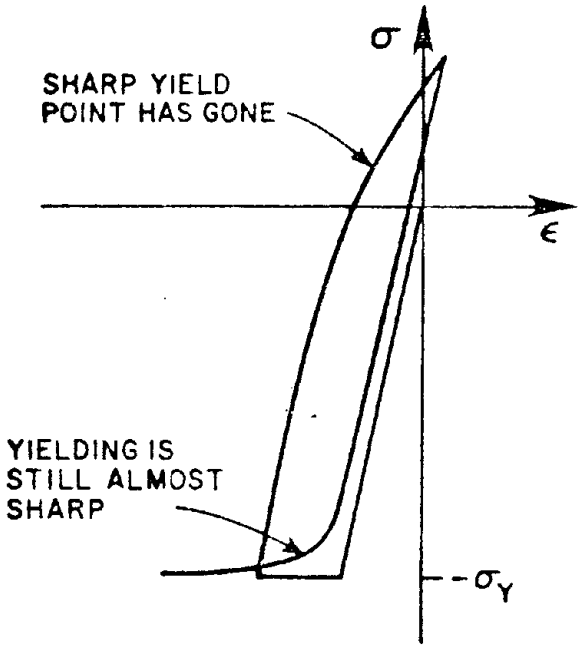

FIG. 4.3 - LOSS OF SHARP YIELD

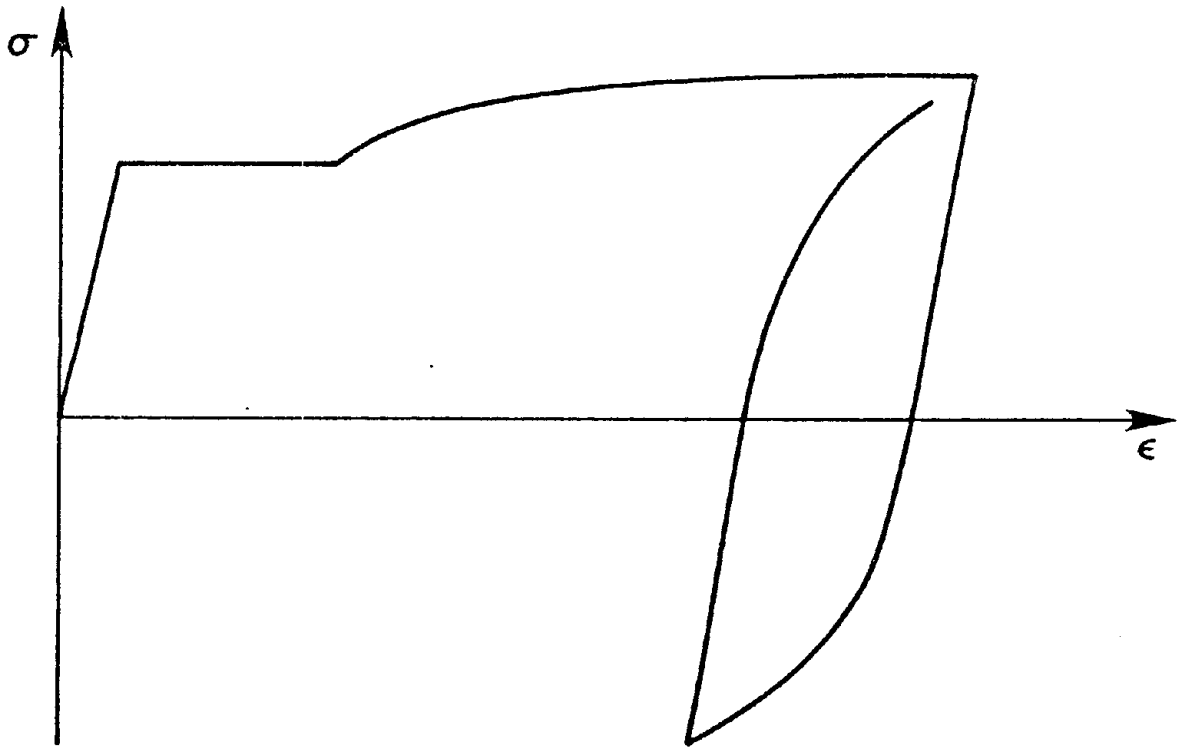

FIG. 4.4 - EXPERIMENTAL STRESS-STRAIN CURVE FOR STEEL

correct because the third half loop displays a distinctly rounded yield, while the cumulative plastic strain maintains the same sense (tensile). But the comparison is dubious because the material was loaded well into the strain hardening region before the first reversal. For want of better information, the first criterion was used in the analytical model.

4. On reversal, the loading path can be thought of in terms of branch curves and an envelope curve. The branch curves are always contained within, and are asymptotic to, the envelope. If only a small amount of plastic work has been done on the material, then the envelope is identical to the monotonic stress-strain curve. But if a significant amount of plastic work has been done, then the envelope is no longer the same as the monotonic loading curve and, furthermore, the difference between them appears to depend on the strain history.
5. The first part of any branch curve is linear elastic. Each curve has a different modulus which decreases as the test progresses.
6. The curvature of the "knee" of the branch curve decreases with each load cycle.
7. Half loops in tension and compression between the same stress limits are not symmetric (i.e., if one is rotated 180°, it cannot be superimposed on the other).

Before strain hardening has set in, the effects of (3) above predominate, but once it has started, the tension loops are more sharply curved, regardless of the direction of the first loading. (This same tendency can be seen in the published results of Aktan, Karlsson, and Sozen's tests [30]).

8. Ma's cyclic load tests were conducted on specially prepared, machined specimens. He performed monotonic tests on two unmachined specimens, one from a #5 bar and one from a #6 bar, to find out if the preparation affected the test results. For both bar sizes, machining did not influence the yield stress, but strain hardening started at a smaller strain and a higher modulus in the machined specimens. Ma suggested that a difference was caused by a change in the distribution of residual stresses. Unfortunately, the unmachined bars were not tested to failure, so it is not possible to compare the ultimate tensile strengths. Such a comparison would indicate whether the explanation is correct or not, because the ultimate tensile strength of such a ductile material should be independent of the residual stresses.

4.2.3 Discussion of Behavior

The concept of a "dynamic envelope" curve is widely used by metallurgists in describing response to cyclic loading. For all types of loading most metal alloys have a dynamic envelope wich differs significantly from the corresponding monotonic load curve, and the two are established independently. However, tests show that for reinforcing steel in simple tension-compression the two curves are close enough that we may approximate the dynamic envelope by the monotonic curve, shifted slightly in the stress and strain directions. It should be emphasized that this is done for convenience and is not based on logical argument.

Morrow [37] describes the phenomenon of "means stress relaxation". If a specimen is loaded cyclically between two strains ε_1 and ε_2, then

the "mean stress," defined as $\left|\frac{\sigma(\varepsilon_1) + \sigma(\varepsilon_2)}{2}\right|$ decreases with cycling (see Fig. 4.5). Morrow's interest is primarily with high cyclic fatigue, but he observes that the largest decrease happens in the first cycle. The relaxation he describes is a different manifestation of that same effect which causes the stress envelope to vary with cyclic loading and is due to some work-dependent slipping of two adjacent atomic layers.

Morrow [38] also reports the existence of "cyclic strain hardening" (or softening). This behavior is shown in Figs. 4.6 and 4.7. When the specimen is loaded cyclically between two (constant) strains ε_1 and ε_2, it is said to harden if the stress range $|\sigma(\varepsilon_2) - \sigma(\varepsilon_1)|$ increases with cycling, and vice versa. He finds that, in general, hard metals soften and soft metals harden with cycling. Smith, Hirschberg and Manson [39] studied different steels and came to much the same conclusion, and report that the metal hardens or softens depending on whether $\sigma_u/\sigma_y > 1.4$ or < 1.2. σ_y is taken as the 0.2% offset yield in cases where there is no sharply defined yield stress. In Ma's specimens, $\sigma_u/\sigma_y = 1.5$ and so they should harden, but most of his tests consist of load cycles which are arbitrary rather than being between constant strain limits, in which case it is not clear what form the hardening will take, or how to detect it.

Morrow's definition of hardening implies an increase in tangent modulus, but if we assume that two successive loading half loops (i.e., $-P \rightarrow +P$ in each) are asymptotic to the same envelope, such an increased modulus would imply a longer linear elastic segment and, therefore, a sharper knee. A few of Ma's tests did include cycles of load between approximately fixed strain limits, but any hardening was small enough to be swamped by other effects and by the limits of experimental accuracy. Therefore, no attempt was made to account for the effect in the model.

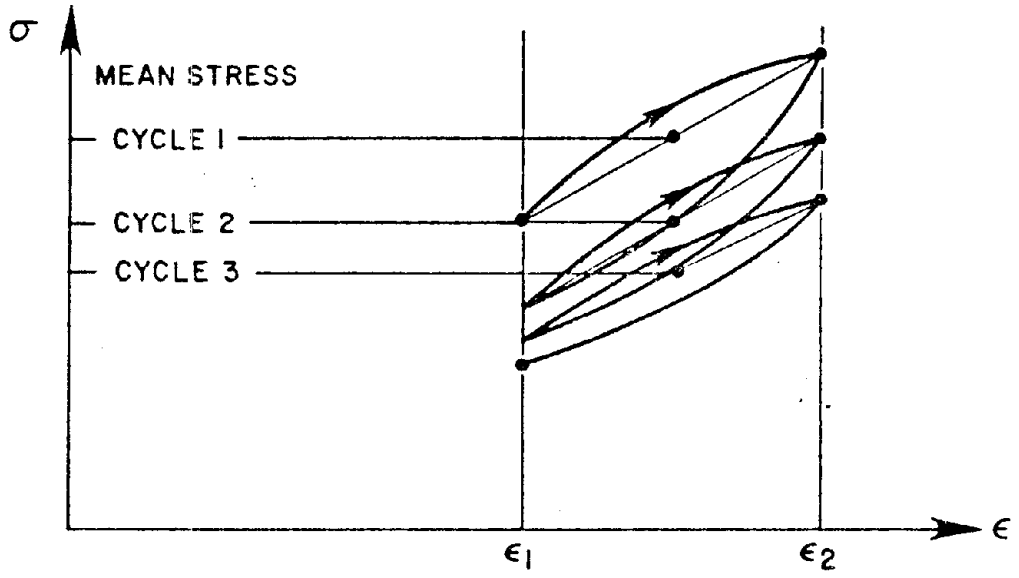

FIG. 4.5 - MEAN STRESS RELAXATION

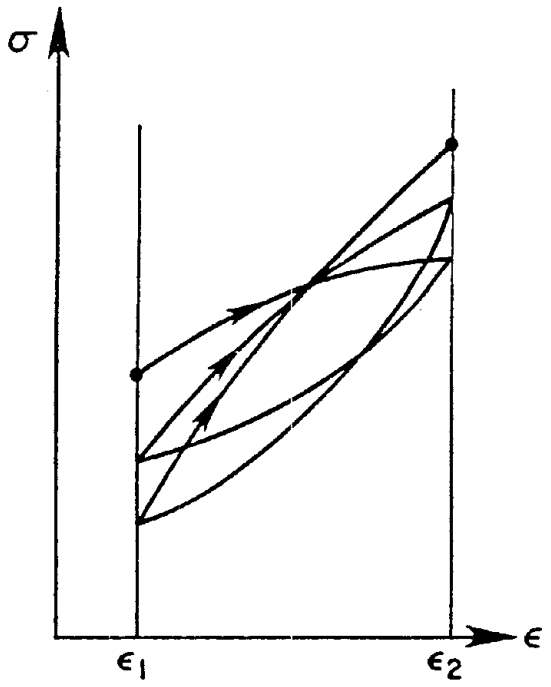

FIG. 4.6
CYCLIC STRAIN HARDENING

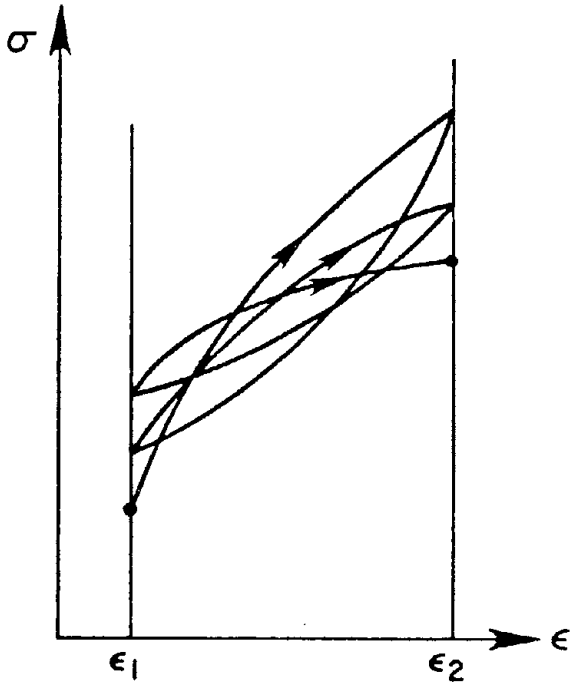

FIG. 4.7
CYCLIC STRAIN SOFTENING

From the above discussion, it is clear that we do not yet have a full, clear and precise understanding of the effects which take place when metals, and steels in particular, are loaded cyclically. Moreover, their isotropy is at best statistical if it exists at all. So we need to know more, not only about the nature of the effects, but also about the statistical distribution of their magnitudes.

It is not surprising, then, that the analytical models which have so far been proposed seek only to fit the stress-strain curve traced out by the test apparatus without attempting to use any knowledge of the material behavior at the microscopic level.

The analytical model should, therefore, be able to reproduce the following features:

1. The true monotonic stress-strain curve, should that be the manner of the loading.
2. Branch curves which are asymptotic to an envelope.
3. Branch curves with knees whose curvature varies as a function of the strain history.
4. An envelope which is obtained by adding suitable stress and strain shifts to the monotonic curve, which can itself be specified arbitrarily. The shifts should be variable functions of the strain history.
5. The ratio of the initial modulus (E_0) of the branch curves to Young's modulus (E) should decrease as a function of some aspect of the strain history.

4.3 Analytical Models

4.3.1 Discussion of Existing Models

The nonlinear analytical models published in the literature have fallen into the three broad categories: multilinear, fixed-parameter nonlinear, and variable parameter nonlinear. Aoyama's [9] is a typical multilinear model. It is simple and cheap to use, but it cannot describe the Bauschinger effect, nor can it include an arbitrary dynamic envelope. Its accuracy is therefore limited.

McNiven and Matzen [40] used the fixed parameter formulation originally suggested by Ramberg and Osgood [22] combined with Masing's [41] assumptions. The context was slightly different to the present one but the goal was the same. Singh, Gerstle and Tulin [25] used their own exponential equation. In all cases the curves are defined by expressions with at least C^1 continuity. With suitably chosen values for their coefficients, these models can mimic the Bauschinger effect but are restricted to describing either the initial sharp yield or the subsequent rounded one, but not both.

The most successful models have all used parameters which vary with the strain history [33,18,19,32,42]; and, indeed, this seems the most promising way of attacking the problem. Within this third group, the nonlinear expressions take three different forms:

(a) An explicit algebraic equation for stress of the form

$$\sigma = \sigma(\varepsilon) \tag{4.1}$$

(b) An implicit algebraic equation of the form

$$f(\varepsilon,\sigma) = 0 \tag{4.2}$$

(c) A first order differential equation of the form

$$\frac{\partial \sigma}{\partial \varepsilon^p} = E^p = f(\sigma) \tag{4.3}$$

where ε^p is the plastic strain. This can be solved for stress if strain is the independent variable.

Layered global models, such as the one used in this study, require an iterative solution for the bending moment, and this must be considered when choosing the type of steel model. For a given curvature, different positions of the neutral axis are tried until axial-force equilibrium is satisfied. But at each iteration, the material stresses must be solved as functions of strain, so in principle option (a) is the most attractive because it involves the least computational effort. Since the calculations will need to be done a large number of times, it may be important to use explicit expressions.

The best explicit formulation is due to Menegotto and Pinto [32]. They propose:

$$\sigma^* = b\varepsilon^* + \frac{(1-b)\varepsilon^*}{(1+\varepsilon^{*R})^{1/R}} \tag{4.4}$$

where

$$\varepsilon^* = \frac{\varepsilon - \varepsilon_r}{\varepsilon_o - \varepsilon_r}, \qquad \sigma^* = \frac{\sigma - \sigma_r}{\sigma_o - \sigma_r}$$

σ_o, ε_o are the stress and strain at the point where the asymptotes of the curve meet, and

ε_r, σ_r are the values at the last reversal.

The equation represents a curved transition from one straight line asymptote (slope E_o) to another (slope E_∞), where

$$b = E_\infty/E_0 \qquad \text{and} \qquad E_0 = \frac{\sigma_0 - \sigma_r}{\varepsilon_0 - \varepsilon_r}$$

R = an independent parameter which defines the curvature of the transition.

The asymptotes are

$$\sigma^* = \varepsilon^* \qquad \text{(initial)} \qquad (4.5)$$

$$\sigma^* = (1-b) + b\varepsilon^* \qquad \text{(final)} \qquad (4.6)$$

and are illustrated in Fig. 4.8.

When ε^* and R are both >>1, the curve can be approximated by

$$\sigma^* = [(1-b) + (b\varepsilon^*)] - \Delta\sigma^* \qquad (4.7)$$

where

$$\Delta\sigma^* \doteq \frac{1-b}{R\varepsilon^{*R}} \qquad (4.8)$$

is the stress difference between the asymptote and the curve.

The advantage of using the approximation is that it contains one exponentiation rather than two and so is about twice as fast to compute. The error in using it is

$$\text{error} = \frac{(1+R)(1-b)}{2R^2\ \varepsilon^{*2R}} + \text{higher order terms} \qquad (4.9)$$

Lazan [43] and Davidenkov [44] suggested a simpler expression, but it is unable even to approximate an elastic-perfectly plastic response, so holds little promise.

Models using an implicit algebraic equation [18,19,33] have generally been based on the Ramberg-Osgood [22] three-parameter model

$$\varepsilon^* = \beta\sigma^*(1 + \alpha|\sigma^*|^{n-1}) \qquad (4.10)$$

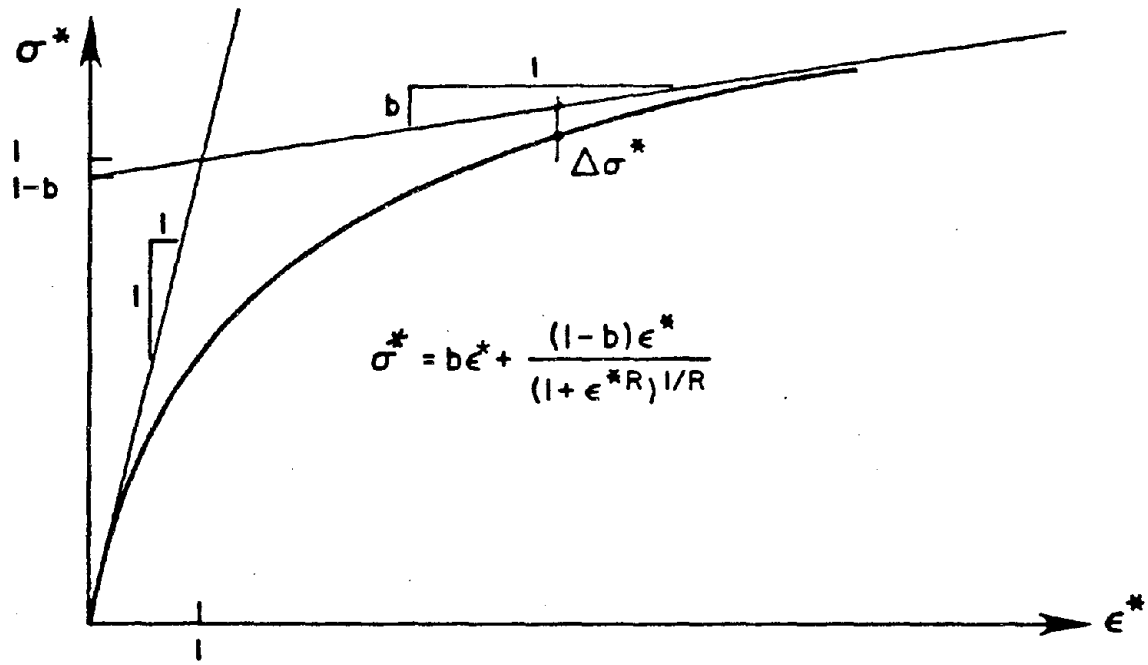

FIG. 4.8 - MENEGOTTO-PINTO EQUATION

where

$$\varepsilon^* = \frac{\varepsilon - \varepsilon_r}{2\varepsilon_y} \qquad \sigma^* = \frac{\sigma - \sigma_r}{2\sigma_y}$$

which is illustrated in Fig. 4.9. The individual models differ in the way in which the coefficients are defined and the manner in which control is transferred from a branch to an envelope curve. The basic equation (Eq. 4.10) has a number of disadvantages, but has been widely used despite them. First, it must be solved by an iterative method if strain is the independent variable (which it is in our case). Second, the conditioning of the parameters is poor since they have typical values of $\beta = 1$, $\alpha = 10^{-4}$, $R = 7$, but α is constrained to be > 0. Last, there is no final asymptote and so the branch curve intersects the envelope rather than approaching it asymptotically.

Dafalias [42] used a differential equation to define the branch curves, but his resulting curves are not dissimilar to Menegotto and Pinto's. He proposes tension and compression asymptotes which are straight lines of slope E_o^p. The branch curve starts with a linear elastic segment extending from (ε_r,σ_r) to some point P (see Fig. 4.10). δ_{in} is then set equal to the distance from P to the asymptote. Thereafter, the curve is defined by a plastic modulus

$$\frac{\partial\sigma}{\partial\varepsilon^p} = E^p = E_o^p \left[1 + h \frac{\delta}{\delta_{in} - \delta}\right] \qquad (4.11)$$

where

δ is the instantaneous distance to the asymptote

h is a function (usually of δ_{in}) chosen to fit the particular material.

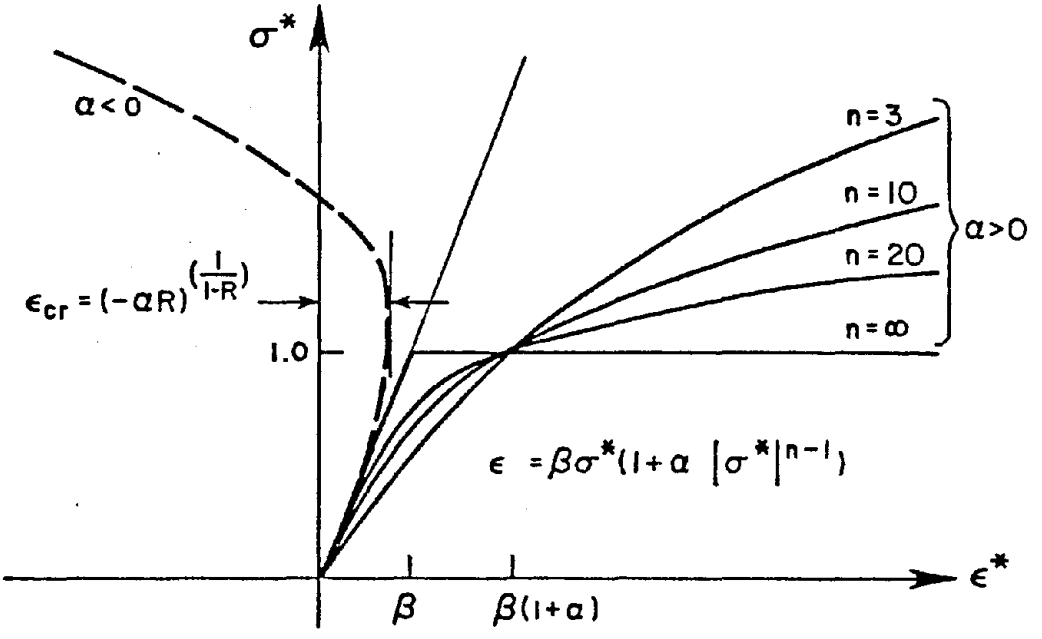

FIG. 4.9 - RAMBERG-OSGOOD EQUATION

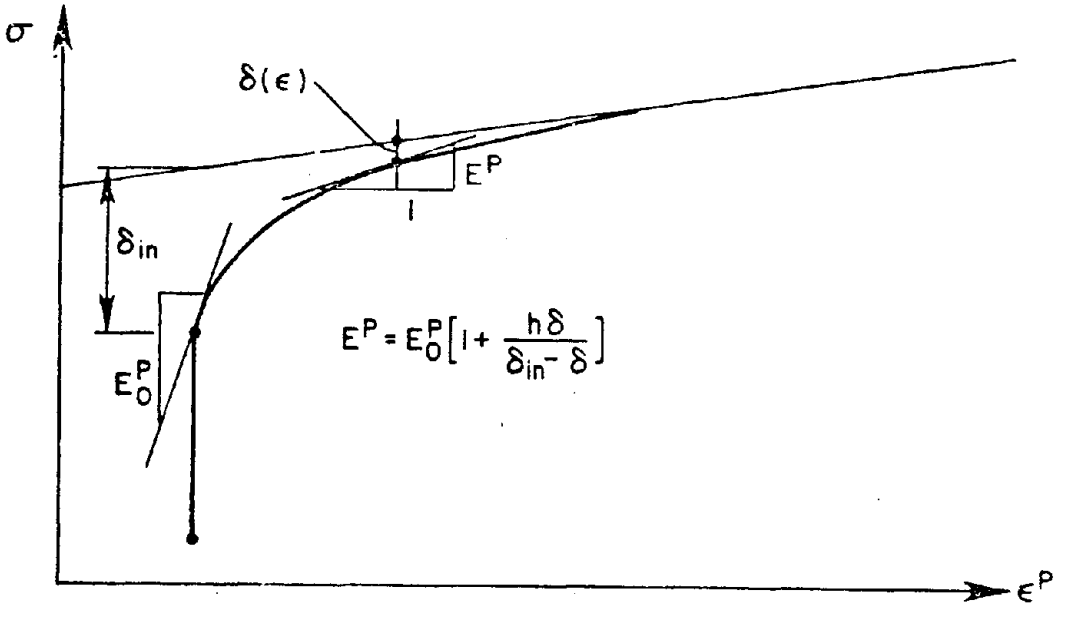

FIG. 4.10 - DAFALIAS' EQUATION

The model shares with Menegotto and Pinto's the elegance of defining a branch curve which is automatically asymptotic to the envelope, thus creating a continuous curve and avoiding the need to check if a boundary curve has been crossed. However, the response is governed by a differential equation, which has two disadvantages. One is that in principal a differential equation is harder to solve than an algebraic one. The second concerns the accuracy of solution. If the stress is needed at several points along a curve, the differential equation has to be solved to a greater accuracy than the corresponding algebraic one because in the former case the errors at each point accumulate, whereas in the latter they do not. The formulation could prove expensive to use.

4.3.2 Choice of Model

The most promising models are Menegotto and Pinto's, Dafalias', and some variant of the Ramberg-Osgood equation. The Ramberg-Osgood equation was solved to a number of different tolerances in order to find out how many iterations are needed for a reasonably accurate solution. The number depends on the accuracy of the initial estimate, which is obtained from the converged solution at the previous point. The closer together the points are located, the smaller is the number of iterations required. The tests showed that for 5-10 points evenly spaced along a typical curve, 3-4 iterations give adequate accuracy. In view of this, and the fact that Ma had achieved good results with his model, the Ramberg-Osgood equation was selected at the preliminary stage.

As will be seen, this choice turned out to be at the same time good and bad. Bad, because it caused problems with the identification routine, and good, because the problems were brought out at this early stage of

the research. Several typical half cycles from Ma's steel tests were digitized, and identification was then used to find the set of Ramberg-Osgood parameters β, α, and n which best fit each curve. These curve fitting tests were also the first experiments with the minimization routines (see Chapter 8), and the Modified Gauss-Newton method was being used in two different versions. One calculated the gradient analytically and the other used finite differences to approximate it.

For some curves the program converged to a set of parameters which gave rise to an error function whose value was close to zero and theoretical stresses which were very close to the experimental ones. The final error function value and the number of iterations required for convergence were both smaller when the gradient was calculated analytically.

For the other curves, however, the program either stopped or failed to converge. It stopped because the search entered the infeasible region of parameter space. The parameter α in Eq. 4.10 must be positive, yet it has a minimizing value which is very close to zero. If during the search it becomes negative, the Ramberg-Osgood equation traces out the dashed rather than the solid curve in Fig. 4.9, and there are either two or no real solutions for the stress, depending on whether the strain is less than or greater than the critical value

$$\varepsilon_{cr} = \beta\left(1-\frac{1}{R}\right)\left(-\alpha R\right)^{\frac{1}{1-R}} \qquad (4.12)$$

The minimizing parameters must lie within the feasible region, and so we must find a way of preventing the search from leaving it, even if the departure is to be only temporary. There are a number of possible

ways. First, the parameters can be constrained to approach the boundary of the feasible region no closer than some small distance ξ. If the line search requires a point beyond this constraint, it should stop and a new direction should be calculated. McNiven and Matzen [40] used an approach similar to this. It is somewhat inelegant, because it means that the minimization program is no longer independent of the error function, and so changing the model involves some work.

This can be avoided by the use of a penalty term which is added to the error function and whose value tends to infinity as the boundary is approached. An appropriate form might be

$$F = f\{|\frac{1}{\xi}|\} \tag{4.13}$$

Another alternative is to rescale the coordinate axes. This alters the scale of the feasible region, and if the scale factors are well chosen, it moves the minimum of the critical parameter α away from the boundary. The ideal scaling appears to be one which equilibrates the Hessian matrix both row and column-wise. However, the true Hessian is generally not available, so this cannot be done, but experiments proved successful in which the parameters were rescaled so that they were all approximately equal at the minimum. The search remained in the feasible region and convergence was more rapid than it had been on those curves where a minimum was located without rescaling.

Perhaps the most obvious remedy is to use a different model. Menegotto and Pinto's model was therefore programmed and the minimization converged rapidly every time. In most cases where both the Ramberg-Osgood and the Menegotto and Pinto equations were applied to the same

data, the Menegotto-Pinto model gave a smaller minimum error. However, great importance should not be attached to this fact because the predictions of both models are good enough for practical purposes and are probably close to the limit of experimental accuracy.

The Menegotto-Pinto model (Fig. 4.8) has two distinct advantages. First, each parameter defines a separate aspect of the curve's geometry, so these can be manipulated independently. Second, good initial estimates of three of the four parameters can be obtained by taking measurements directly from the curve. Figs. 4.11a-c show some of the curves which the model can assume (elastic-perfectly plastic, elastic-strain hardening with a positive or negative strain hardening modulus).

The only parameter which appears difficult to estimate initially is R, but the curves possess a property which simplifies the task. Suppose we define by an arbitrary set of parameters a curve A whose origin is at (0,0), then digitize it. A second curve B, with origin at some point (-c,-c), with c arbitrary, can then be fitted through the digitized points and the parameters found which give the best fit. It turns out that the best fit occurs when the value of R/σ_0 is almost exactly the same for curves A and B, regardless of the value of c, and furthermore the fit is extremely good. The usefulness of this property can be seen in Fig. 4.11d, which shows that two branch curves can easily be made to have knees which are almost identical, although the curves start at different distances from the asymptote. If we define $R = r\sigma_0$, and use r as a parameter instead of R, then r is found to vary only between about 0.55 and 0.75 for all the experimental curves, and so 0.65 can be used universally as a good initial estimate.

The Menegotto-Pinto model possesses many characteristics which make

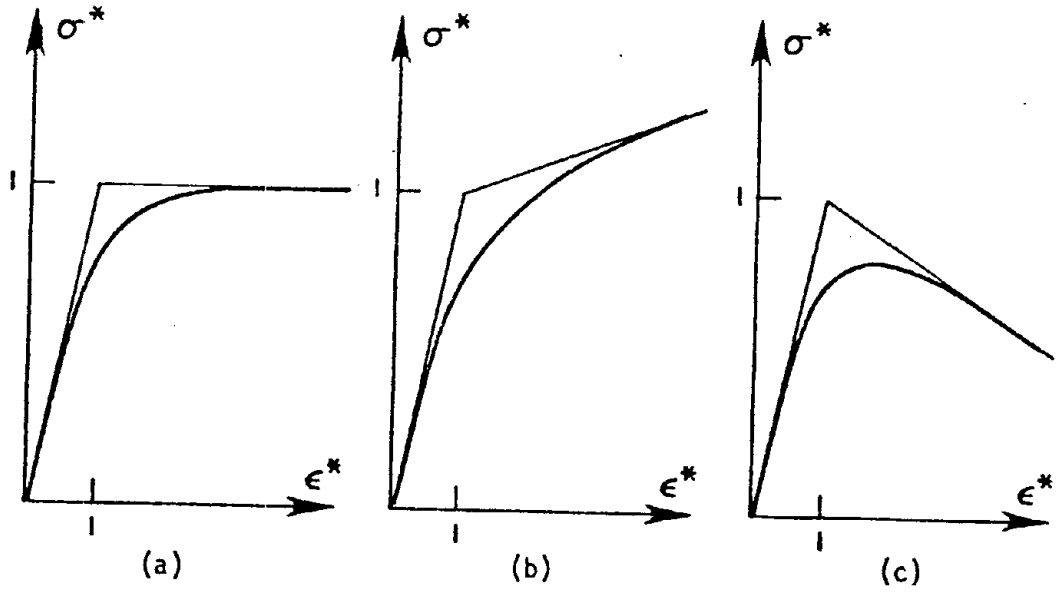

FIG. 4.11(a-c) - POSSIBLE SHAPES FOR MENEGOTTO-PINTO CURVES

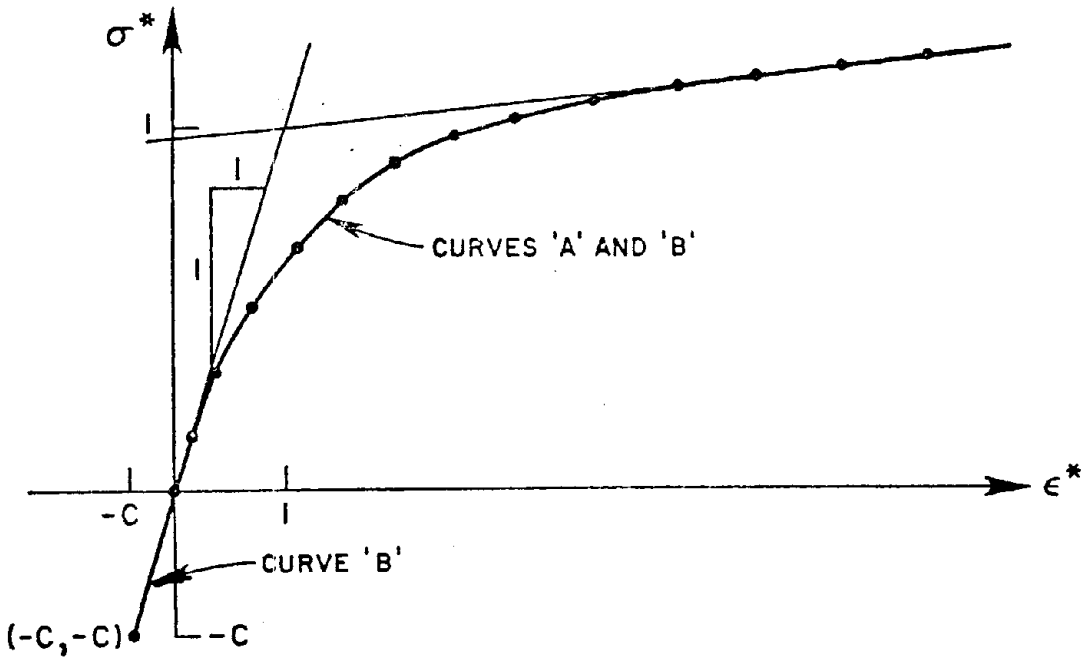

FIG. 4.11(d) - SUPERPOSITION OF MENEGOTTO-PINTO CURVES

it preferable to Ramberg-Osgood, but as suggested by the authors, its final asymptote is a straight line, and this is definitely not the shape of the dynamic envelope curve for a typical steel. It was therefore modified as shown in Fig. 4.12. An arbitrary envelope is defined in such a way that the stress (σ_1) and tangent modulus (E_1) on it can be calculated easily at any strain ε. To define the stress on the branch curve at strain ε, the envelope values σ_1 and E_1 are first calculated. E_∞ in Eq. 4.4 is then set equal to E_1, and σ_0 is calculated from E_0, E_1, σ_1, ε_r and σ_r.

By this means the branch curves are made asymptotic to an envelope of arbitrary shape. Furthermore, the two variables E_∞ and σ_0 in Eq. 4.4 become known functions of the envelope data which are calculated at each step, rather than parameters whose values must be found by identification.

This modified form of the Menegotto-Pinto model was felt to be more suitable than any of the alternatives, and so was used throughout the rest of the study.

The arbitrary envelope used was the monotonic curve, shifted in the stress and strain directions. The stress shifts are expected to depend in some way on the strain, and the coefficients in the dependence relation are treated as parameters to be identified. The monotonic curve forms part of the input data to the program. It is defined by any number of points whose stress and strain coordinates are read in (see Fig. 4.13). A cubic polynomial is then fitted between each pair of adjacent points on the strain hardening curve in such a way that the total curve has C^2 continuity. The coefficients of the cubics and their derivatives are stored for later use. The details of the process are given in Appendix B.

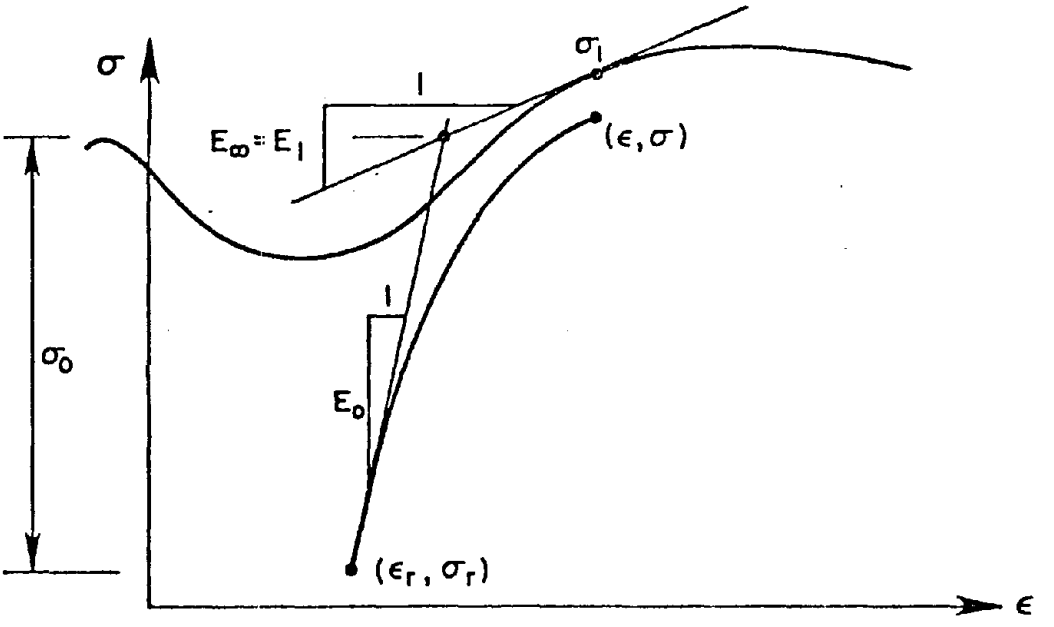

FIG. 4.12 - MODIFIED MENEGOTTO-PINTO CURVE

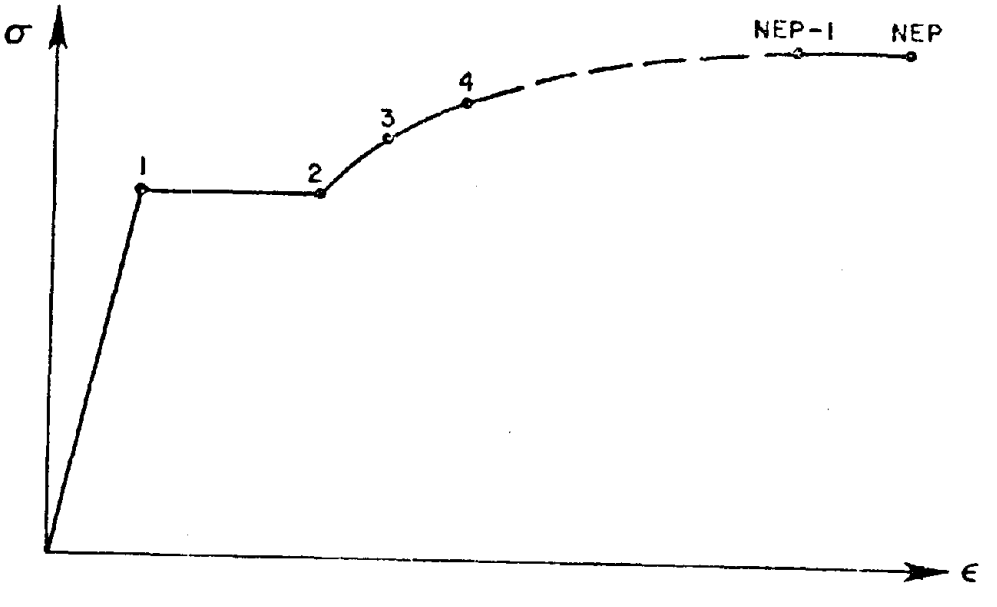

FIG. 4.13 - DIGITIZATION OF MONOTONIC CURVE

4.3.3 Description of the Model Adopted

The development of the model was a gradual process requiring several cycles of refinement, each of which consisted of an assessment of the performance of the model in its current state, modifications to the model form, and identification of the new parameters. Because the processes of identification and selection of the model form were interwoven in this way, they are described together in this section.

The basic rules for prediction of stresses are:

1. If the bar has not previously reached its yield stress in either direction, response is linearly elastic.
2. After yielding for the first time, response follows the monotonic curve until the first post-yield reversal.
3. Thereafter, the path follows a series of branch curves, each of which is asymptotic to the appropriate (compression or tension) envelope. The envelope is defined by the monotonic curve, suitably shifted in the stress and strain directions. The branch curves are defined by the Modified Menegotto-Pinto equation (Eq. 4.4) in which the variables E_∞ and σ_0 are calculated directly from the envelope stress and tangent modulus at each strain value. (This is not strictly true because the program was modified slightly in the interests of economy. If the initial asymptote meets the envelope at (ε_e,σ_e), then for strains between ε_r and ε_e the shape of the branch curve is rather insensitive to E_∞ and σ_0, which do not change much in this region. Therefore, upon each strain reversal, the E_∞ and σ_0 corresponding to (ε_e,σ_e) were calculated and used for all strains between ε_r and ε_e.)

These basic rules alone are not sufficient to predict stresses, because definitions are lacking for E_o and R in the Memegotto-Pinto equation and for the envelope stress and strain shifts.

We use Kent's [18] definition for the strain shift, which is illustrated in Fig. 4.14. For the tensile stress envelope, the monotonic curve is shifted along the strain axis so that its origin lies at (ε_{zmx},o), where ε_{zmx} is the minimum value of ε_z. ε_z has a different value in each load cycle and is the residual strain remaining after reloading to zero stress. The point (ε_z,o) lies on a branch curve which is defined by Menegotto and Pinto's equation. Therefore, to find ε_z exactly we would need to solve the equation for strain at a known stress, which can only be done iteratively. However, the coefficients in the equation are not known until the envelope is defined and this cannot be done without knowing ε_z! To avoid a tedious calculation, an approximate value $\bar{\varepsilon}_z$ is used, where $\bar{\varepsilon}_z$ is the point where the initial asymptote E_o to the branch curve intersects the strain axis.

If the strain shift is nonzero, the reloading curve will have lost its sharp yield point. The yield plateau of the envelope is then replaced by a straight line passing through the start of the strain hardening curve with a slope equal to the initial strain-hardening modulus. This is shown in Fig. 4.14. The compression strain shift is similarly defined.

E_o, R, and the envelope stress shift, σ_{sft}, remain to be defined. As a first attempt, σ_{sft} was taken as zero, E_o and R were assumed constant, and their values were found by identification over a number of half cycles of load. The resulting match was poor, and it was evident that E_o, R, and σ_{sft} would have to be made dependent on the strain in some way. The simplest way of achieving this is to keep them constant throughout

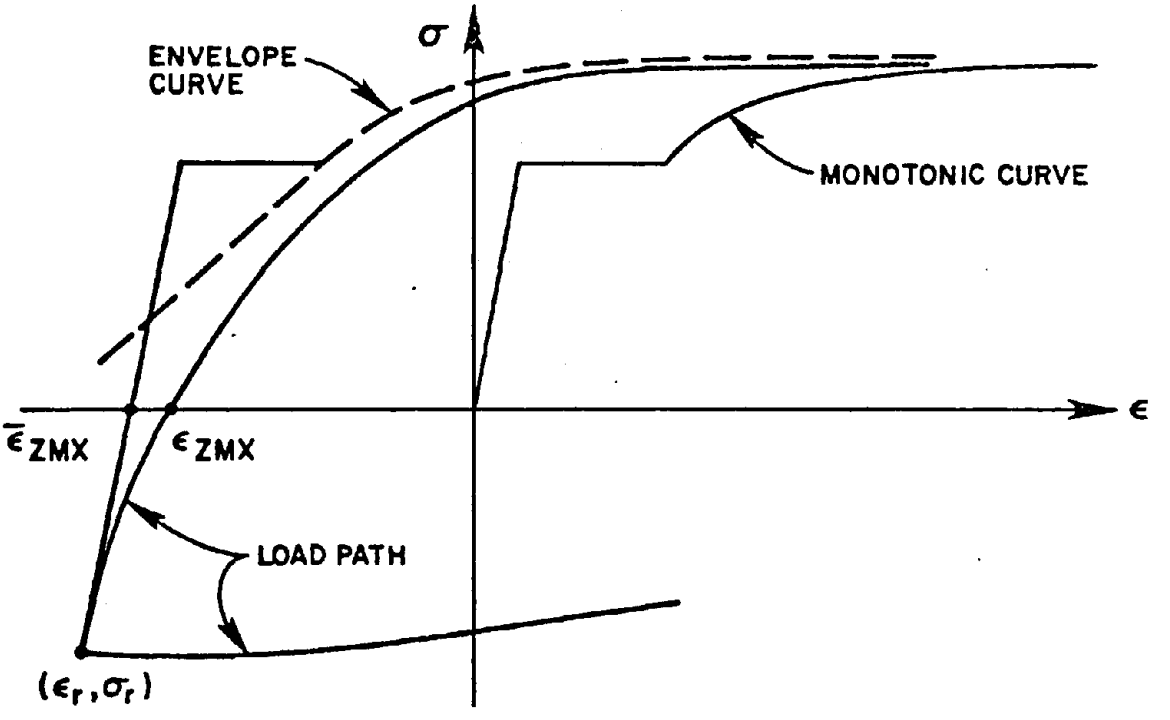

FIG. 4.14 - ENVELOPE STRAIN SHIFT

any half cycle of load and to recalculate their values at each reversal point. Such a procedure requires three functions of strain from which to evaluate E_o, R, and σ_{sft}. These can be established by taking the half cycles of load separately and identifying for each the optimum values of the three variables. These are then plotted against different aspects of strain (e.g., reversal strain, maximum plastic strain, cumulative plastic strain, etc.), the most suitable of which is then chosen as the independent variable on which each function is to depend.

To assume that the three variables E_o, R, and σ_{sft} are independent seemed unduly optimistic, so their functional relations were selected sequentially. First a functional form was chosen for E_o, and R and σ_{sft} were kept constant while the parameters in the functional relationship for E_o were identified from a number of half cycles of load. Next, calculating E_o from the function just established, optimum values for R and σ_{sft} were once again identified for each half loop separately. These values differed from the previous ones because the calculated values of E_o were not identical to the optimum ones for each half loop, but rather the best approximations which could be accommodated in simple functional form. The values of R were then plotted against several independent strain variables, a functional form chosen, and the parameters in it identified using a series of half loops. The same procedure was then used for σ_{sft}.

E_o was dealt with first because it was observed in practice to decrease with increasing strain, and this tendency is supported by theory. If Young's modulus, E, is assumed to be a constant relating true stress and strain, the measured modulus, E_m, at a reversal point (ε_r,σ_r) will be

$$E_m = \frac{E}{(1+\varepsilon_r)^2} \tag{4.14}$$

due to the differences between true and observed stress and strain.

In the experiments, the degradation in E_m was about twice this theoretical value. The difference may have been caused by a variation in strain along the gage length of the specimen and the initiation of necking.

The functions chosen to define E_o, r and σ_{sft} are:

$$E_o = 30.0 - 0.108\ \varepsilon_r - 1.928\ (1.0 - \exp\{-0.39\ \varepsilon_r\}) \tag{4.15}$$

but not less than 22.0

$$r = 0.7439 - 0.01092\ \varepsilon^p_{maxc} \quad \text{in tension} \tag{4.16}$$

$$r = 0.6923 - 0.006323\ \varepsilon^p_{maxt} \quad \text{in compression} \tag{4.17}$$

$$\sigma_{sft} = 2.482 - .0406\ \varepsilon^p_{sum} \quad \text{in tension} \tag{4.18}$$

$$\sigma_{sft} = 0.4123 - 0.0364\ \varepsilon^p_{sum} \quad \text{in compression} \tag{4.19}$$

but

σ_{sft} = 0.0 if the material has not yet yielded in that direction.

In the above,

ε_r = strain at last reversal

ε^p_{maxt}, ε^p_{maxc} = maximum plastic strain in a half loop in tension and compression, respectively

ε^p_{sum} = the sum of the absolute values of the plastic strains in all half loops to date (both directions together)

Stress is measured in ksi and strain in 10^{-3} in/in, thus the material modulus is in ksi/10^{-3} in/in or 10^6 psi.

A few points are worth noting. First, the different values of r in tension and compression reflect the fact that the tension branch curves have slightly sharper knees. Also, r is governed by the maximum plastic strain in the opposite direction, so that a large tensile inelastic excursion will reduce the curvature of the subsequent compression curves and vice versa.

Equation 4.15 and the points which led to its selection are plotted in Fig. 4.15. The data for r and σ_{sft} is more scattered and so their equations are simpler. The use of different data undoubtedly would have altered the coefficients in the equations, but since r is approximately constant and σ_{sft} is small, the possible variations were considered relatively unimportant.

Some typical experimental results are plotted in Fig. 4.16, with the corresponding predictions of the model. The worst error is seen to be about 3 ksi, and generally the agreement is much better. The exact shape of the analytical curve and the values of the optimum parameters are influenced by the locations of the discrete points at which the stress is calculated. However, the differences between theory and experiment are of the same order of magnitude as both the experimental error and the differences in mechanical properties between bars from the same batch of steel, so there is little to be gained by further refinement.

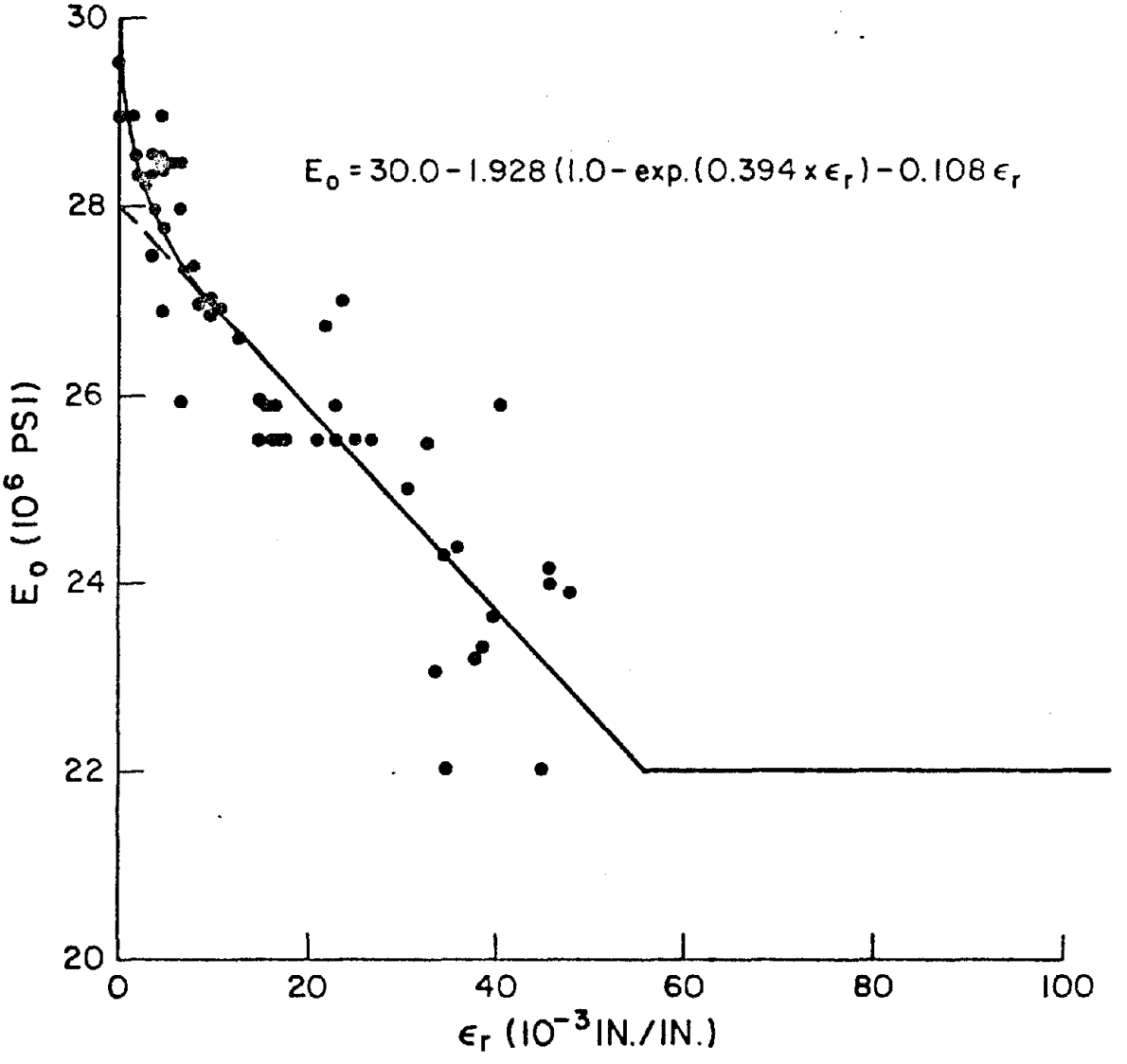

FIG. 4.15 - INITIAL TANGENT MODULUS EXPRESSION

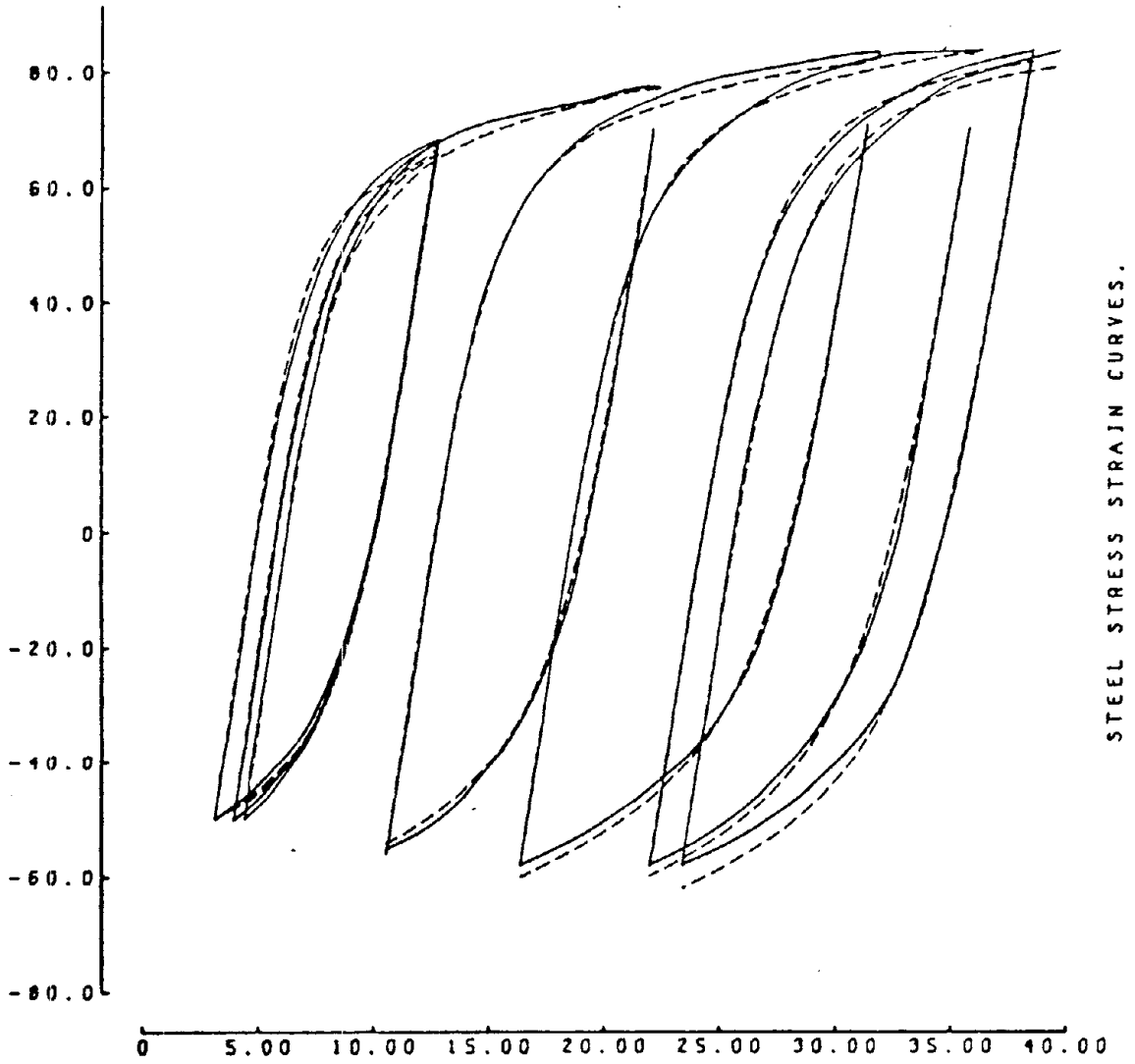

FIG. 4.16 - COMPARISON OF THEORETICAL AND EXPERIMENTAL RESULTS

Chapter 5

ANALYTICAL MODEL FOR CONCRETE

5.1 General

This chapter discusses the model adopted to describe the behavior of plain concrete. The model for concrete is not treated in the same way as the one for steel, the difference lying in the manner in which the parameters are estimated. Those for steel are obtained by comparing the predictions of the model to the results of axial tests on steel bars, and they are then held constant when the steel model is incorporated into the global one. This is done in order to reduce the number of parameters to be identified in the global model and is justified on the grounds that the mechanical behavior of the steel remains the same whether or not it is embedded in concrete. There is no explicit proof that this assumption is valid, but numerous investigators have used it and no evidence to the contrary has been published. The behavior of plain concrete, on the other hand, is demonstrably not the same in a reinforced beam as it is in a simple compression test on a cylinder. Special tests have been devised [12,45] to simulate the conditions in a beam, but they are beset by the difficulty of measuring stress experimentally and this, above all else, has prevented the complete definition of the relationship between stress and strain in concrete. The deficiency has two direct consequences. The first is that a sophisticated analytical model is unwarranted, especially since the relative importance of the factors influencing the concrete behavior has not been properly established. This is illustrated by the experience of Agrawal et al [27] who found that a crude model predicted their experimental results more closely than a sophisticated one.

It is worth noting that the concrete model has only a modest influence on the overall predicted behavior of a beam, but a large influence on that of a column, if each is subjected to a cyclic load. This is because the axial compression on a beam is generally very small, so flexural cracks form right across it and remain open for most of each load cycle. While they are open, the concrete is unstressed and the behavior of the beam depends only on the response of the steel.

Second, the optimum parameters should be identified not by using tests on plain concrete but by incorporating the concrete model into the global one and using results of tests on reinforced concrete members. This is the approach that was used, and the results are discussed in Chapter 9. But in order to do this, a form is needed for the model. Clearly, it should simulate as closely as possible our best estimate of the behavior of the concrete in the beam, but to achieve this end, we must first establish the range of shapes which the response curve can assume, and then choose as parameters quantities which will allow the model to reproduce those shapes. If the parameters can at the same time be made to represent specific physical quantities, the usefulness of the model will be increased.

5.2 Behavior of Concrete in Compression

Figs. 5.1 and 5.2 show typical stress-strain curves for concrete subjected respectively to monotonic and repeated loads. In each case, however, the exact shape of the curve will be influenced by a number of physical factors which are examined in this section for the purpose of determining their effect on the stress-strain curve.

5.2.1 Monotonic Behavior

The monotonic stress-strain curve for concrete is characterized by

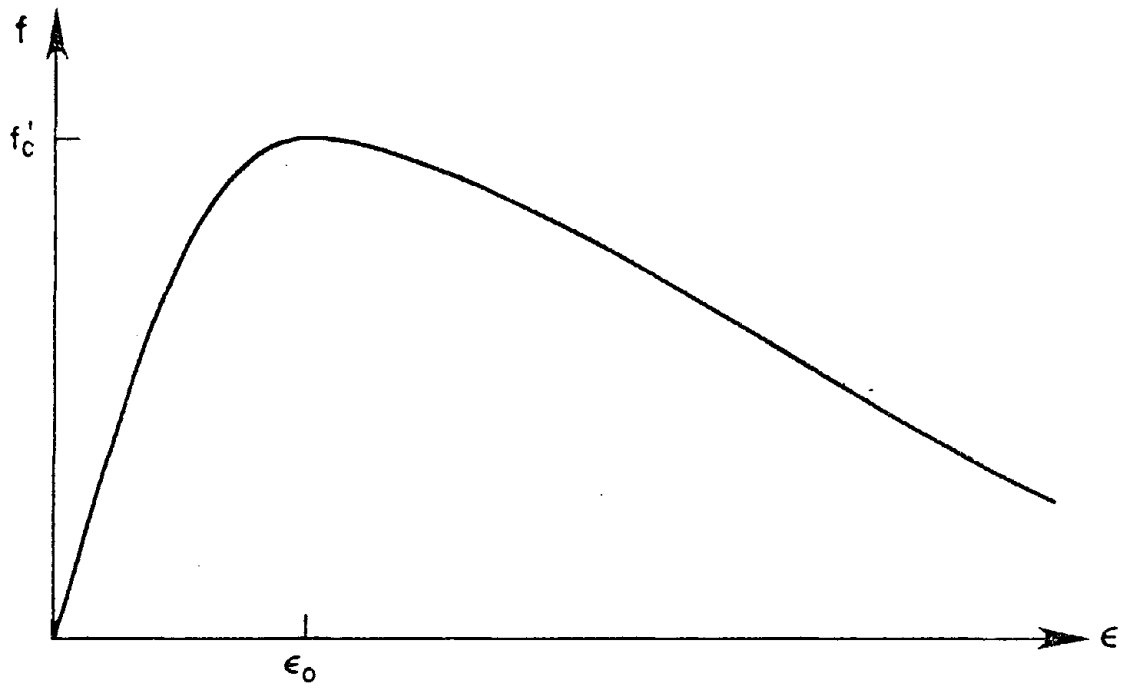

FIG. 5.1 - MONOTONIC STRESS-STRAIN CURVE FOR CONCRETE

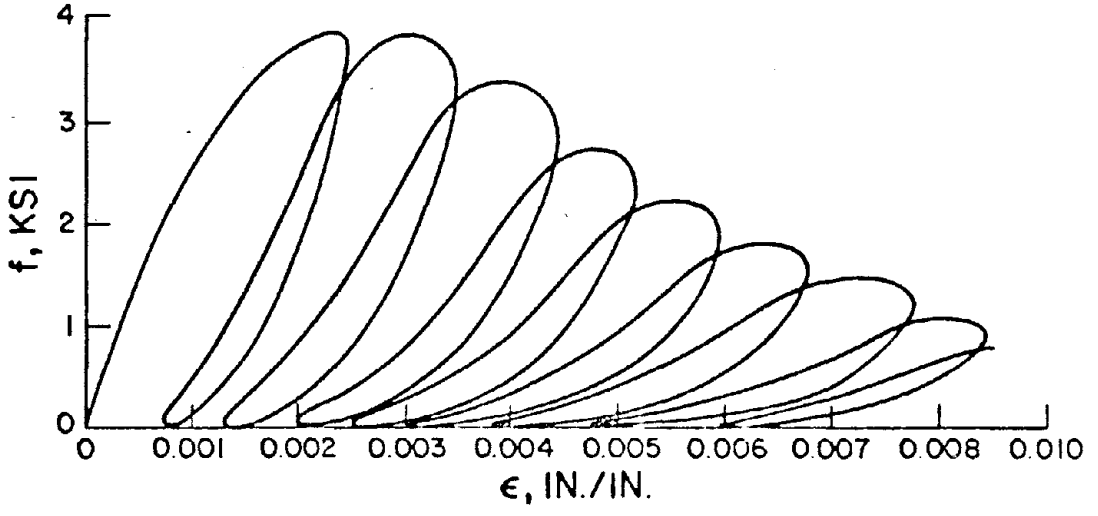

FIG. 5.2 - RESPONSE OF CONCRETE TO REPEATED LOADS

three regions. Initially, response is linear, then at 40%-60% of maximum stress, the tangent modulus starts to decrease and it continues to do so until the maximum stress is reached, after which the stress falls rapidly to zero. The physical effects which have the most important influence on this basic behavior pattern are:

(a) Concrete Composition. The design of the concrete mix controls the maximum stress, f'_c, which can be imposed. As the strength increases, the strain (ε_o) at which it is achieved decreases, and the slope of the descending part of the curve becomes steeper.

(b) Effect of Confinement. Concrete fails by propagation of internal microcracks [46]. Their growth can be inhibited by the application of lateral pressure to the specimen [47], which is generally provided by steel binders. However, unless the confining steel is prestressed, some transverse expansion of the concrete must take place in order to mobilize the confining pressure and, until it does, the axial strength of the concrete is not affected by the presence of the steel. At strains below ε_o the transverse expansion is so small that it is convenient to assume that the portion of the curve before the maximum stress is independent of the binding steel, whereas the unloading portion is totally dependent on it. Experiments support such an assumption. Park and Kent [20] discuss in detail the binding effectiveness of various hoop configurations. In a beam which undergoes significant inelastic deformation, most of the concrete is strained beyond ε_o, where the stress is determined almost entirely by the confining effect of the binders. Confinement, therefore, has more influence than anything else on the concrete behavior.

(c) Effect of Loading Rate. Both the maximum stress and the strain at which it occurs are sensitive to loading rate. A standard rate of

approximately 2 ksi/min is used for cylinders [48] so that comparisons between tests may be meaningful. Faster loading increases the maximum stress and reduces the corresponding strain, and vice versa [49]. If the model is to be used in dynamic analysis, the effective loading rates will be higher than those in Ref. [49], but the principle remains the same.

Little quantitative information is available on very high rates of loading, largely because the dynamic properties of the testing apparatus start to contaminate the results. Information on the rate-dependency of the unloading part of the curve for bound concrete is equally sparse. It is, therefore, assumed that the concrete properties are unaffected by the rate of loading.

(d) Influence of Strain Gradient. Opinions differ over the influence of a strain gradient across the cross section. Sturman, Shah and Winter [46] found that eccentrically loaded specimens failed at a 20% higher stress and a 50% higher strain than concentrically loaded ones. On the other hand, Hognestad, Hanson, and McHenry [50] and Karsan and Jirsa [51] found no differences. Barnard [52] suggested that the changes in behavior quoted by Winter affect the rotation capacity much more than the flexural strength and so are not very important in strength analysis. In the absence of conclusive evidence, we assume that a strain gradient has no influence.

(e) Behavior of Concrete Cover. Many investigators recognize that the concrete cover behaves differently from the concrete in the core of the beam, so they use separate equations to describe its response. It is not confined by the steel binders and so it displays stress-strain characteristics different from those of the concrete core. Under sufficiently severe loading, cracks form in the horizontal planes containing the top

and bottom reinforcement and eventually the cover physically breaks away from the beam. It obviously contributes nothing to the beam's flexural strength once this has happened. Since the cover has a greater lever arm and is subjected to a greater compressive strain than any other concrete element, it is in a sense the most critical; so it is unfortunate that the conditions which govern its spalling are not yet understood. Studies [15] have indicated that high cyclic stresses in the bars, thin cover, and closely spaced bars (which form a separating layer between the cover and the concrete core) all hasten the onset of spalling, but practically every model for cyclically loaded concrete contains a different assumption for the magnitude of strain at which spalling begins. Agrawal et al [27] do not consider the problem at all (with some justification, because their test beam had no stirrups and was reinforced with only one bar). Kent and Park [20] assume that spalling occurs at a compressive strain of .004 in/in. Ma [33] assumes that the cover can carry a small load even at very large strains, and Thompson [19] performed separate analyses with four different assumptions. The general consensus is that the load-carrying ability of the cover is reduced to nothing or some small value when the strain reaches about $2\varepsilon_o$. In this study we assume that both the cover and the core can sustain a stress of af'_c at infinitely large strains, as illustrated in Fig. 5.3. However, the stress in the cover drops from f'_c to this value at a strain (ε_c) which is lower than the comparable strain (ε_a) for the concrete core.

5.2.2 Behavior of Concrete Subjected to Repeated Loads

The stress-strain curves for concrete subjected to repeated loads all lie within an envelope for which the monotonic curve is a good approximation. Thus, all the factors which influence the shape of the monotonic

curve affect the cyclic curves as well. Inspection of the typical unloading and reloading curves shown in Fig. 5.2 reveals three main characteristics:

(1) Unloading and reloading follow nonlinear paths which together form a hysteresis loop.

(2) Both paths have about the same stiffness, which is a function of the strain at which the cyclic curve departs from the envelope.

(3) The reloading path crosses the unloading path at some point inside the envelope.

Karsan and Jirsa [51] developed a model which predicts accurately the response of plain concrete specimens subjected to many cycles of repeated load. However, it is too complicated for our purposes, and it fails to take into account the influence of tension cracks opening and closing. Ma's work indicates that the cracks become partially filled by small particles of finely ground concrete rubble and so some load can be transferred across them before they close fully. The reloading curves for the concrete in the beam will then differ from those in Fig. 5.2 and Karsan and Jirsa's expression will no longer be applicable. The definition adopted here for unloading and reloading paths is a simple one which includes the first two characteristics but not the third. It is explained in the next section.

5.3 Model Adopted for Concrete

The model adopted produces behavior as shown in Figs. 5.3 and 5.4 and is defined by the following rules. The sign convention used in the rules is that compressive stress and strain are both positive.

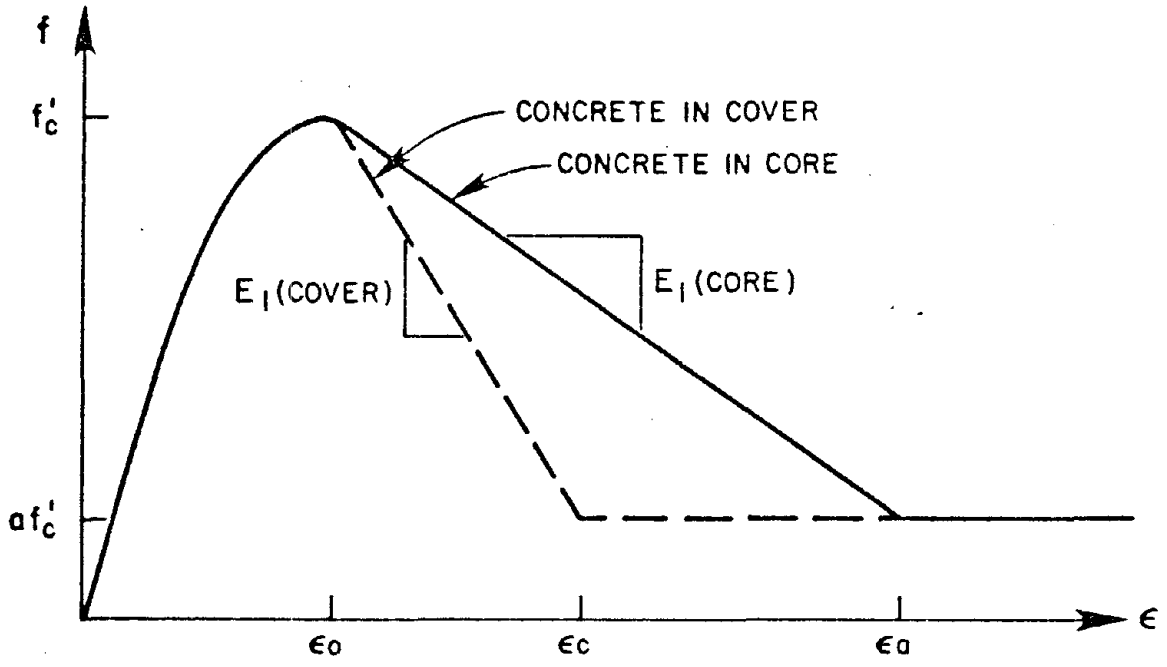

FIG. 5.3 - CONCRETE MODEL ENVELOPE DEFINITION

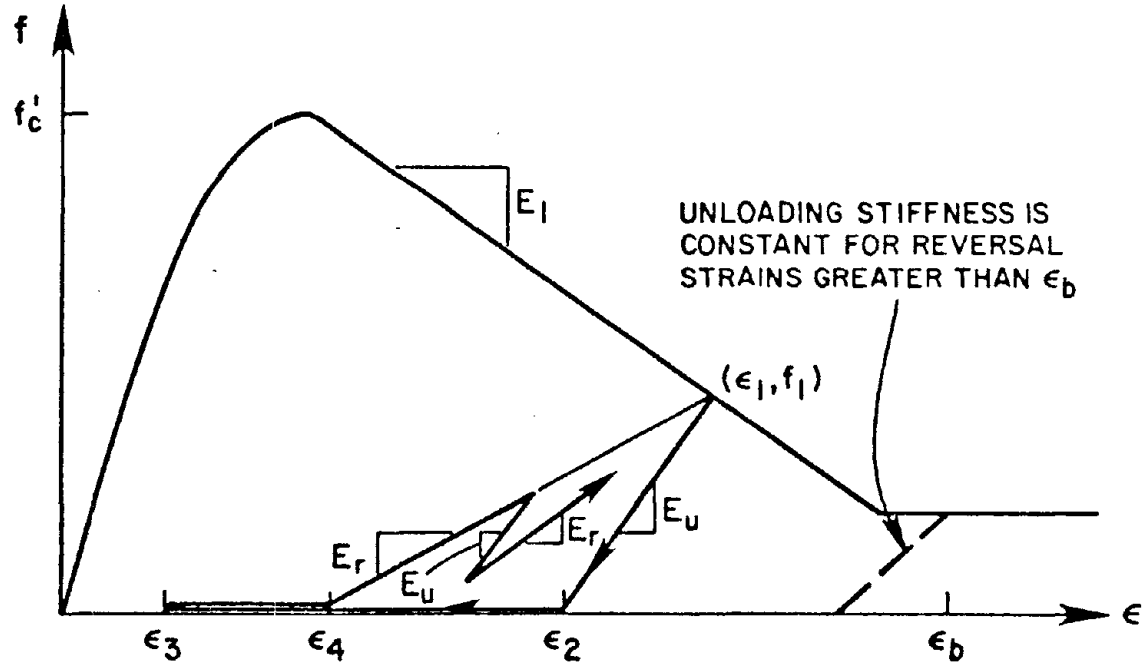

FIG. 5.4 - CONCRETE MODEL UNLOADING AND RELOADING

(1) All cyclic stress-strain curves are contained within an envelope which is taken to be the monotonic curve. The concrete is assumed to have no tensile strength.

(2) The envelope is made up of three regions in each of which it is governed by a separate equation:

$$f/f'_c = \varepsilon/\varepsilon_o\ (2 - \varepsilon/\varepsilon_o) \qquad 0 \le \varepsilon \le \varepsilon_o \qquad (5.1)$$

$$f = f'_c + E_1\ (\varepsilon - \varepsilon_o) \qquad \varepsilon_o \le \varepsilon \le \varepsilon_a \qquad (5.2)$$

$$f = af'_c \qquad \varepsilon_a \le \varepsilon \qquad (5.3)$$

The four parameters, f'_c, ε_o, ε_a, and a, are needed to define the envelope. E_1 is defined in terms of them as:

$$E_1 = f'_c\ \frac{a-1}{\varepsilon_a - \varepsilon_o} \qquad \text{for the confined core} \qquad (5.4)$$

$$E_1 = 2f'_c\ \frac{a-1}{\varepsilon_o} \qquad \text{for the cover} \qquad (5.5)$$

(3) Unloading and reloading are governed by stiffnesses E_u and E_r, and by strains ε_1, ε_2, ε_3, and ε_4. The meaning of each is illustrated in Fig. 5.4.

ε_1 and f_1 are the strain and stress at which the unloading curve departs from the envelope.

ε_2 is the strain at which the stress becomes zero.

ε_3 is the minimum (i.e., most tensile) strain reached during the unload-reload cycle.

ε_4 is the strain at which reloading starts.

(3a) Unloading from the envelope is defined by:

$$E_u = E_o (1 - b Z) \tag{5.6}$$

where

$$E_o = 2f'_c/\varepsilon_o \tag{5.7}$$

$$Z = \min (\varepsilon_1, \varepsilon_b)$$

b is a parameter which defines the rate at which the unloading stiffness decreases with increasing strain.

(3b) Unloading from a point inside the envelope takes place at a stiffness equal to the most recently calculated E_u.

(3c) If unloading stops before the stress has reached zero (Fig. 5.4), then reloading follows a straight line from the reversal point to (ε_1, f_1), the point of departure from the envelope.

Opening and closing of cracks both occur at zero stress. When the strain becomes less (i.e., more tensile) than ε_2, cracks open. In the absence of rubble, they would close again when the average strain returned to ε_2. If, however, rubble enters the cracks, compression will start to be transmitted at some strain ε_4 less than ε_2. So

$$\varepsilon_4 = \varepsilon_2 - r (\varepsilon_2 - \varepsilon_3) \tag{5.8}$$

and

$$E_r = \frac{f_1}{(\varepsilon_1 - \varepsilon_4)} \tag{5.9}$$

where

ε_4 = strain at which reloading starts

r = the proportion of the crack filled by rubble

If $(\varepsilon_2 - \varepsilon_3)$ is greater than a limiting value CMX, then $(\varepsilon_2 - \varepsilon_3)$ is replaced by CMX. Values of b, ε_b, r, and CMX are needed to define unloading and reloading. The complete concrete behavior is specified by the above set of rules and the numerical values of f'_c, ε_{co}, ε_a, ε_b, a, b, r, CMX. The program was arranged in such a way that each of these constants can be either established by system identification or given a fixed value.

A few points deserve further comment. First, many equations have been proposed [53] to define the first segment of the envelope. The main difference between them is the ratio between the initial tangent modulus, E_o, and the secant modulus, f'_c/ε_o. The ratio is a constant in almost all of the equations, although its value varies from one formulation to another. Equation (5.1) was selected because it is simple, the most commonly used, and it implies

$$E_o = 2f'_c/\varepsilon_o,$$

which agrees well with the results of tests on cylinders [33]. But for the purposes of this study, any other choice would probably have been equally suitable because the maximum deformations of the beams were large enough to strain some 85% of the concrete beyond ε_o, where the equation does not apply.

Second, no attempt is made to correlate the value of ε_a (or E_1) with the properties of the binding steel. To perform such a correlation using identification, we would need to include in the error function results from many tests each with different binding steel. This was considered to be outside the scope of the work, and instead the model was set up in such a way that the slope E_1 of the second segment could be varied and the

optimum value found for the experimental results in question. The initial value of E_1 was calculated from Kent and Park's formula [20].

Chapter 6

ANALYTICAL MODEL FOR BOND-SLIP

6.1 Introduction

This chapter concerns the bond-slip model which was incorporated into the global model for the reinforced concrete section.

A layered system with separate constitutive relationships for steel and concrete was chosen for the global model in the interests of accuracy, but at the price of considerable complexity. In order to prevent the model's becoming so cumbersome as to be unusable, efforts must be made to avoid the addition of further complications unless they are essential to the central purpose. We hoped that by selecting a sophisticated model form good results could be obtained without the refinement of an explicit allowance for bond-slip. As will be seen in Chapter 9, this was not to be the case.

The first theoretical moment-curvature relations were derived for beams R4 and T2, and they show that if perfect bond is assumed between steel and concrete, the model predicts the moments in the first positive half-cycle of loading well; but at the beginning of the ensuing half-cycle of negative moments, the theoretical values are too large and the model is too stiff. During this part of the load history, the concrete is cracked from top to bottom and is therefore in a state of zero stress, so the applied moment is carried by the steel couple alone. Since the theoretically derived moments do not agree with the experimentally observed ones, either the constitutive relation for steel or the assumed steel strains are incorrect. The latter explanation seems the more likely.

The steel strains are derived from the rotation of the yoke relative

to the face of the anchor block. This rotation contains one component which is due to the integral of the curvature along the relevant length of the beam, and another due to the end rotation of the beam caused by the bars pulling out of the anchor block. Ma allowed for this latter component either by using the measured value of fixed-end rotation (beams T2 and T3) or by estimating its value from other measurements. However, no allowance was made for the slipping of the bars in the cantilever itself, and the bond-slip relation described in Section 6.4 was introduced to overcome the deficiency.

6.2 The Nature of the Problem

There are many physical mechanisms concealed behind the generic term "bond-slip." Most of them are complicated and few are well understood. The present state of knowledge, though advancing rapidly, is too poor to include them all explicitly; but even if this were possible, the resulting equations relating bond stress to bar slip would be so complicated as to be virtually unusable. We therefore resort to a practice common in reinforced concrete engineering, namely that of observing the overall physical behavior and then using an empirical expression to describe it. In this section, in spite of this intent, we consider the physical behavior.

Bond is the name given to those shearing stresses which transfer axial load from a reinforcing bar to the concrete surrounding it. They may be true stresses uniformly distributed over the surface of the bar (for example, the chemical adherence of concrete to a smooth bar) or equivalent shear stresses, as in the case of a deformed bar whose bond

resistance is developed almost entirely by local bearing forces between the concrete and the surface deformations (lugs) on the bar. Slip is the axial displacement of the bar relative to the surrounding concrete.

Bond stresses are important in two different situations. The first is at mid-span of a beam where the shear is small and the moment is almost constant. The tension in the steel might be expected to be constant, but it is not, because the concrete surrounding the bars also undergoes extension, and cracks as shown in Fig. 6.1a. At each crack, the whole tensile force is carried by the steel, but between cracks bond stresses transmit some of the load to the concrete, thus reducing the tension in the steel. Typical bond and steel stress distributions are shown in Figs. 6.1b and 6.1c. Bond forces are important in this context because they are transferred by the bar lugs bearing on the surrounding concrete. But these bearing forces also have a radial component which tends to split the concrete away from the bars. If the beam is loaded cyclically, the direction of the forces alternates but the radial component is always outwards, and so the concrete cover tends to spall off to the obvious detriment of the beam's performance.

Bond stresses must also be considered wherever bars are anchored by embedding them in concrete, and this is the case which concerns us here. The beam-column joints of reinforced concrete frames are examples which have received much attention, because slipping of the beam bars at the joint contributes significantly to the stiffness degradation of the frame under cyclic load. Most of the experimental work for this latter case has been done either on some form of cantilever specimen [13,54,55] or, in cases where an effort was made to isolate the bond behavior, on pull-out specimens [16,56,57]. The usefulness of the results

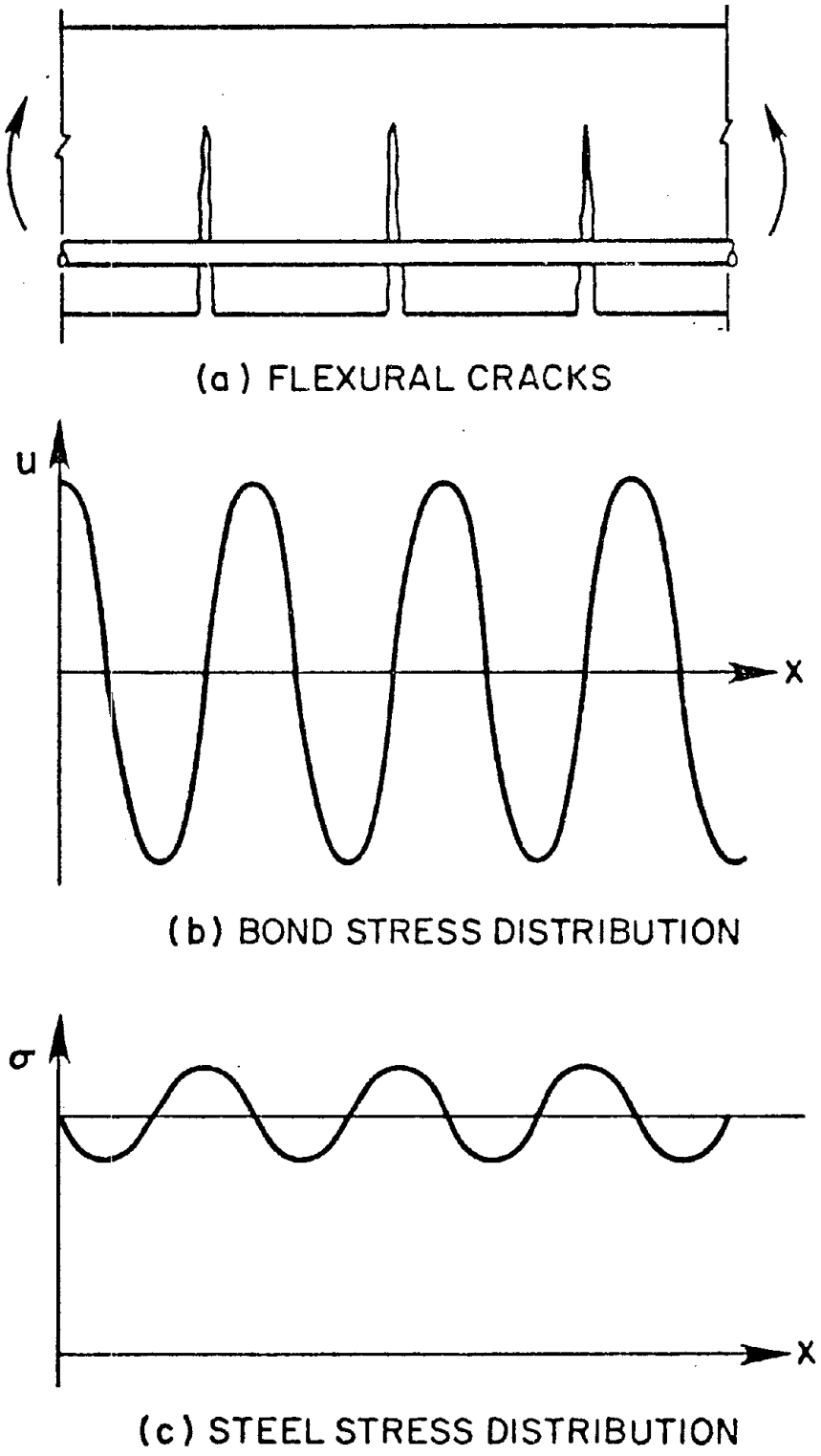

FIG. 6.1(a-c) - STRESS AND CRACK DISTRIBUTION IN A REINFORCED CONCRETE MEMBER

varies because, as Hassan and Hawkins [57] point out, care must be taken to reproduce in the specimen the boundary conditions found in practice if the test results are to be meaningful. Their analytical work with that of Viwathanatepa [16] is useful in understanding the mechanisms which act in a pull-out specimen.

Consider the bond behavior of a deformed bar embedded in concrete and subjected to monotonic tension. Figs. 6.2a-d show qualitatively the distribution of bond stress along the bar as the load is increased from zero to failure. At very low loads (below about 2 ksi axial stress) the mechanism is essentially elastic, and the tensile stress in the bar decays smoothly to zero at its far end (Fig. 6.2b). Hassan and Hawkins assumed an exponential distribution

$$\sigma(x) = \sigma_o \exp\left\{-\frac{4x}{L-x}\right\} \tag{6.1}$$

Stanton [58] developed a closed-form solution under modest simplifying assumptions for a bar embedded in a cylinder of concrete

$$\sigma(x) = \sigma_o \frac{\sinh cL\,(1-x/L)}{\sinh cL} \tag{6.2}$$

which implies a bond stress distribution

$$u(x) = \frac{cr}{2}\,\sigma(x)\,\tanh cL \tag{6.3}$$

where

$$c = \frac{1}{r}\sqrt{\frac{2G_c}{E_s \ln (R/r)}}$$

and

G_c = shear modulus of concrete

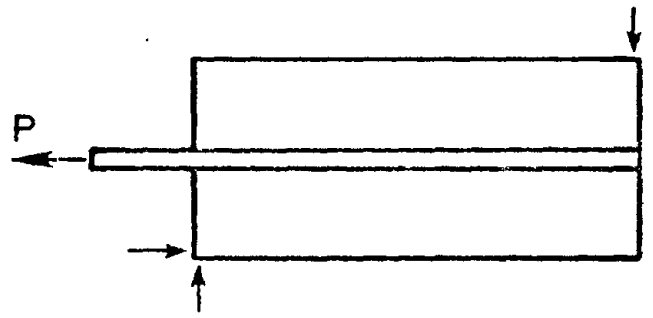

(a) PULL-OUT SPECIMEN

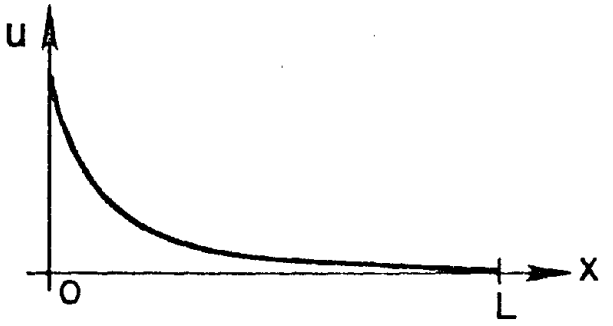

(b) BOND STRESS AT LOW LOAD

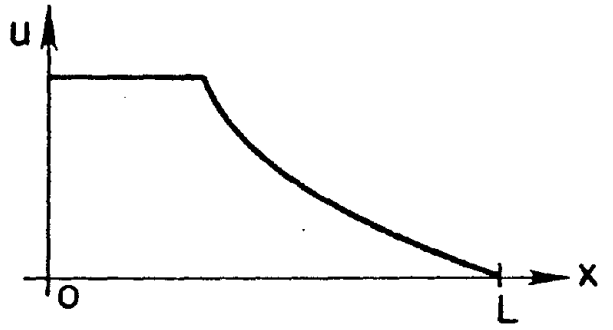

(c) BOND STRESS AT MODERATE LOAD

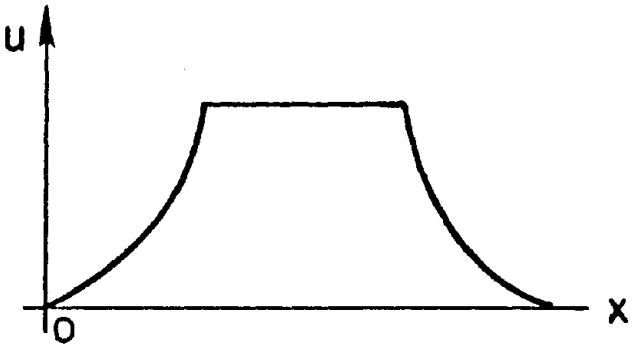

(d) BOND STRESS AT HIGH LOAD

FIG. 6.2(a-d) - BOND STRESS IN A PULL-OUT SPECIMEN

E_s = Young's modulus of steel

R = radius of concrete cylinder

r = bar radius

L = bar length

x = distance along the bar

The dimensions of Hassan and Hawkin's specimen give $cL \doteq 4$ in equations (6.2) and (6.3), so the two distributions are the same at the loaded end, after which equation (6.1) decays more rapidly. However, the differences are unimportant because the elastic region contributes so little to the total bond resistance.

The principal stresses in the concrete radiate diagonally from the bar as shown in Fig. 6.3. When the tensile strength of the concrete is exceeded, cracks form and, as the load increases further, they propagate until the damage caused by them and the local concrete crushing at the bar lugs prevents the boundary layer from carrying any higher level of bond stress. The bar then starts to slip and the bond stress along the cracked length is approximately constant. The distribution of bond stress then resembles that shown in Fig. 6.2c.

As the load increases further, so does the damage to the concrete. Eventually the bar yields at its loaded end and it undergoes inelastic deformations large enough to destroy the boundary layer locally, and so the bond stresses over the yield length are reduced to zero. Indeed, this must be the case for equilibrium to be satisfied. If the bar does not possess a sharp yield point, the bond stresses are reduced to some small value instead of zero. Their approximate distribution is shown in Fig. 6.2d. This last stage of loading is frequently accompanied by

the spalling of a cone of concrete around the bar at its loaded end (see Fig. 6.4).

Propagation of the cracks is inhibited by the presence of stirrup ties in the concrete, or by generous cover (3 in.-4 in. or more) to the bar. Thin cover which is not tied spalls off at an early stage of loading and significantly reduces the pull-out strength of the bar.

Bars loaded monotonically in compression perform much better than those in tension, primarily because:

1. Some load can be taken in bearing on the end of the bar.
2. The concrete at the loaded end of the bar does not spall as it does in tension. This allows very large bond stresses to build up close to the loaded end of the bar. Popov [59] quotes an extreme case of their reaching 8000 psi.
3. The Poisson effect causes the bar to expand laterally, improving any adhesion between steel and concrete. This last is probably the least important of the three effects.

Under cyclic load the mechanism differs in one important respect. Once the response becomes nonlinear, conical cracks, similar to the pattern observed under monotonic load, open up in each direction. They cross each other, as shown in Fig. 6.5, thus breaking the boundary layer into individual particles of rubble. After several cycles of load, the rubble is so crushed and ground that it can no longer transmit any bond stress, and the bar slips through it with almost no resistance. The slip is only halted when the lugs come to bear on concrete which has not yet been ground into rubble. However, even this concrete will have undergone some damage, and so it will be destroyed by crushing and cracking more readily then if it had been in its virgin state. The bar

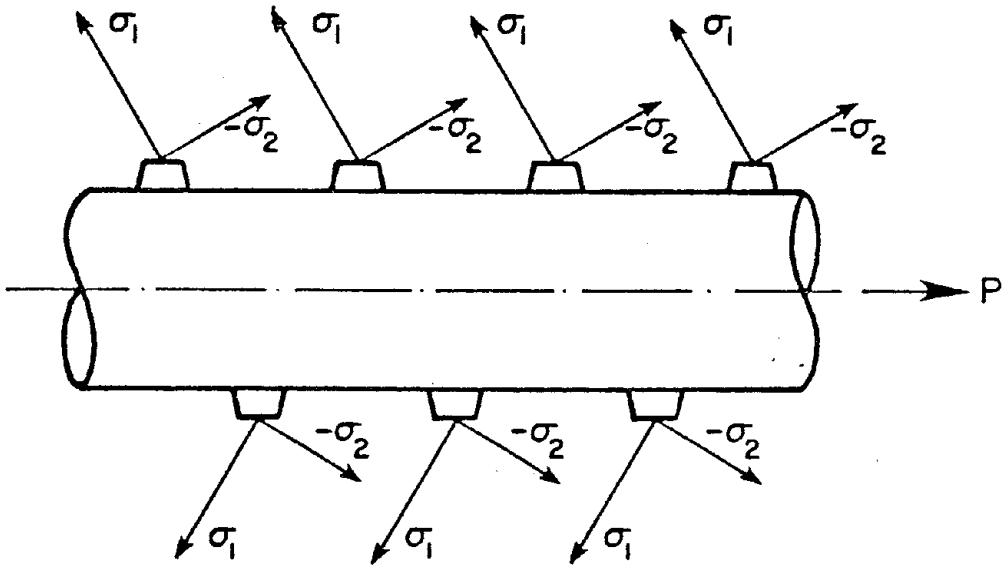

FIG. 6.3 - PRINCIPAL STRESS IN CONCRETE

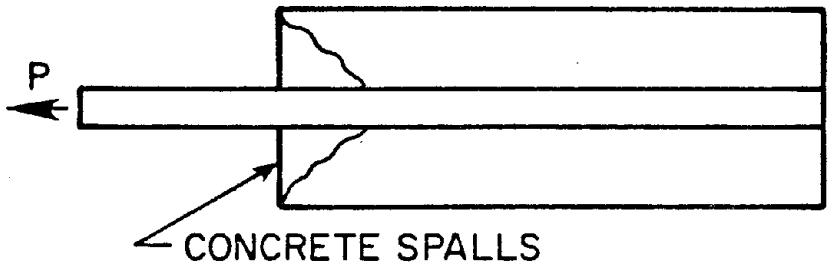

FIG. 6.4 - SPALLING OF CONCRETE IN PULL-OUT SPECIMEN

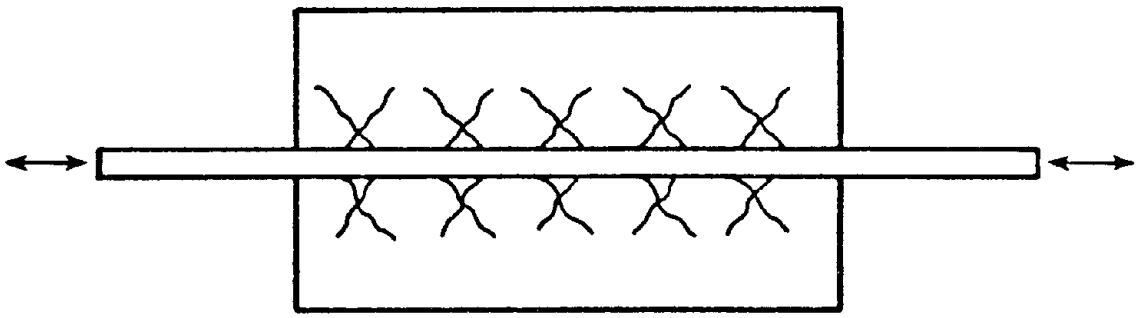

FIG. 6.5 - DIAGONAL CRACKS UNDER CYCLIC LOAD

thus displays a reduced stiffness.

This physical description is a necessarily simplified view of a complicated series of events. However, it is in agreement with two of the most commonly reported facets of bond behavior, namely

1. Several cycles at high load drastically reduce the stiffness displayed in subsequent cycles at low load.
2. Repeated cycles at the same load do not significantly change the maximum slip.

The second of these assertions appears to be true only at low levels of slip. At higher levels Viwathanatepa's results [16] show that the stress amplitude falls off markedly with cycling if the specimen is loaded between constant slip limits.

For this idealized behavior, the relationship between slip and bar force at the loaded end can be divided into three separate ranges, which are shown in Fig. 6.6.

The first (A) represents free slipping of the bar through the crushed rubble. The stiffness is negligible, and the nominal resistance is provided by friction.

The second (B) shows the response when the lugs on the bar meet the unbroken concrete and subsequently crack and grind it into rubble.

The third (C) is an elastic unloading of the system.

The length of the free slip in A, the stiffness and peak resistance in B, and the unloading stiffness in C may all be expected to vary with the amount of damage that the concrete boundary layer has suffered. Typical results from Viwathanatepa's work are reproduced in Fig. 6.7, and the idealization can be seen to be in general agreement with them.

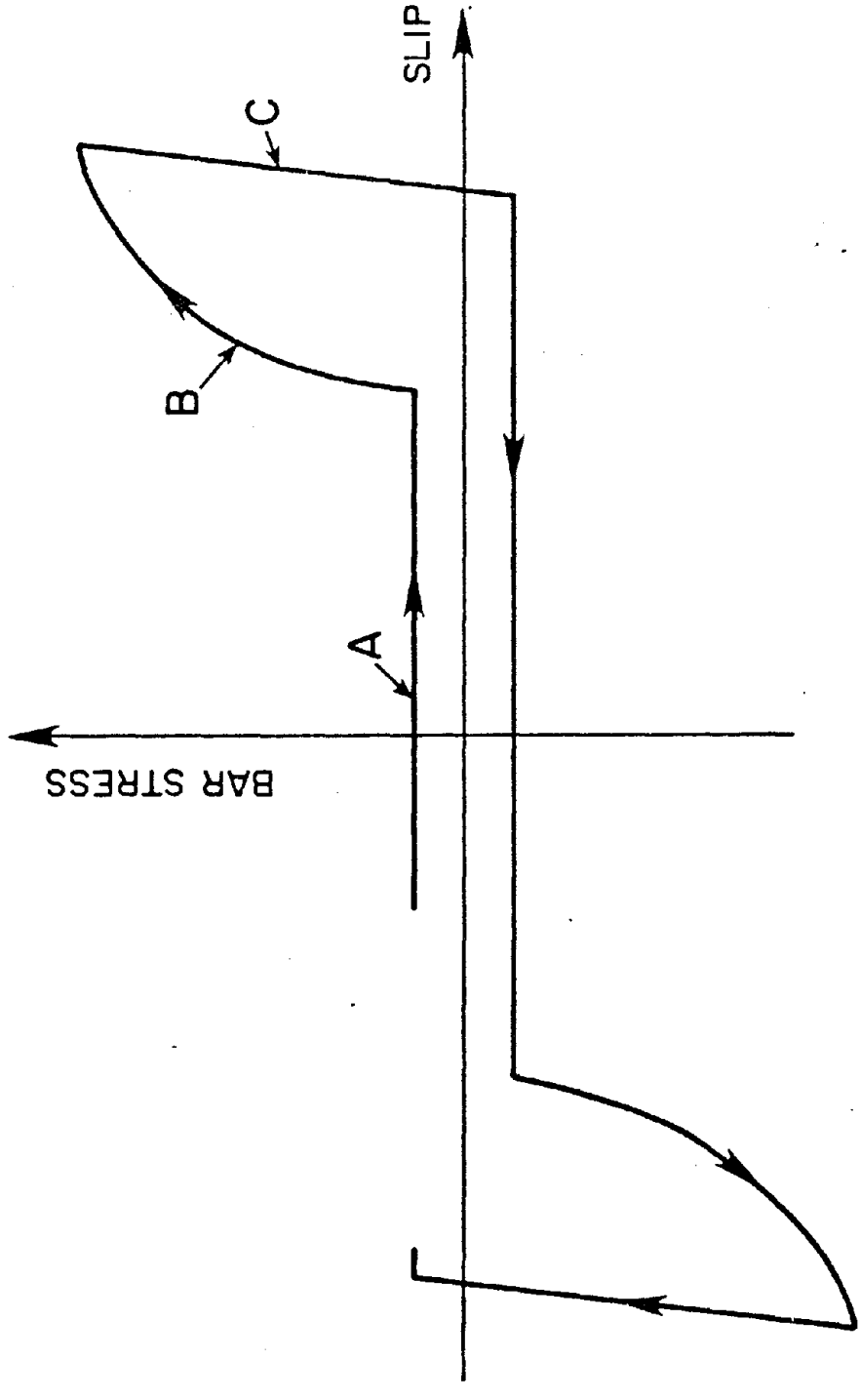

FIG. 6.6 - IDEALIZED BOND-SLIP BEHAVIOR

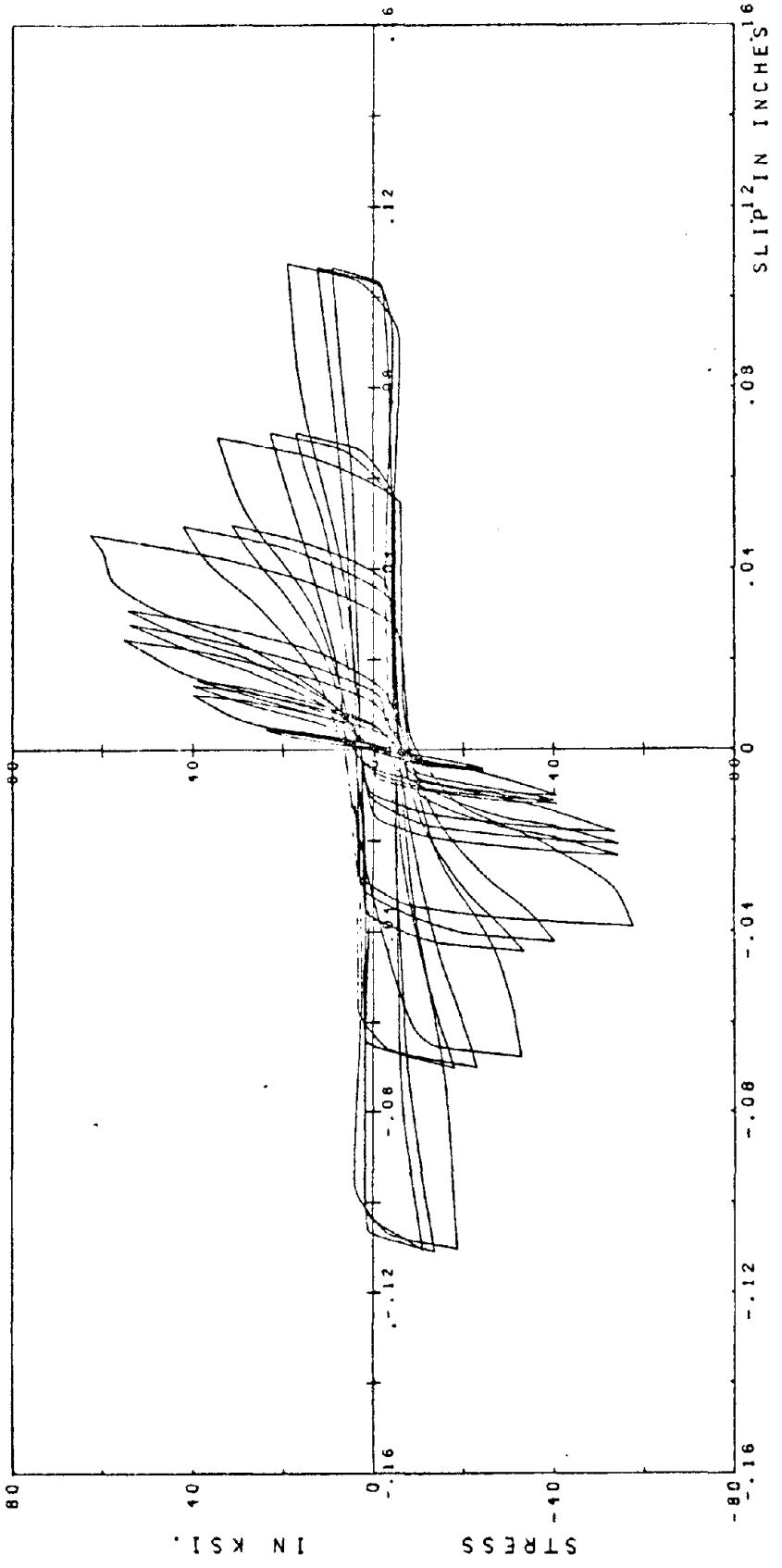

FIG. 6.7 - EXPERIMENTAL BOND-SLIP BEHAVIOR

Although we have a global understanding of the bond-slip mechanism, many details still require further study. One particularly pressing need is to establish the nature and extent of the interaction between the yielding of the bar and the larger slips which accompany it. Without the benefit of further research, we will have to continue to rely on empirical relations such as the one proposed in Section 6.4. They can give us numbers for use in calculations, but they can do little for our understanding of the true behavior.

6.3 Incorporation of Bond-Slip into the Global Model

The bond-slip model is described in Section 6.4. It relates bar stress to slip, measured relative to the appropriate concrete face, which in this case is the end face of the beam in contact with the anchorage block.

Bond-slip is included in the global model by assuming that, at the level of the reinforcing bars, the displacement of the yoke relative to the anchorage block is composed of three parts, namely the extension of the steel over the 7-in. gage length, the slip of the bar in the beam, and the pull-out of the bar from the anchorage block. Ma's values for average curvature have already been purged of this last component, so average strain values calculated from them will contain only the first two components. The bond-slip relation and the constitutive law for steel are then used to find the steel strain which simultaneously satisfies equilibrium

$$\sigma_{(\text{steel strain})} = \sigma_{(\text{bond slip})}$$

and compatibility

$$\delta_{(\text{steel strain})} + \delta_{(\text{bond slip})} = \delta_{(\text{total})}$$

The problem is nonlinear and must be solved by iteration. This is unfortunate because it adds an extra level of iteration to a problem which is already complicated enough. The incorporation of the bond-slip model roughly doubles the computer time requirements.

6.4 Model Adopted to Describe Bond-Slip Behavior

The model must have a form capable of reproducing the sort of behavior illustrated in Fig. 6.8 and is to express bar stress as a function of slip. The formulation proposed here has eleven parameters, and either singly or in groups of two or three, they represent separate geometric properties of the model and are related to some physical property of the steel or concrete. The rules which define the bond-slip behavior are introduced in what follows, and the meaning of many of the parameters can be seen in Fig. 6.8. The bar stress is designated by σ and the slip by d.

1. Segment A of the curve (see Figs. 6.6 and 6.7) is described by $\sigma = \sigma_F$ = constant, $d < d_2$ and increasing.

This is a region of "free slip" where the slip increases at a constant (small) bar stress. It represents the bar's being pulled through a distance d_2 of crushed rubble before the lugs come to bear on undamaged concrete.

2. If the slip exceeds d_2, the lugs are in contact with undamaged concrete.

The curves in Fig. 6.7 show that any increase in slip beyond this point consists approximately of an elastic and an inelastic component joined by a rounded transition. Menegotto and Pinto's equation is ideal for describing such a curve and consequently is used. It is

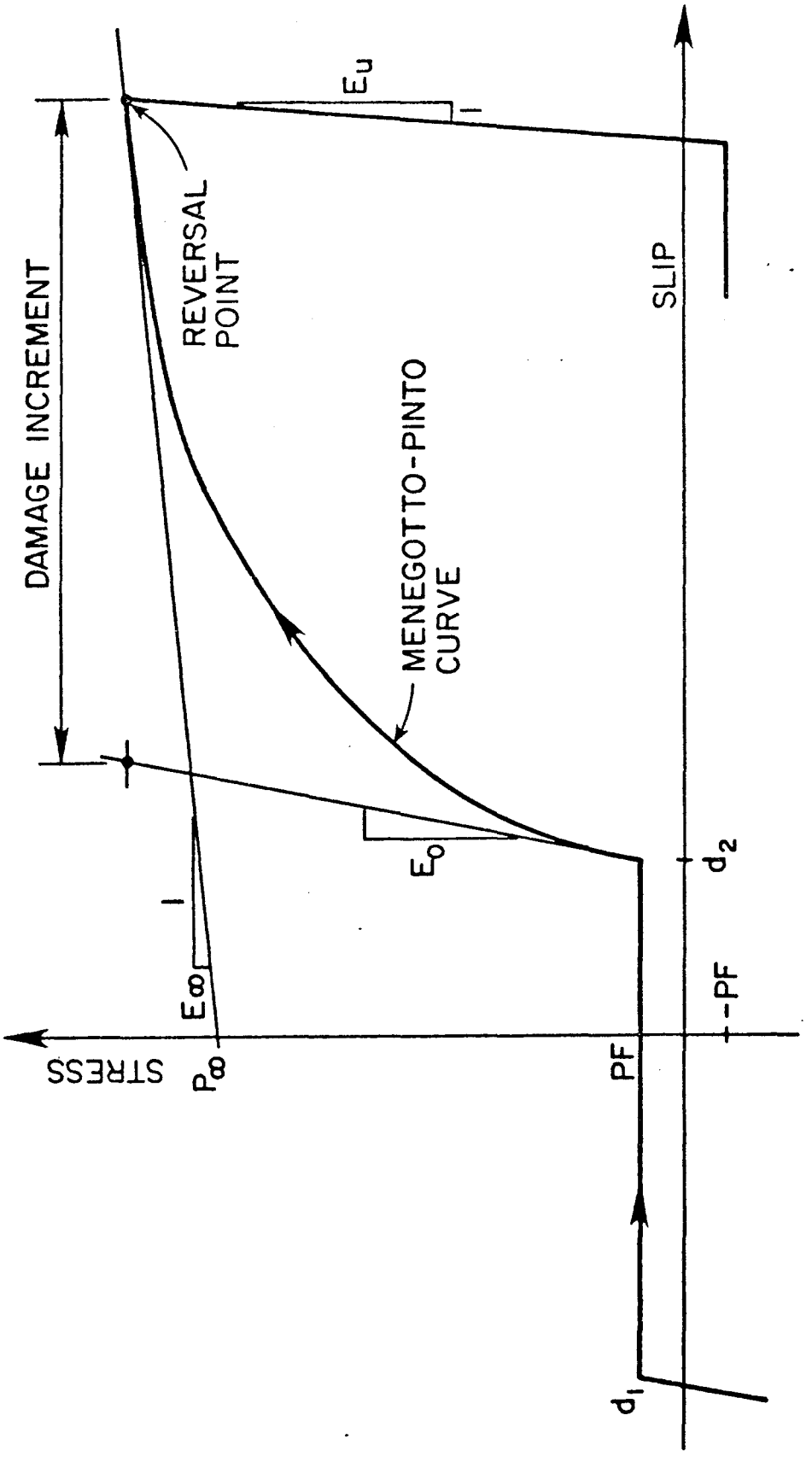

FIG. 6.8 - BOND-SLIP MODEL

$$\sigma^* = bd^* + \frac{(1-b)d^*}{(1+d^{*R})^{1/R}} \qquad (6.4)$$

where

$$\sigma^* = \frac{\sigma-\sigma_F}{\sigma_0} \qquad \varepsilon^* = \left(\frac{d-d_F}{\sigma_0}\right)\Xi_0$$

$$\sigma_0 = (\sigma_\infty - \sigma_F + E_\infty \cdot d_2)/(1 - b)$$

$$b = E_\infty/E_0 \qquad \text{and} \qquad R = r\,\sigma_0$$

The geometric interpretation of each variable is illustrated in Fig. 6.8. The subscript F stands for friction, because the resisting force in that segment of the curve has the appearance of friction. Note that we use Menegotto and Pinto's original formulation, with a straight line final asymptote, rather than the modified version used for the steel model which permitted arbitrary definition of the asymptote.

3. Unloading is defined by

$$(\sigma - \sigma_r) = E_u\,(d - d_r), \quad \sigma \geq -\sigma_F$$

where d_r and σ_r are the slip and stress at the reversal point.

4. The values of E_0, E_∞, E_u, d_2, σ_∞, σ_F, and r are needed to define the behavior.

The experimental results (Fig. 6.7) indicate that E_0, E_∞, d_2, and σ_∞ should vary with cycling, and so they are made functions of the damage to the concrete boundary layer. In the interests of simplicity, E_u and r are kept constant. The damage is measured independently in compression and tension and is equal to the cumulative sum of the inelastic parts of

all the Menegotto-Pinto curves in the appropriate direction. It is re-evaluated at each reversal point and then held constant throughout the ensuing half cycle of load. E_0, E_∞, d_2, and σ_∞ are calculated as functions of DAM, the damage, each time its value is updated, using the functional relationships given in Table 6.1. The relationships contain eight coefficients x_2, x_3, x_5-x_8, x_{10}, x_{11}, which, with σ_F, E_u, and r (renamed x_1, x_4, and x_9) make up the eleven parameters of the system whose values are to be found by identification.

This particular definition of damage is selected because it is in some sense a measure of the physical crushing of the concrete boundary layer. The functional relationships in Table 6.1 were chosen purely for their ability to match typical experimental results, without recourse to physical reasoning.

6.5 Appraisal of the Bond-Slip Model

We felt that the bond-slip model needed careful, separate review before it is incorporated into the global model. The form of the model and the values of its parameters are studied independently, although in both cases the appraisal is based on a comparison of the model's predictions with the results of appropriate experiments.

The objective of the first study is to find out if the model can reproduce experimental bond-slip curves with reasonable accuracy. The results from Viwathanatepa's tests on a #6 bar were used and are shown in Fig. 6.7. System Identification requires data in numerical form so the curve must be digitized by reading the coordinates of a number of points along its length. Since the values of the parameters $E_u(x_4)$ and $PF(x_1)$ can be read directly from the graph, and do not need to be

$PF = x(1)$

$d_2 = x(6) * DAM$

$E_o = x(10) * \exp\{-DAM * x(11)\}$

$E_\infty = x(5) * \exp\{-DAM * x(7)\}$

$E_u = x(4)$

$P_\infty = x(2) * \exp\{-DAM * x(8)\}$ tension

$P_\infty = x(3) * \exp\{-DAM * x(8)\}$ compression

$r = x(9)$

TABLE 6.1

DEPENDENCE OF BOND-SLIP PARAMETERS ON DAMAGE

established by identification, all of the points were located on the parts of the curve described by the Menegotto-Pinto equation. This choice permits identification of all of the unknown parameters with the minimum amount of data. Such efficient use of data is important because the whole curve consists of many load cycles, all of which must be included if the parameters governing the decay in strength and stiffness are to be found.

The best values of the coefficients x_1 - x_{11} were obtained by identification and are given in Table 6.2. The experimental and best theoretical curves are plotted together in Fig. 6.9, which shows that the model is well able to match the general trend of decay in bond resistance. However, the detailed shape of each individual half loop is not matched perfectly, particularly in the first few cycles of the test. Despite such discrepancy, the response of the model appears good enough to provide hope for a significant improvement in the performance of the global model. The values of the coefficients given in Table 6.2 will be used as initial estimates for the parameters in the bond-slip model when it is incorporated into the global model.

In the second study the relative sensitivity of the error function to changes in each parameter x_1 - x_{11} is determined. The motivation for this is to cut down the number of parameters to be established by identification in the global model. The values of the parameters may be expected to vary from one reinforcing bar size to another; and since the reinforced concrete beams contained up to three different bar sizes, thirty-three more parameters would be added to the eight already existing in the global model. The identification program is so arranged that each parameter can either be left free to be adjusted by the minimization

$x_1 = 5.0$	$x_5 = 3.84$	$x_9 = 0.05$
$x_2 = 46.92$	$x_6 = 0.267$	$x_{10} = 39.0$
$x_3 = 43.62$	$x_7 = 0.140$	$x_{11} = 0.136$
$x_4 = 39.3$	$x_8 = 0.037$	

TABLE 6.2

VALUES OF $x_1 - x_{11}$ OBTAINED BY IDENTIFICATION
FROM VIWATHANATEPA'S TEST

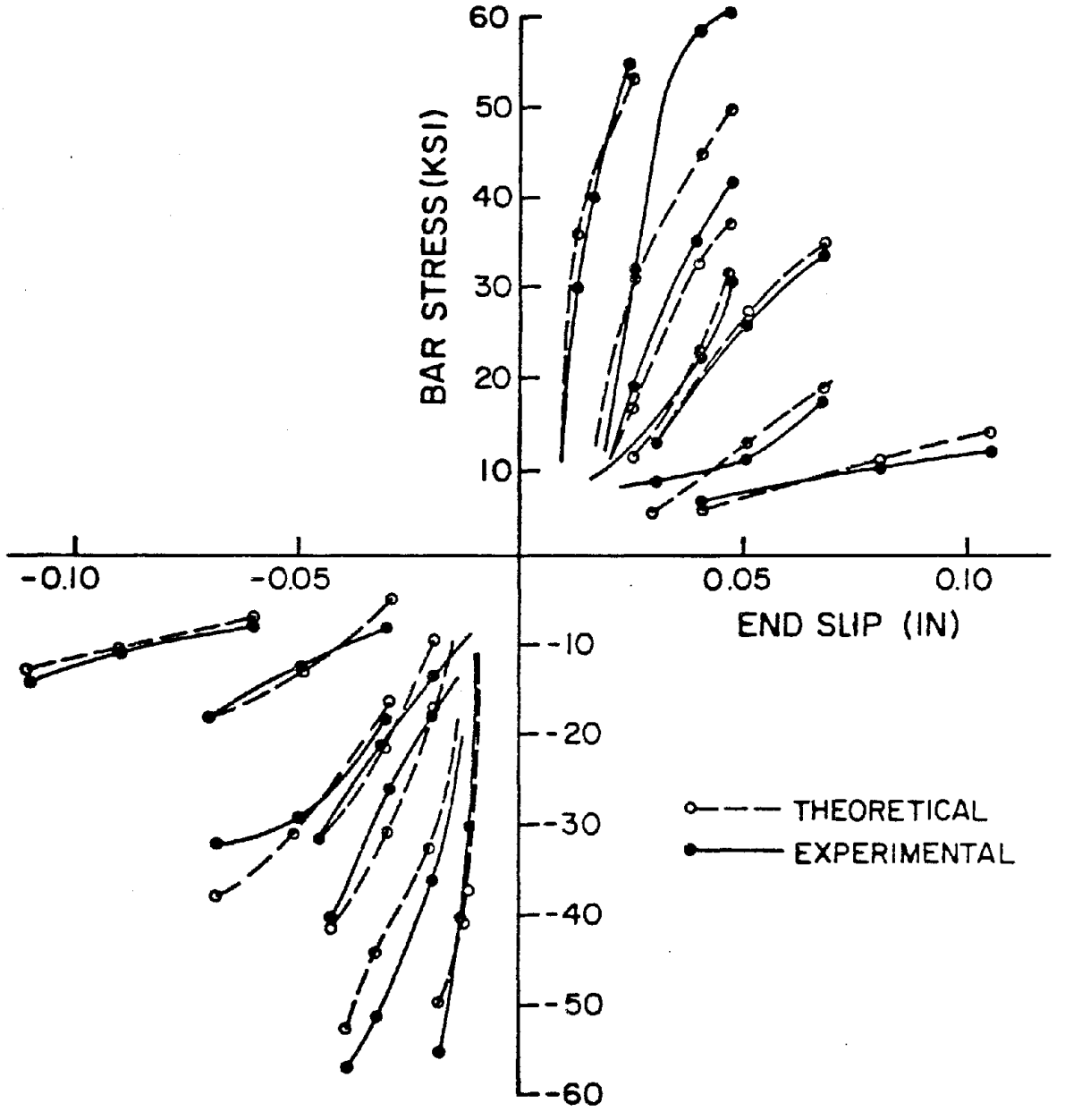

FIG. 6.9 - COMPARISON BETWEEN THEORETICAL AND EXPERIMENTAL BOND-SLIP CURVES

algorithm or it can be assigned a fixed value, so the existence of a large number of parameters does not in itself pose insuperable problems. However, it is still preferable to cut out as many of them as possible before attempting identification with the global model.

The parameters were varied separately and the error function was re-evaluated each time. In every case the error function changed sufficiently that none of the parameters could be cut out without detracting from the model's ability to reproduce the experimental results. On the one hand, this is encouraging because it indicates that the model is well formulated and that each parameter plays a useful role, but it is at the same time discouraging because such a large number of parameters are added to the global model. The error function proved most sensitive to x_6, which defines d_2, and to x_2 and x_8, which define P_∞. So the test at least established which parameters should be varied first in any attempt to fit the model to experimental results.

Chapter 7

INTEGRATION OF STRESSES OVER THE CROSS SECTION

7.1 General

The global model is designed to calculate the resisting moment of a reinforced concrete cross section which is subjected to a specified curvature and a specified axial load where one exists. The moment depends on the stress distribution across the cross section, which in turn depends on the strain distribution. For simplicity, this is assumed to be linear. Consequently the strain field can be completely defined by two variables, namely, its slope (which is the beam curvature, and is known) and either d_{NA}, the position of the neutral axis, or ε_g, the strain at the centroid of the section, neither of which is known. Recall that we are dealing with average strains (see Section 3.1) which spread out the discontinuous effects of the cracks in the concrete, so any assumption for strain distribution more complicated than linear is probably not justified.

The neutral axis position is found by satisfying axial force equilibrium. This is done most simply by treating the strain distribution as a function of ε_g rather than d_{NA}, because for small curvatures d_{NA} can vary over a very large range of values while the axial force changes only a little, and for zero curvature d_{NA} is indeterminate. This is not so for ε_g. Knowing the beam curvature and estimating ε_g, we can calculate the strains in each material layer and hence obtain the corresponding stresses. These are summed over the cross section to give a predicted axial force, which is then compared to the applied axial load. If the two are sufficiently close, the process stops; otherwise a new estimate of ε_g is made and the cycle of calculation is repeated.

If we define a function

$$F(\varepsilon_g) = P_{calc} - P_{app} \tag{7.1}$$

where

ε_g is the strain at the centroid

P_{calc} is the calculated axial load

P_{app} is the applied axial load

the problem reduces to one of finding the zero of a function of one variable. The function $F(\varepsilon_g)$ is nonlinear and so Equation (7.1) must be solved numerically and to some specified tolerance.

7.2 Method of Solution

A zero of a function is generally found in two stages. First, two points ε_1 and ε_2 must be found for which

$$F(\varepsilon_1) \cdot F(\varepsilon_2) < 0 \tag{7.2}$$

and then some form of interpolation is used to locate the ε_3, which gives

$$|F(\varepsilon_3)| < TOL \tag{7.3}$$

The first stage depends on the particular function, and any available insight into its behavior should be used to obtain suitable ε_1 and ε_2. The method used here is discussed in Section 7.2.2. The interpolation is discussed first in Section 7.2.1.

7.2.1 Interpolation

For the set of all real continuous functions, bisection is the optimum interpolation method because it is the fastest one which always works.

Unfortunately, the price of this security is that the method is slow. In general, $\log_2 \left(\frac{b-a}{\delta}\right)$ iterations are needed to locate ε within a tolerance δ on an interval [a,b]. If δ is 10^{-6} and the interval is [0,1], then 20 iterations are needed. Satisfaction of a tolerance on F rather than ε obviously depends on the local slope of the F-ε curve. Faster methods exist, but they all risk breaking down on poorly behaved functions. Brent [60] and Dekker [61] propose algorithms which combine a faster method (e.g. linear interpolation) with bisection in such a way as to reap the benefits of both. At best, they are much faster than bisection, and at worst, only a little slower.

The method used here is similar to theirs in its approach and combines parabolic interpolation with bisection in the following way. Suppose that we have three points, $\varepsilon_1 < \varepsilon_2 < \varepsilon_3$ such that either $f(\varepsilon_1)\cdot f(\varepsilon_2) < 0$ or $f(\varepsilon_2)\cdot f(\varepsilon_3) < 0$. Interpolation is then used to find a fourth point ε_4 which we hope will be better than any of ε_1, ε_2, and ε_3. The worst point of the four is then rejected, the other three renumbered, and the process repeated until the required tolerance is satisfied. Interpolation is parabolic unless one of the end points (ε_1 or ε_3) has been retained without change for the two consecutive steps, in which case bisection is used. In order to guarantee that ε_4 lies within $[\varepsilon_1, \varepsilon_3]$, the parabola must express stress as a function of strain and not the other way around. Also parabolic interpolation requires three starting points rather than the two implied by Equation (7.2), but if two are available which satisfy the equation, any point between them will suffice as a third. This combination of parabolic interpolation with bisection is referred to hereafter as "hybrid interpolation."

7.2.2 Method of Establishing First Points

The approach used is a modification of the one proposed by Ma [33]. The first change is to use ε_g and not d_{NA} as the independent variable, for reasons described in Section 7.1. Centroidal strains ε_1 and ε_2 are then chosen in such a way that the strains in the top and bottom steel respectively are the same as they were at the last curvature point (see Fig. 7.1). Then Equation (7.2) will be satisfied, point ε_3 found by bisection, and hybrid interpolation used thereafter.

While this method always provides an ε_1 and ε_2 to satisfy Equation (7.2), it suffers from the disadvantage that ε_1 and ε_2 form a very wide bracket to the solution. Experiment shows that a refinement of this basic method generally gives a better set of initial points $\bar{\varepsilon}_1$, $\bar{\varepsilon}_2$, and $\bar{\varepsilon}_3$. If ε_0 is the converged value from the last curvature point, and ε_1 and ε_2 are defined as before, $\bar{\varepsilon}_1$ and $\bar{\varepsilon}_2$ are the refined estimates of ε_1 and ε_2 where

$$\bar{\varepsilon}_1 = b\varepsilon_0 + (1-b)\varepsilon_1 \tag{7.4}$$

$$\bar{\varepsilon}_2 = b\varepsilon_0 + (1-b)\varepsilon_2 \tag{7.5}$$

b is a coefficient selected by the user such that $0 < b < 1$. (7.6)

Strain distributions for b = 0.5 are shown in Fig. 7.2.

If $F(\bar{\varepsilon}_1) \cdot F(\bar{\varepsilon}_2) < 0$, $\bar{\varepsilon}_3$ is found by bisection. Otherwise, $\bar{\varepsilon}_3$ is set equal to ε_1 or ε_2, whichever is appropriate. This ensures that $\bar{\varepsilon}_1$, $\bar{\varepsilon}_2$, and $\bar{\varepsilon}_3$ bracket the required solution. Hybrid interpolation is used thereafter. If b is 0.0, the refinement reduces to the basic method. And, if it is 1.0, $\bar{\varepsilon}_1$ and $\bar{\varepsilon}_2$ are the same and there is no way of telling whether $\bar{\varepsilon}_3$ should be equal to ε_1 or ε_2. Thus the inequality (7.6) must be strictly

adhered to. A number of trials with different values of b were conducted, and 0.5 was selected as giving the best results. The advantage of the refinement is that it provides a bracket to the solution which is one-half or three-quarters as wide as that given by the basic method while using the same number (three) of function evaluations.

7.3 Problems

The shape of the F-ε curve was unexpected, and it appears to control the minimum number of material layers that can be used. It is also such that hybrid interpolation, rather than pure linear or parabolic interpolation, is a necessity for fast convergence. Typical shapes for the curve, with different numbers of concrete layers, are shown in Fig. 7.2. It can be seen that the effect of using layers (or elements) of finite thickness is to superimpose ripples on the smooth curve which would be the result of using an infinite number of layers. The ripples become larger as the number of elements decreases. Furthermore, the zero of the rippled function occurs at a different ε value to that of the smooth one. Consequently, a false position is predicted for ε_g and the bending moment is inaccurate. If the elements are too large, the function may even possess multiple roots, and the hybrid interpolation will converge to any one of them depending on the initial three points. This is clearly undesirable, and the condition that the function has a single root provides a criterion for a minimum number of layers. Trial and error shows that at least 20 are needed in the present analysis. A more restrictive criterion is that the error in the bending moment calculation should be less than some preset amount. (The error here refers to the difference between calculated moment values using a finite and an infinite number of elements. It was

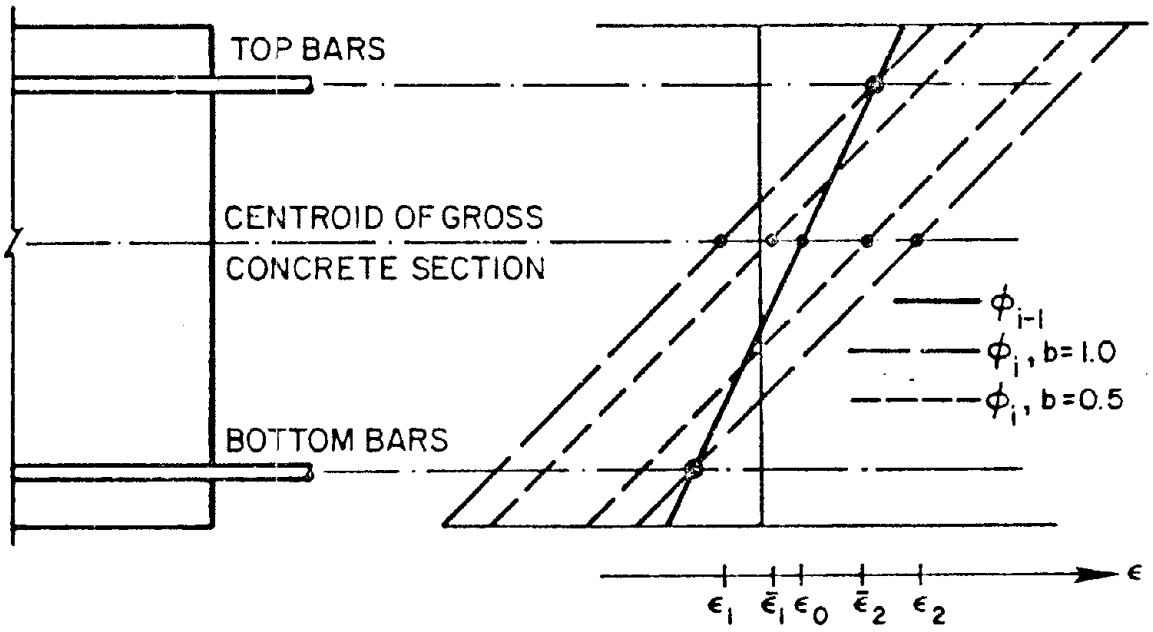

FIG. 7.1 - INITIAL ESTIMATE OF CENTROIDAL STRAIN

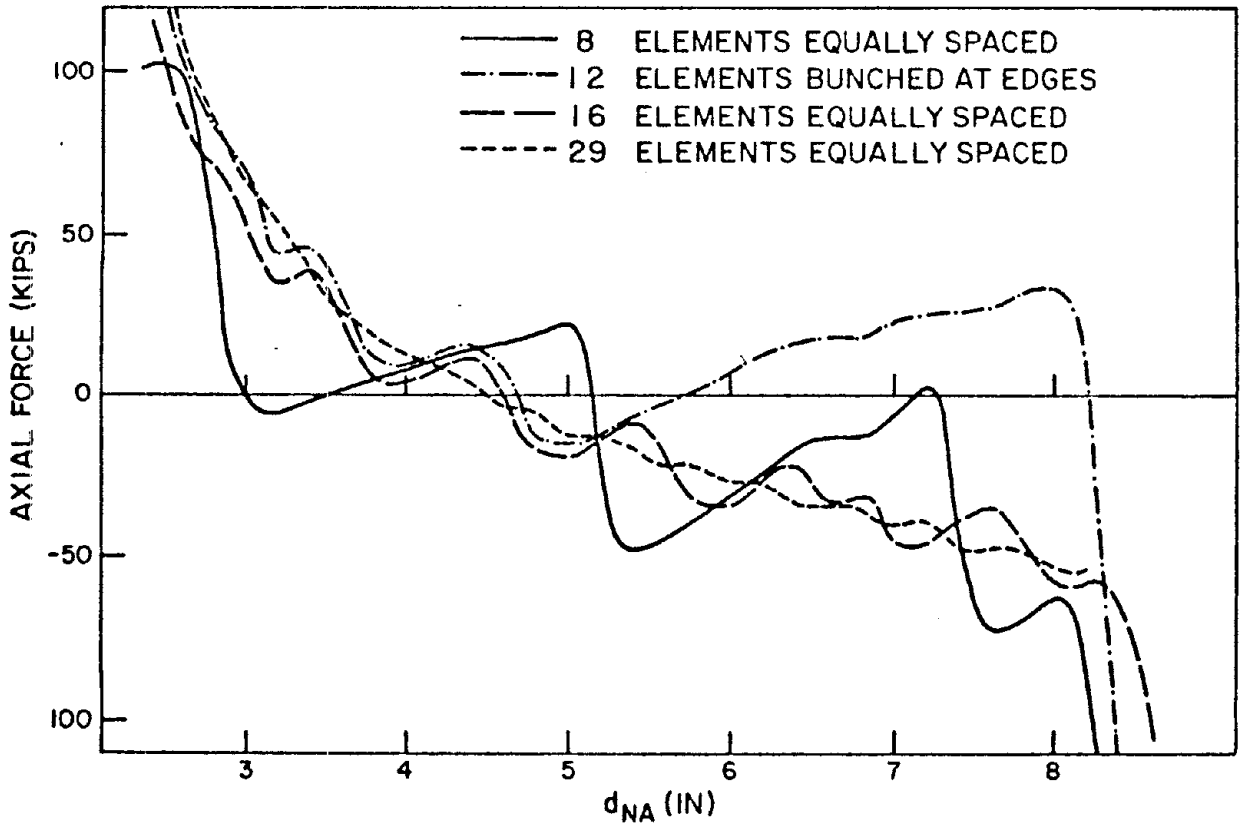

FIG. 7.2 - AXIAL FORCE VS. CENTROIDAL STRAIN FOR DIFFERENT LAYER ARRANGEMENTS

estimated by performing the calculations a number of times, each with a different number of elements.) It appears to depend on both the properties of the cross section and the sequence of applied curvatures but, in general, the 20 elements needed for a unique solution for ε_g also provided errors in the moment of less than 2%. We hoped that the number of elements might be reduced by bunching them at the point where the neutral axis is expected to occur, but this proved impossible because the neutral axis position varied over such a wide range.

The ripples are caused by the discontinuity in the slope of the stress field, which is a direct consequence of assuming that the concrete can carry no tension. In theory, the problem can be overcome quite simply by using a higher order integration method (e.g. trapezoidal), rather than the rectangle rule, to integrate the stresses and calculate the axial force. Fig. 7.3 illustrates the use of each. However, the implementation of the trapezoidal rule is tedious because special conditions need to be introduced in four locations. These are the cover elements, the first elements inside the cover, the element in which the stress falls to zero, and, if the beam is a tee, the elements adjacent to the joint between the web and the flange. It seems easier to use more elements and the rectangle rule.

For most of the runs, the section is divided into 29 layers. The outside pair represent the concrete cover and the remaining 27 are distributed fairly uniformly throughout the core. With this configuration, the neutral axis is located so that the error in the axial force is less than 0.1 kips. (This is approximately 0.01% of the beams axial strength.) The average cost is five and one quarter function evaluations.

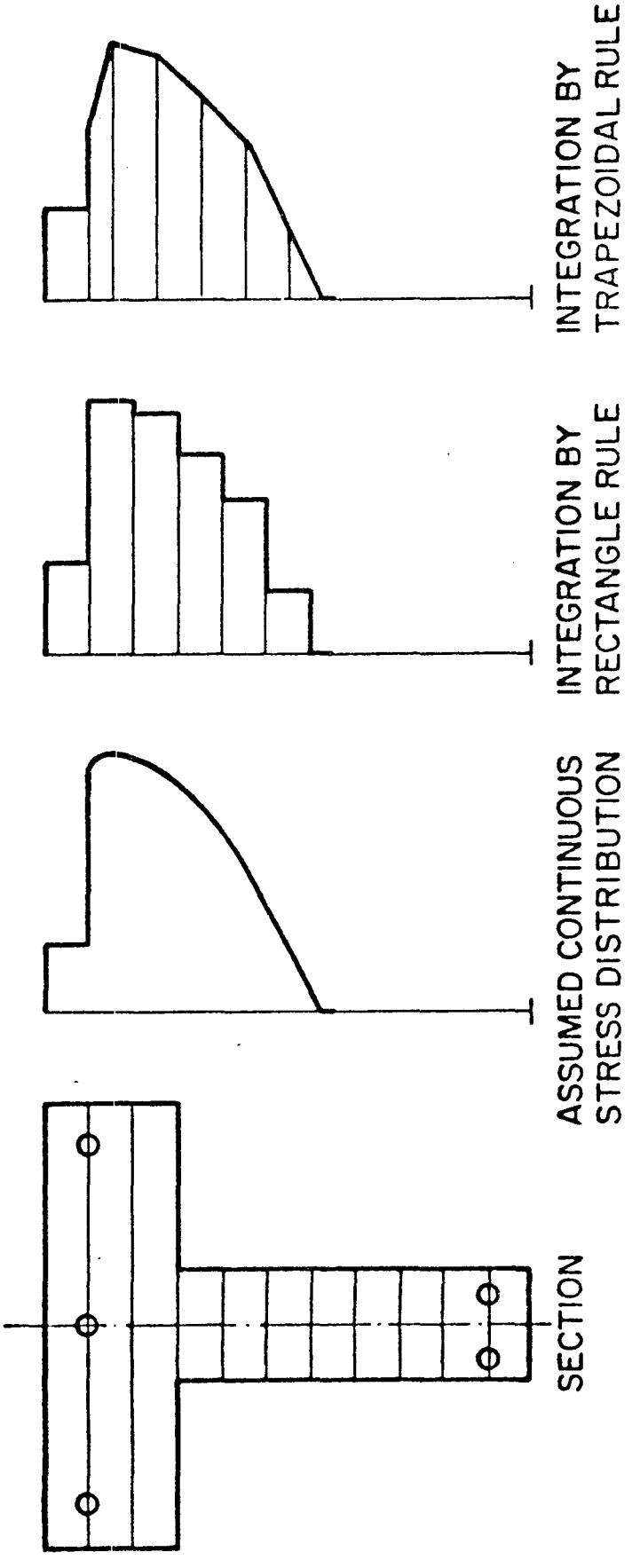

FIG. 7.3 - INTEGRATION BY TRAPEZOIDAL AND RECTANGLE RULES

Chapter 8

MINIMIZATION ALGORITHMS

8.1 General

This chapter is concerned with the minimization of the error function, which is the objective measure of how well the model fits the experimental data.

We seek the minimum of a function of N variables. If the function can be defined by a simple, explicit, analytical expression, the task is relatively easy. However, to locate the minimum of a function which is defined numerically (such as the error function in this study) is more difficult and requires the use of nonlinear programming techniques. The last fifteen years have seen rapid advances in the nonlinear programming field, but most of them have been made in disciplines such as Operations Research and Electrical Engineering and are not well known to civil engineers. This chapter attempts to review some of the objectives of the minimization process and to investigate briefly the characteristics of some of the better algorithms in order to select one which is suited to our purposes.

8.2 Properties Desirable in a Good Algorithm

Virtually all minimization methods fall into one of two broad categories, random search or iterative search. The first is largely self-explanatory. The second possesses a more thoroughly developed background and is the one considered here. We specialize the discussion further by considering only unconstrained problems, because physical reasoning suggests that the minimizing vector lies in the interior of the feasible region of the parameter space rather than on its boundary.

If f is a function of the N variables $\underset{\sim}{x}$, and $\underset{\sim}{x}^i$ is the vector which contains the values of $\underset{\sim}{x}$ at iteration i, then an ideal iterative minimization algorithm would perform in the following way. It would start at some arbitrary point $\underset{\sim}{x}^0$ in the parameter space and would then choose a sequence of steps leading rapidly to the exact global minimum of the function. In practice, such performance can only be obtained with relatively simple functions which satisfy very restrictive conditions; and for more general functions, we have to be satisfied with considerably less. It is thus worth considering what characteristics an algorithm needs to possess in order to be effective.

The first is that it must converge globally, by which we mean that it must be capable of converging to a stationary point. This is illustrated by a counter example. A high order method may be considered desirable on account of its good convergence properties in the neighborhood of a stationary point, but away from that neighborhood, the steps which it chooses may actually increase the function value. If this happens to the step starting at $\underset{\sim}{x}^i$, point $\underset{\sim}{x}^{i+1}$ is rejected and the search remains forever at $\underset{\sim}{x}^i$. To be globally convergent, the method would need to take occasional steps which are guaranteed to reduce the function value, even though they are less efficient near the stationary point than those calculated using the higher order method.

The second desirable property is that the stationary point should be at least a local minimum. A rigorous assurance of this requires information about second derivatives of the function which is probably not available, but in practice, a one-dimensional minimization in a random direction almost invariably reveals the true character of the stationary point. If it is a minimum, it is accepted. If it is not, then

the search is restarted from a new arbitrary point.

The last property we seek is good local convergence, which means that the algorithm must converge rapidly when it is in the neighborhood of a minimum. It is cold comfort to know that an algorithm is guaranteed to reach a minimum if it is going to take 10^8 steps to get there!

A very large number of individual algorithms exist, as can be seen from the extensive literature on the subject [60,62]. However, almost all of them are variations on a few basic themes. These we present to give an idea of the characteristics which the different methods display.

8.3 Basic Methods for Determining the Search Direction

Any step is completely defined by its direction and its length. It can be expressed as

$$\underset{\sim}{x}^{i+1} - \underset{\sim}{x}^{i} = \mu \underset{\sim}{d} \tag{8.1}$$

where $\underset{\sim}{d}$ is the direction vector and the scalar μ is the step length. Individual methods vary in their choice of μ and $\underset{\sim}{d}$.

There are four fundamental methods for determining a search direction on which almost all others are based.

The first is usually called coordinate descent. The function is minimized along each coordinate direction in turn, so the directions, $\underset{\sim}{d}$, are the coordinate axes themselves. The method is globally convergent, but its local convergence properties are poor.

The classical method of steepest descent uses

$$\underset{\sim}{d} = -\underset{\sim}{g} \tag{8.2}$$

where $\underset{\sim}{g}$ is the gradient of the function, so $\underset{\sim}{d}$ is the direction in which the downhill slope is the steepest. This choice ensures that each step

will reduce the function value, provided that the derivatives are continuous and that the gradient is not zero (in which case a stationary point has been located). Thus it is globally convergent and is useful as a spacer step to ensure global convergence in more sophisticated methods.

Newton's method uses

$$\underset{\sim}{d} = -\underline{H}^{-1}\underset{\sim}{g} \tag{8.3}$$

where $\underline{H}$ is the Hessian matrix of second partial derivatives. Eq. (8.3) is obtained from a truncated Taylor series expansion for the gradient.

$$\underset{\sim}{g}(\underset{\sim}{x} + \Delta\underset{\sim}{x}) = \underset{\sim}{g}(\underset{\sim}{x}) + (\Delta\underset{\sim}{x})^T \underline{H}(\underset{\sim}{x}) + O(\Delta\underset{\sim}{x}^2) \tag{8.4}$$

If $\underset{\sim}{x} + \Delta\underset{\sim}{x}$ is to be a stationary point, then $\underset{\sim}{g}(\underset{\sim}{x} + \Delta\underset{\sim}{x})$ must be zero, and Eq. 8.3 follows directly.

If the second derivatives of the function are continuous, the truncated series may be expected to be a reasonably accurate representation near the minimum, so the method should give good local convergence. Global convergence, however, is not guaranteed. The method can also be viewed as an approximation of the function locally by a quadratic. In predicting the new point $\underset{\sim}{x}^{i+1}$ we are assuming that the Hessian remains constant for the duration of the step. Far from a stationary point, the steps are relatively large and the value of the true Hessian may change appreciably between $\underset{\sim}{x}^{i}$ and $\underset{\sim}{x}^{i+1}$. However, as we approach a stationary point, the steps shorten, the Hessian changes less in each, and so the iterations become increasingly accurate.

The fourth fundamental idea is a little more subtle and forms the basis of all the conjugate direction methods. The theory is developed for a quadratic function and is then extended to general functions.

A quadratic function has a Hessian matrix $\underline{H}$ which is constant. If we have N direction vectors $\underset{\sim}{u}^i$ (i = 1,...,N) which are H-orthogonal, that is, which satisfy

$$(\underset{\sim}{u}^i)^T \underline{H} \underset{\sim}{u}^j = 0 \qquad i \neq j \tag{8.5}$$

then we can find the minimum of the quadratic function by a single one-dimensional minimization (or line search) in each direction. The difficulty obviously lies in finding the directions $\underset{\sim}{u}^i$, when $\underline{H}$ is not available. Fletcher and Reeves' conjugate gradient method [63] is one of the most efficient of these techniques.

These four fundamental ideas for establishing search directions form the basis of almost all of the algorithms commonly used today.

8.4 Practical Methods for Finding Good Search Directions

Newton's method has particularly good local convergence properties but suffers from two drawbacks. First, the Hessian matrix may be tiresome and even impossible to compute; and second, the method is not globally convergent. Both difficulties can be overcome without ruining the local convergence properties if we substitute for $\underline{H}$ a positive definite matrix $\underline{A}$ which converges to $\underline{H}$ as $\underset{\sim}{x}$ approaches its minimizing value of $\underset{\sim}{x}^*$. Such methods are called Quasi-Newton.

The modified Gauss-Newton method is an example. It works only for sums of squares functions, namely those which can be expressed in the form

$$F(x) = \sum_{k=1}^{m} f_k^2(x) \tag{8.6}$$

but these are so common that the method enjoys widespread use. The true

Hessian matrix is given by

$$H_{ij} = 2 \sum_{k=1}^{m} \left[\left(\frac{\partial f_k}{\partial x_i} \right) \left(\frac{\partial f_k}{\partial x_j} \right) + f_k \left(\frac{\partial^2 f_k}{\partial x_i \partial x_j} \right) \right] \qquad (8.7)$$

If the second term is dropped, and $\underline{A}$ is set equal to the first term, it is positive definite, thus ensuring global convergence, and can be calculated using only first derivatives. Furthermore $\underline{A}$ converges to $\underline{H}$ if $f_k \to 0$, so $\underline{A}$ is the desired approximation. Note that the direction

$$\underset{\sim}{d} = -\underline{A}^{-1} \underset{\sim}{g} \qquad (8.8)$$

is calculated from information at point $\underset{\sim}{x}^i$ only.

Variable metric methods (rank one correction [64], Davidon-Fletcher-Powell [65], Davidon [66]) are Quasi-Newton methods but are also closely allied to the conjugate direction method. They are applicable to any type of function and avoid the matrix inversion inherent in the Modified Gauss-Newton method, but they take N steps rather than one to generate an approximation $\underline{A}$ to $\underline{H}^{-1}$. Also, they do not depend for their success on the function values becoming very small at the minimum.

The methods outlined above represent some of the most widely used. Many variations of each exist, both for specialized and general applications, and these should be considered when choosing a method. However, the majority of useful algorithms are based on the ideas presented in this section.

8.5 Step Length

The previous section shows how some of the different methods choose their search directions, but to define a step completely, we also need to know its length. Some methods, such as Modified Gauss-Newton and

Davidon's second method, use a fixed step length, whose value is generally 1.0. The majority, however, use a line search (or one-dimensional minimization) in the chosen direction. We need to consider how it should be carried out, and to what accuracy, if the overall search procedure is to be as efficient as possible. Three factors influence the decision:

(i) Are the calculations of subsequent search directions affected by the outcome of this line search?

(ii) How large is N?

(iii) How easy are the derivatives to compute compared to the function value itself?

In methods such as the Modified Gauss-Newton in which each search direction is calculated using only information at the point $\underset{\sim}{x}^i$, the accuracy of the line search does not affect the computation of future search directions. In this case, the optimum accuracy is decided solely on grounds of efficiency. Let us assume that a line search requires between two and ten function evaluations, depending on the desired accuracy. If N is, say, 50, and the derivatives are each as hard to compute as the function value itself, then the cost of finding a new search direction is 51 equivalent function evaluations. It is thus worth expending a relatively large amount of effort (e.g., ten function evaluations rather than two) on the line search. For small N, or derivatives that are relatively easy to compute, the reverse is true, and the line search should be terminated after only a few function evaluations.

For methods which accumulate information on the approximate Hessian over a number of steps (such as the Davidon-Fletcher-Powell method),

there are conflicting opinions about the optimum accuracy. Luenberger [62] reports that the method is very sensitive to the accuracy of the line search and recommends using a relatively fine tolerance. Bard [64] finds that a "moderate" amount of effort should be expended in the line search. Perhaps the optimum results would be achieved with a variable tolerance, which is initially coarse but is refined as the search progresses and the function becomes more nearly quadratic.

8.6 Methods Which Do Not Require Analytical Expression For The Derivatives

All but one of the methods so far discussed require the use of the gradient vector, for which we have implicitly assumed that analytical expressions exist. However, calculation of the gradient numerically rather than analytically may be desirable or even necessary. If, for example, the expressions for each element of the gradient vector are significantly more involved than the one for the function evaluation, then the use of finite differences would save computer time. More important, however, is the gain in flexibility of use, particularly for large numbers of variables, because the function can be modified without having to rewrite all of the expressions for the derivatives. This advantage is bought at the price of limited accuracy, caused by the twin constraints of truncation and round-off.

The problem of accuracy is most clearly illustrated in one dimension. If we use the forward difference approximation

$$f'(x) \doteq \frac{f(x+h) - f(x)}{h} \tag{8.9}$$

and ε is the relative machine precision and h is the finite difference step length, then the total error, composed of truncation and round-off,

is bounded by

$$|\text{error}| \leq \frac{h}{2}|f''| + \frac{2\varepsilon}{h} \tag{8.10}$$

This bound is minimized by choosing

$$h = h^* = \left(\frac{2f}{f''}\right)^{1/2} \tag{8.11}$$

Even if we choose this optimal step length, we still risk an error in the approximation of the derivative of up to $2(\text{eff}'')^{1/2}$. For any other step length, say αh^*, the error is bounded by

$$|\text{error}| \leq \left(\alpha + \frac{1}{\alpha}\right)\left(\text{eff}''\right)^{1/2} \tag{8.12}$$

which is larger than the error bound for h^*. The essential point is that the use of finite differences involves an error which cannot be reduced below a certain value by choice of step length alone. It can be reduced by using double precision arithmetic (which has the effect of replacing ε by ε^2 in Eqs. (8.10)-(8.12)) or by using a higher order approximation such as the central difference method

$$f'(x) \doteq \frac{f(x+h) - f(x-h)}{2h} \tag{8.13}$$

in which case the minimum error bound is $(1.125\ \varepsilon^2 f^2 f''')^{1/3}$ at an optimal step length of $\left(\frac{3\varepsilon f}{f'''}\right)^{1/3}$. The central difference method uses twice as many function evaluations as the forward difference, and double precision costs about twice as much as single precision, both in computer storage and execution costs. These improvements reduce the error bound by factors of $\varepsilon^{1/2}$ and $0.52\left(\frac{\varepsilon f}{f'''}\right)^{1/6}\left(\frac{f'''}{f''}\right)^{1/2}$, respectively, so the choice of method depends on the function and the computer. However, in both cases, the increased accuracy is hard-won. For example, using double

precision, the error bound improves only with the square root of the increased effort. These error bounds are applicable only if the optimal step length h* is used, and any other step length will lead to a larger bound. However, most methods permit approximate information about the higher derivatives to be accumulated which can be used to optimize the step length.

The bounds on the relative error are $\left(\frac{4\varepsilon f f''}{(f')^2}\right)^{1/2}$ and $\left(\frac{9\varepsilon^2 f^2 f'''}{8(f')^3}\right)^{1/3}$, both of which are singular at the minimum. The consequence is that the search method will have the same convergence properties as the analogous version which calculates the gradient analytically until that neighborhood of the minimum is reached in which the errors dominate the gradient calculation. From this point on, the convergence deteriorates because the calculated search directions are so inaccurate. Thus, under optimal conditions, the adverse effects of using finite differences can be restricted to a neighborhood around the minimum. In practice, the penalty may be negligible if the minimum does not need to be located very accurately.

These arguments apply to methods which use finite difference approximations explicitly. Powell's method [67] without derivatives does not, and so is subject to different restrictions. It is explained in detail in Sec. 8.8.

8.7 Relative Merits

For sums of squares functions the Gauss-Newton methods should work best, provided that the minimum function value is small and the gradient can be calculated analytically. Assuming that operations other than function evaluations consume negligible computer time and that calculation

of the gradient is as expensive as N equivalent function evaluations, then the Gauss-Newton methods require N equivalent function evaluations to generate a search direction close to $H^{-1}g$, compared to N^2 for the variable metric and conjugate gradient methods. But if f_{min} is sufficiently large, then the Gauss-Newton methods may actually perform worse than the other two.

For more general functions, the Davidon-Fletcher-Powell method is considered by many authors to be the best. However, it requires storage of the approximate Hessian, and if this is a problem, the Fletcher-Reeves conjugate gradient method may be preferable.

The relative economy of the methods remains the same if the derivatives are calculated numerically. Powell's method needs some 2.5 (N^2+N) equivalent function evaluations per cycle compared to Gauss-Newton with finite differences which needs N or 2N (forward or central difference).

In the present case we expected to modify the model form as the study progressed, which would be facilitated by using a method which does not require analytical expressions for the derivatives. Furthermore, to suppose that the model would fit the data perfectly (giving $f_{min} = 0$) seemed unduly optimistic. Thus, after some early experiments with finite difference versions of the Gauss-Newton and Davidon-Fletcher-Powell methods, which were beset by the problems of accuracy near the minimum described above, they were discarded in favor of the computer program POWBRE, which is an improved version of Powell's method and is described in detail in the next section.

8.8 Algorithm Used

8.8.1 General

This section describes program POWBRE, the algorithm used in this study. It is a modification of Powell's method of minimizing a function without the use of analytical expressions for the derivatives.

Powell's basic procedure is described first. Then its drawbacks and Brent's modifications for overcoming them are presented.

8.8.2 Powell's Basic Algorithm

We examine first the application of the algorithm to quadratic functions. Consider a quadratic function of N variables

$$f(\underset{\sim}{x}) = \underset{\sim}{x}^T \underline{A}\, \underset{\sim}{x} - 2\underset{\sim}{b}^T \underset{\sim}{x} + c \qquad (8.14)$$

where $\underline{A}$, $\underset{\sim}{b}$, and c are constant, and $\underline{A}$ is positive definite.

The problem is to find the vector $\underset{\sim}{x}$ which minimizes f if $\underline{A}$, $\underset{\sim}{b}$, and c are unknown, and f can only be evaluated numerically. The basis of Powell's solution is as follows.

Suppose we have N nonzero vectors $\underset{\sim}{u}_i$[†] (i=1,...,N) which are mutually $\underline{A}$-orthogonal. Then, by definition of orthogonality,

$$\underset{\sim}{u}_i^T \underline{A}\, \underset{\sim}{u}_j = 0 \qquad i \neq j \qquad (8.15)$$

The $\underset{\sim}{u}_i$ span the N-dimensional space and so any vector $\underset{\sim}{x}$ can be expanded in terms of them

$$\underset{\sim}{x} = \sum_{i=1}^{N} \alpha_i \underset{\sim}{u}_i \qquad (8.16)$$

[†] In this section, subscripts refer to the number of the vector in the set, and superscripts refer to the cycle number.

Substituting Eqs. (8.15) and (8.16) into Eq. (8.14),

$$f(\underset{\sim}{x}) = \sum_{i=1}^{N} \left[\left(\alpha_i^2 \, \underset{\sim}{u}_i^T \, \underline{A} \, \underset{\sim}{u}_i \right) - 2b\alpha_i \, \underset{\sim}{u}_i \right] + c \qquad (8.17)$$

Since Eq. (8.17) contains no cross products of the form $\alpha_i \alpha_j$, $f(\underset{\sim}{x})$ can be minimized by searching once along each $\underset{\sim}{u}_i$ for the local minimum in that direction. If each line search starts from the minimum of the previous one, the finishing point is the global minimum of f. (Recall that f is quadratic and $\underline{A}$ is positive definite, so f has a global minimum.)

The difficulty lies in finding the $\underline{A}$-orthogonal vectors $\underset{\sim}{u}_i$ when we do not know $\underline{A}$. Powell's method uses an iterative process which starts with any set of linearly independent vectors (the columns of the identity matrix are a convenient choice) and in each subcycle orthogonalizes one more of them. N such subcycles, forming one cycle, are needed to generate the complete orthogonal set.

If we define

$\underset{\sim}{u}_i^k$ = direction $\underset{\sim}{u}_i$ during subcycle k

$\underset{\sim}{x}_i^k$ = the vector which minimizes f along a line in direction $\underset{\sim}{u}_i^k$ starting from $\underset{\sim}{x}_{i-1}^k$

$\underset{\sim}{w}^k = \underset{\sim}{x}_n^k - \underset{\sim}{x}_o^k$

which are shown schematically in Fig. (8.1), the following calculations constitute the k^{th} subcycle:

(1) Compute the β_i to minimize $\phi(\beta_i) = f\left(\underset{\sim}{x}_{i-1}^k + \beta_i \, \underset{\sim}{u}_i^k\right)$ and define $\underset{\sim}{x}_i^k = \underset{\sim}{x}_{i-1}^k + \beta_i \, \underset{\sim}{u}_i^k$, for i=1,...,N

(2) Define a new direction $\underset{\sim}{w}^k = \underset{\sim}{x}_n^k - \underset{\sim}{x}_o^k$

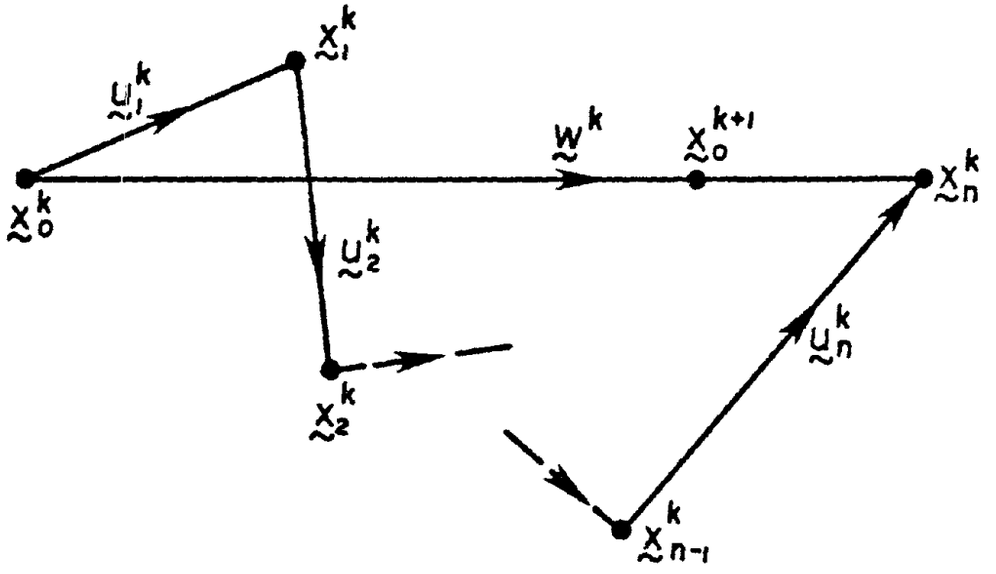

FIG. 8.1 - MINIMIZATION BY POWELL'S METHOD

(3) Compute β to minimize $f\left(\underset{\sim}{x}_0^k + \beta\ \underset{\sim}{w}^k\right)$

(4) Set $\underset{\sim}{x}_0^{k+1} = \underset{\sim}{x}_0^k + \beta\ \underset{\sim}{w}^k$

$$\underset{\sim}{u}_i^{k+1} = \underset{\sim}{u}_{i+1}^k \qquad i=1,\ldots,N-1$$

$$\underset{\sim}{u}_n^{k+1} = \underset{\sim}{w}^k$$

and return to Step 1 for subcycle k+1

The important point is that the new direction $\underset{\sim}{w}^k$ is orthogonal to the last k-1 vectors of the set $\underset{\sim}{u}_i^k$ i=1,...,N, and at the end of the k^{th} cycle it replaces one of the N-k+1 nonorthogonal directions. The proof of its orthogonality is given in Appendix A.

For a quadratic function, a single cycle of this process generates a full set of orthogonal directions and, since the last subcycle includes a minimization along each of them, the cycle ends at the exact minimum of f.

If f is not quadratic, the matrix $\underline{A}$ is a variable function of $\underset{\sim}{x}$ and so the computed directions cannot be mutually orthogonal with respect to it. The minimum will not be found exactly in one cycle, but rather it is approached iteratively in a number of cycles. At the end of each one, the change in $\underset{\sim}{x}$ (equal to $\underset{\sim}{x}_n^k - \underset{\sim}{x}_n^{k-1}$) is compared to the stopping tolerance.

The method is attractive because it is globally convergent and it also has good local convergence properties. As the search approaches a stationary point, $\underline{A}$ changes less, the orthogonality condition is more nearly fulfilled, and the local convergence becomes asymptotically quadratic.

8.8.3 Line Search Strategy

Powell's method uses N(N+1) line searches to generate an orthogonal set of vectors, so a good strategy for these one-dimensional searches is important. The choice is influenced by the fact that we are approximating f locally by a quadratic function. In each line search we seek μ^*, which is the value of μ that approximately minimizes $\phi(\mu) = f(\underset{\sim}{x}_0 + \mu\underset{\sim}{u})$, given $\underset{\sim}{x}_0$ the starting point and $\underset{\sim}{u}$, the search direction.

The simplest way is to use parabolic interpolation, which requires three pieces of information. We already know the function value $\phi(0)$, so either two more function values, or one function value and an estimate of ϕ'', are needed. If μ_1 is the minimum of the interpolating parabola, $\phi(\mu_1)$ is computed and if it is less than $\phi(0)$, μ^* is taken equal to μ_1 and the line search ends. If it is not, μ_1 is replaced by $\frac{\mu_1}{2}$ and the function is re-evaluated. This process is repeated until a μ_1 is found that gives $\phi(\mu_1) < \phi(0)$ or until a limiting number of attempts is reached. When μ^* has been located, the second difference of ϕ is calculated and stored for subsequent use as the estimate of ϕ'' in the next minimization along $\underset{\sim}{u}$. Near the minimum, the estimate of ϕ'' will be good enough that μ^* can be found at the first attempt, so the line search requires only two function evaluations.

Use of such a crude line search technique gives the greatest economy overall, regardless of N. This is in contrast to other methods, such as the Modified Gauss-Newton, in which the optimum accuracy of the line search is governed by the amount of effort required to find a new search direction relative to that needed for a function evaluation. The reason for the difference is that in the Modified Gauss-Newton method the computation of a new search direction and the linear search are two independent

operations. In Powell's method, however, the new search direction is found purely by means of line searches. Since we are approximating the multi-dimensional error surface by a quadratic function, it is inconsistent and uneconomical to approximate to a higher order a line contained within it.

8.8.4 Shortcomings of the Basic Algorithm and Brent's Modification

The main difficulty is that one or more of the β_i calculated in Step 1 of each subcycle may be close to zero, causing the search directions to become nearly linearly dependent, and thus preventing the convergence from becoming quadratic. This is particularly likely if the approximate Hessian $\underline{A}$ is nearly singular, or if N, the number of variables, is large, or both. Powell has suggested two modifications to overcome this difficulty. The first is to reset the search directions $\underset{\sim}{u}_i$ at the end of each cycle to a set of vectors which are truly linearly independent — for example, the columns of the identity matrix. However, in resetting them, all the accumulated information about the approximate Hessian is thrown away. Not only does this mean that the starting vectors are poor approximations to the A-orthogonal set, but also the individual line searches are rendered less efficient due to the lack of second derivative information. The second modification is to replace direction $\underset{\sim}{u}_i$ (rather than $\underset{\sim}{u}_n$) by $\underset{\sim}{w}^k = \underset{\sim}{x}_n^k - \underset{\sim}{x}_o^k$ only if $\det|\underset{\sim}{v}_1,\ldots,\underset{\sim}{v}_n|$ is increased by doing so, where $\underset{\sim}{v}_j = \left(\underset{\sim}{u}_j^T \underline{A}\, \underset{\sim}{u}_j\right)^{-1/2} \underset{\sim}{u}_j$. Furthermore the direction $\underset{\sim}{u}_i$ to be discarded should be chosen in such a way as to maximize $\det|\underset{\sim}{v}_1,\ldots,\underset{\sim}{v}_n|$.

This modification improves the algorithm's convergence with most of the functions on which it has been tested. But with this criterion it is possible that a complete set of n conjugate directions will never be built up (either because the discarded vector $\underset{\sim}{u}_i$ is a conjugate one, or

because no vector is ever replaced by $(\underset{\sim}{x}_n - \underset{\sim}{x}_0)$), in which case quadratic convergence cannot be guaranteed.

Brent's modification is to reset the $\underset{\sim}{u}_i$ after each cycle to the eigenvectors of $\underline{A}$. By doing so, linear independence is preserved (as in Powell's first modification) but without throwing away Hessian information. The eigenvalue extraction is done without explicit knowledge of $\underline{A}$ and uses a singular value decomposition technique. Details are given in [60]. Brent also suggests a reduced form of Powell's second modification, whereby the discarded direction is chosen from the nonconjugate subset in such a way as to maximize the $\det|\underset{\sim}{v}_1,\ldots,\underset{\sim}{v}_n|$. Thus, no conjugate direction is ever discarded.

Convergence will be hindered by poor conditioning of the approximate Hessian. This can be alleviated by rescaling the coordinate axes so that the Hessian is approximately row and column equilibrated.

The choice of a good stopping criterion needs careful consideration. For well behaved functions a simple check on the change in the elements of $\underset{\sim}{x}$ will suffice. But awkward functions, particularly of many variables, can get caught in a "resolution valley," where the simple tolerance criteria are met at a point far removed from the minimum. This occurs if the derivative is almost zero in each search direction, but is relatively large in some intermediate direction. Such a condition can usually be detected by an extra search in a random direction, and this feature is included in the program.

Chapter 9

RESULTS

9.1 General

With the construction of the form of the global model now complete, we may turn our attention to the task of matching the moment-average curvature relations displayed by the test beams.

The global model contains a total of fifty-three parameters for the T-beams and forty-two for the rectangular beams. These are made up of nine for the concrete model, eleven for the steel model, and eleven bond-slip parameters for each bar size. The T-beams contain bars of three different sizes, and the rectangular beams contain two, which is why the T-beams have more parameters. As has already been pointed out, the computer program for finding optimum parameters was arranged so that each parameter could either be left free to be adjusted or be assigned a fixed value. It is therefore much easier to cut out parameters (by declaring them fixed on input to the program) than it is to alter the program itself to include new ones. So every quantity which might influence the model's performance is treated as a potential parameter. Thus there are really fifty-three (or forty-two) potential parameters, and in most of the computer runs only a small number of them are freed to become actual parameters.

If this is the case, why then did we identify the steel behavior separately rather than assembling the complete global model and then identifying the steel parameters? The reasons illustrate a fundamental dilemma in the process of mathematical modelling, which is that we want of the model two things which are not necessarily compatible. Not only

should it predict the measured response as well as possible, but also its parameters should have a clear physical significance so that the model can easily be applied to a reinforced concrete beam of any proportions. We attempt to achieve the first objective by minimizing an error function, and the second, by treating the steel and concrete separately in the model, and assigning to each a group of parameters. But we have to decide which to do first, identify the values of each group of parameters, or assemble the global model. If the parameters in the individual models can be identified before the latter are integrated into a global model (for example, by using separate experimental results such as Ma's axial bar tests), then we can be sure that the parameters do indeed describe the particular material behavior they were intended to. But the resulting parameter set may not minimize the error function. If, on the other hand, the global model is assembled first, we can ensure the best match for any particular set of experimental results, but we can no longer guarantee that the parameters retain their physical significance. In which case there is no way of determining from the system identification study the parameter values needed to predict the behavior of other beams.

We feel that preservation of the parameter's physical significance is essential, so their values are identified from separate tests in the one case (namely, the steel model) where such a procedure is feasible. By so doing we also reduce the cost of identification, because the error function for the individual model is much cheaper to evaluate than the one for the global model.

Before presenting the predictions of the model for the behavior of the test beams, it is well to consider the factors which limit the accuracy we can expect to achieve. The most obvious limitation lies in the experi-

mental data itself. The lateral load on each beam was measured with a load cell, and the rotations were derived from clip gage readings. Both devices depend on electrical resistance strain gages which have an accuracy of about ±1% of their full scale reading. The exact position of the reinforcement in the beam is also important. The top and bottom bars are nominally 12-1/2 inches apart, so if, in practice, each bar is displaced 1/16 inch from its nominal position, an error of 1% will be introduced in the predicted moment.

Errors are also introduced when the data is digitized. We had originally hoped to use the original data recorded in digital form during the experiments, but it was not available. The moment-average curvature plots in Ma's report were therefore digitized on a Calma 685C digitizing bed, and this data used instead. The curves in the report were drawn by a draftsman from the original data, so we should expect discrepancies in moment at a given curvature of perhaps 2% in the regions where the slope is small, but much more where the curve rises or falls steeply.

Last, but not least, are the slight variations in mechanical properties between nominally identical steel bars or samples of concrete.

The existence of the errors listed above suggests that no attempt should be made to match the experimental data to an accuracy of less than about 2%-5%. Any further adjustment of the parameters would in fact be directed towards matching a particular sequence of random errors rather than the mechanical behavior of a reinforced concrete beam.

9.2 Predicted Moment-Curvature Relations

Eleven of Ma's published moment-curvature graphs were selected for digitization. They are:

Beam	Curvature
R1	ϕ_1
R1	ϕ_2
R3	ϕ_1
R3	ϕ_2
R4	ϕ_1
R5	ϕ_1
R6	ϕ_1
T1	ϕ_1
T1	ϕ_2
T2	ϕ_1
T3	ϕ_1

The dimensions and reinforcing details of each beam are given in Table 9.1. ϕ_1 and ϕ_2 refer respectively to the average curvature in the first and second 7-inch segments of the beam, starting at the fixed end. From here on, the notation is used whereby R3/2 signifies the moment-curvature relation displayed in segment 2 of beam R3.

The objective is to investigate the model's ability to reproduce different aspects of physical behavior by comparing results for pairs of beams between which only one variable differed.

Comparisons between R3/1 and R6/1, or T1/1 and T3/1, show the effect of changing the bottom steel. R1/1 and T1/1, or R1/2 and T1/2, show the effect of the existence of a slab. R5/1 and R6/1 compare low and high shear spans, and R4/1 and T2/1 were both loaded to failure in the first cycle rather than being subjected to many cycles of alternating load, as were all of the other beams.

SPECIMEN	ℓ (in.)	h (in.)	b (in.)	d (in.)	ℓ/d (in/in.)	ρ	ρ'	ρ_b	top* Reinf. (bars)	bot.** Reinf. (bars)	Stirrup*** tie (bars)	tie Spacings (in.)	ρ''	f'_c (Ksi)	f_r (Psi)	Slab Size (in. x in.)	Slab reinf. (bars)
BEAM R-1	62.5	16.0	9.0	14.0	4.5	.014	.0074	.030	4#6	3#5	#2	3.5	.0053	5.07	510	None	None
BEAM R-2	62.5	16.0	9.0	14.0	4.5	.014	.0074	.026	4#6	3#5	#2	3.5	.0053	4.19	455	None	None
BEAM R-3	62.5	16.0	9.0	14.0	4.5	.014	.0074	.028	4#6	3#5	#2	3.5	.010	4.58	475	None	None
BEAM R-4	62.5	16.0	9.0	14.0	4.5	.014	.0074	.027	4#6	3#5	#2	3.5	.010	4.38	460	None	None
BEAM R-5	38.5	16.0	9.0	14.0	2.8	.014	.014	.028	4#6	4#6	#2	3.5	.010	4.58	480	None	None
BEAM R-6	62.5	16.0	9.0	14.0	4.5	.014	.014	.027	4#6	4#6	#2	3.5	.010	4.34	450	None	None
BEAM T-1	62.5	16.0	9.0	14.0	4.5	.014	.0074	.030	4#6	3#5	#2	3.5	.010	4.79	530	36 x 2.25	12#2
BEAM T-2	62.5	16.0	9.0	14.0	4.5	.014	.0074	.028	4#6	3#5	#2	3.5	.010	4.61	462	36 x 2.25	12#2
BEAM T-3	62.5	16.0	9.0	14.0	4.5	.014	.014	.028	4#6	4#6	#2	3.5	.010	4.47	470	36 x 2.25	12#2

ℓ = length of the cantilever

h = height of the beam section

b = width of the beam section

d = effective depth

ρ = top steel reinf. ratio

ρ' = bottom steel reinf. ratio

ρ'' = volume of ties/volume of bound concrete core

ρ_b = balanced steel ratio

f'_c = concrete cylinder strength

f_r = modulus of rupture of concrete

* Yield strength = 65.5 Ksi

** Yield strength = 66.5 Ksi

*** Yield strength = 60.0 Ksi

TABLE 9.1 - DIMENSIONS AND REINFORCING DETAILS OF BEAMS

Five separate parameter studies are done, referred to as Series A-E. In all of them except Series D, perfect bond is assumed. Series A is designed to find out which concrete parameters are important. In Series B the same parameters are applied to all of the beams, and the qualities of the predictions for each are compared. In Series C the optimum concrete parameters are found for a number of the beams. The bond-slip relation is introduced in Series D in an effort to improve the fit between theoretical and experimental results. In Series E the steel parameters, previously regarded as fixed, are adjusted.

9.2.1 Test Series A

Series A was exploratory and was based on the data for a single beam. Beam R4 was chosen because it has a short load history and so is relatively cheap to run. The intention was to investigate the sensitivity of the error function to changes in the values of the parameters. A set of initial values were assigned (based as far as possible on physical data) and the error function was evaluated. The eight concrete parameters were then varied in turn, and the error function re-evaluated each time. The values of the parameters and the error function are given in Table 9.2. Inspection of the table shows that the function value is hardly dependent at all on the two unloading parameters $\frac{\partial k}{\partial \varepsilon}$ and ε_{lim}. This appears reasonable because the concrete unloads completely in only a very small strain increment. It is quite possible that the first point at which the moment is calculated after a reversal occurs after the concrete has unloaded.

The error function appears to be about equally sensitive to the values of ε_a, a, cmx, and the rubble. The last two variables control in only slightly different ways the absolute amount of rubble in a crack, and their effects on the error function are likely to be similar.

Run	A1	A2	A3	A4	A5	A6	A7	A8	A9
Parameter									
ε_o	- 2.45	- 2.45	- 2.45	- 2.45	- 2.45	- 2.45	- 2.45	- 2.45	-15.0
ε_a	-23.23	-15.0	-23.23	-23.23	-23.23	-23.23	-23.23	-23.23	-23.23
f_a/f'_c	0.15	0.15	.05	0.15	0.15	0.15	0.15	0.15	0.15
cmx	50.0	50.0	50.0	5.0	50.0	50.0	50.0	50.0	50.0
r	0.7	0.7	0.7	0.7	0.1	0.7	0.7	0.7	0.7
$\partial k/\partial \varepsilon$	0.1	0.1	0.1	0.1	0.1	0.0	0.1	0.1	0.1
ε_{lim}	-18.0	-18.0	-18.0	-18.0	-18.0	-18.0	-10.0	-18.0	-18.0
f'_c	4.38	4.38	4.38	4.38	4.38	4.38	4.38	3.000	4.38
Error Function	2.81E6	2.25E6	2.57E6	2.34E6	2.40E6	2.82E6	2.82E6	1.82E6	3.85E6
RMS Error	335	300	321	306	310	336	336	270	392
Max. Error	737	737	737	737	737	737	737	641	763

TABLE 9.2 - SERIES B RESULTS. VARIATION OF PARAMETERS IN BEAM R4

Therefore some effort can be saved in subsequent runs by varying only one of them.

f'_c and ε_o exert an influence on the error which was unexpected, but which illustrates the dilemma outlined in the last section. The Series A results indicate that in order to provide the best fit with the experimental data f'_c and ε_o must assume values which are radically different from the ones which we would expect them to have.

There is overwhelming evidence to suggest that both quantities can be estimated reasonably reliably from standard cylinder tests, and so the large discrepancy indicates that, for these experimental results at least, the parameters have lost their physical significance. The model predicts a strength for the beam greater than that observed in the experiments, even in regions of the curve where the resisting moment is provided by the steel couple alone. Thus either the steel or the bond-slip model must be contributing to the difference between the two response curves. Yet we are attempting to rectify it by adjusting only the concrete parameters, so it is hardly surprising that their physical meaning has been distorted. The inaccuracies in the steel model are probably attributable to buckling of the compression bars because the steel behavior is well modelled in other beams.

The policy we adopt in future identification calculations is to assign to f'_c and ε_o the values obtained from cylinder tests. Thus they are treated not as adjustable parameters but rather as fixed constants.

Test Series A brought out one more point. The steel model has a larger influence than the concrete one on the accuracy of the overall behavior prediction. Therefore, if a relatively small error in the steel model is to be accounted for by adjusting only the concrete parameters,

then that adjustment will have to be relatively large.

9.2.2 Test Series B

The Series B study compares the model's predictions for a number of beams when the same parameter values are used for each. The values used are the standard ones from the Series A study except that the rubble parameter is given its optimal value of 0.7, and ε_0 and f'_c are given the values obtained from the test cylinders.

This set of parameters was then assigned to each beam in turn, for which a moment-curvature relation was calculated. Table 9.3 gives the error function value, the worst error and the root mean square error for each beam. Each beam is digitized into a different number of points, so the root mean square error between measured and predicted moments is the best indication of how good or bad the fit is. The curves are plotted in Figs. 9.1a-k in which the solid lines depict the measured response. Beam R5/1 displays the worst fit, but this is to be expected because it has the shortest shear span and is therefore subjected to the highest shear forces. Beam T3 shows a fit which is almost as bad, but the reasons for it are not clear. The predicted moments are everywhere too large. Beams R1/1, R1/2, R3/1, R4/1, R6/1, T1/1, T1/2 all have a root mean square error between 225 and 300 kip/in (approximately 10-15% of maximum moment). In most cases the bulk of the error is incurred at the points in the middle of each half-loop, indicating that the unloading stiffness of the steel bars is not well modelled. The maximum moment in each half cycle is generally predicted to within an error smaller than the root mean square, which is encouraging because the maximum moment is generally the most important for design purposes.

Beam	No. Pts.	Error fn. Value	RMS Error	Max. Error (pt)	Max/RMS Error
R1/1	81	4.24 E6	229	492 (11)	2.15
R1/2	66	4.07 E6	248	666 (20)	2.69
R3/1	109	7.67 E6	265	610 (7)	2.30
R3/2	90	2.02 E6	150	466 (15)	3.10
R4/1	33	2.90 E6	296	714 (4)	2.41
R5/1	99	38.20 E6	621	1316 (74)	2.12
R6/1	120	8.40 E6	265	1016 (104)	4.00
T1/1	92	8.09 E6	307	681 (37)	2.22
T1/2	76	5.85 E6	278	1079 (67)	3.88
T2/1	15	0.12 E6	90	267 (13)	2.97
T3/1	92	29.39 E6	565	1061 (71)	1.88

TABLE 9.3 - SERIES B RESULTS. SAME PARAMETERS APPLIED TO ALL BEAMS.

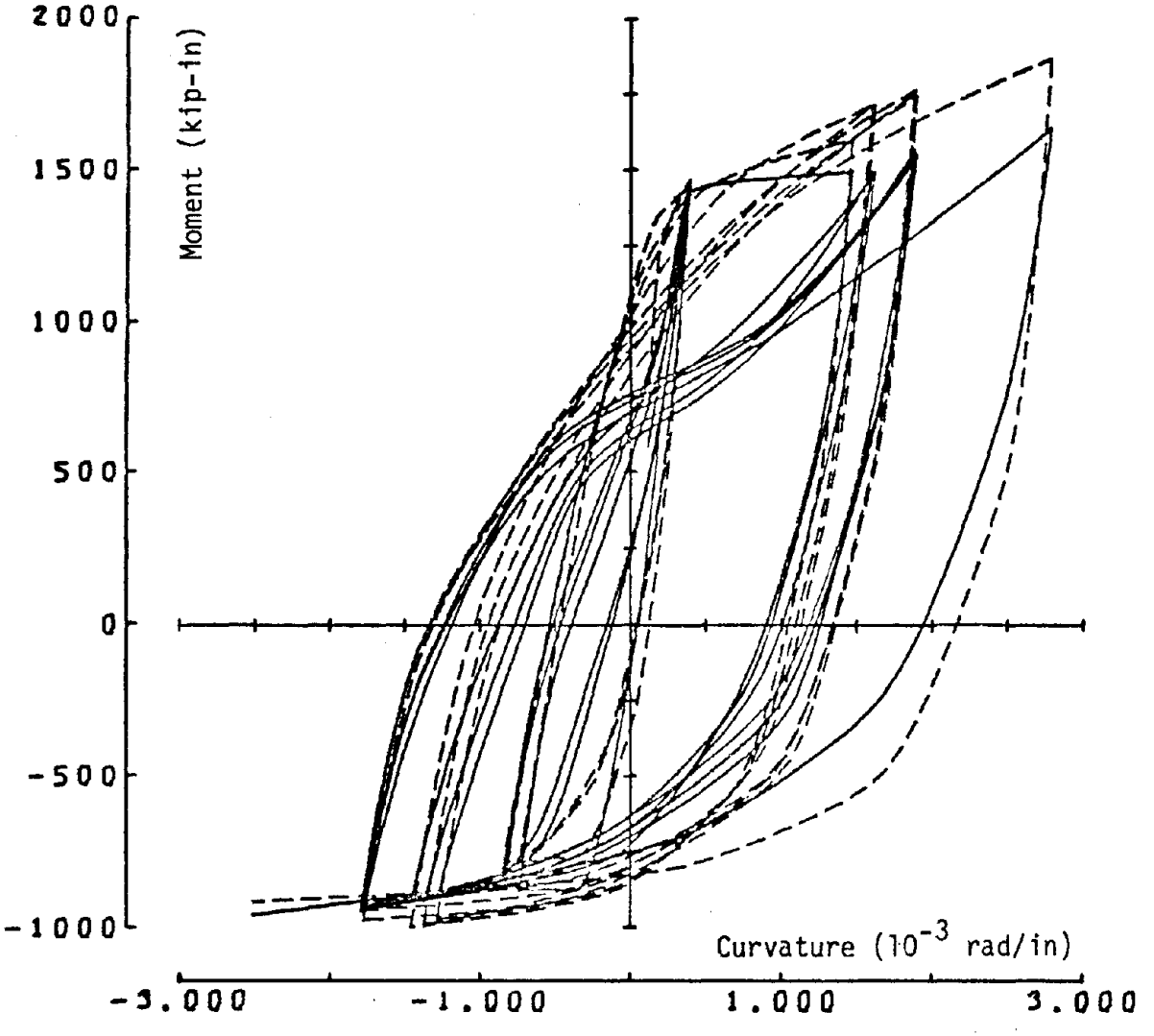

Fig. 9.1a

Series B. Moment-Curvature. Beam R1/1

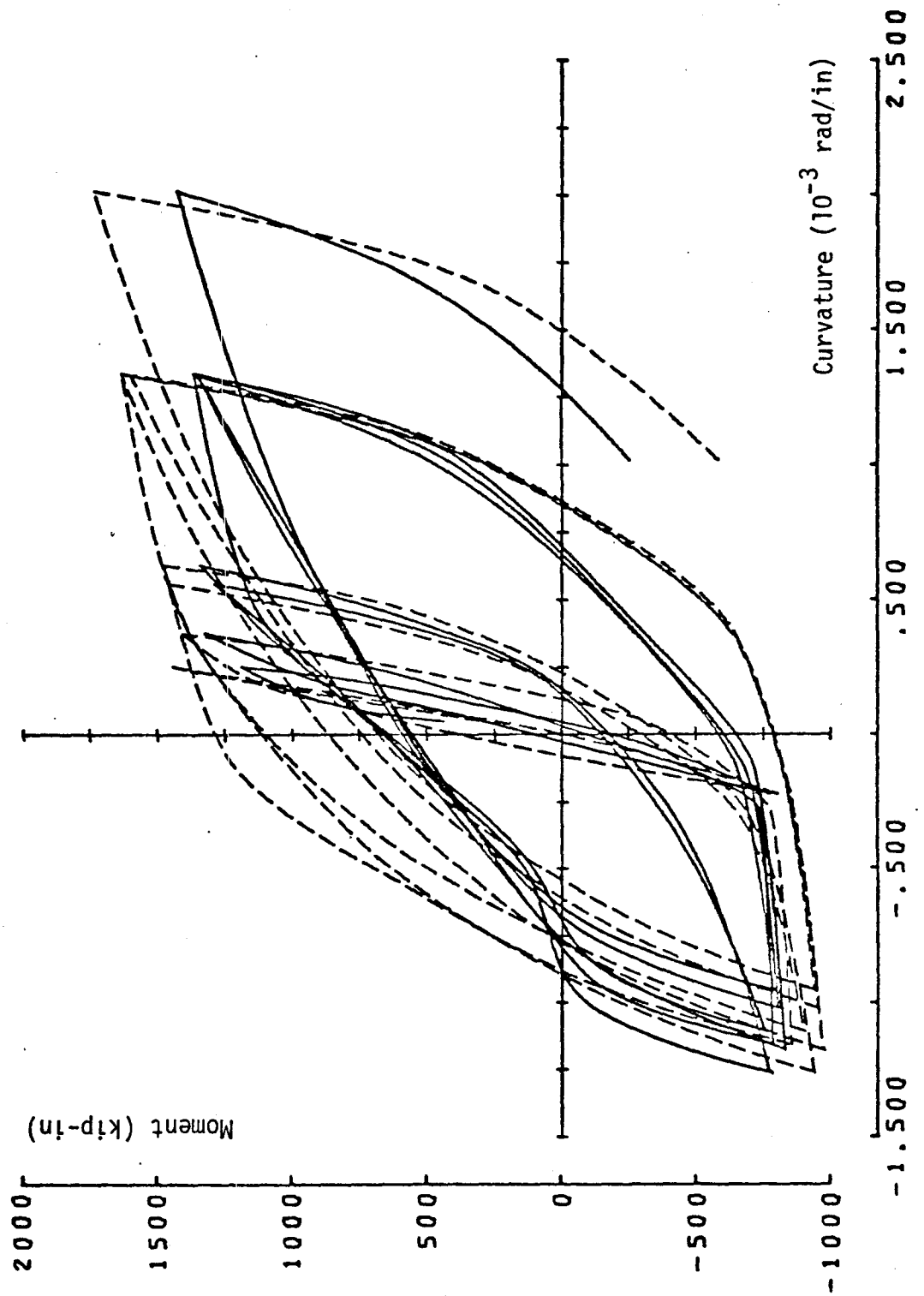

Fig. 9.1b

Series B. Moment-Curvature. Beam R1/2

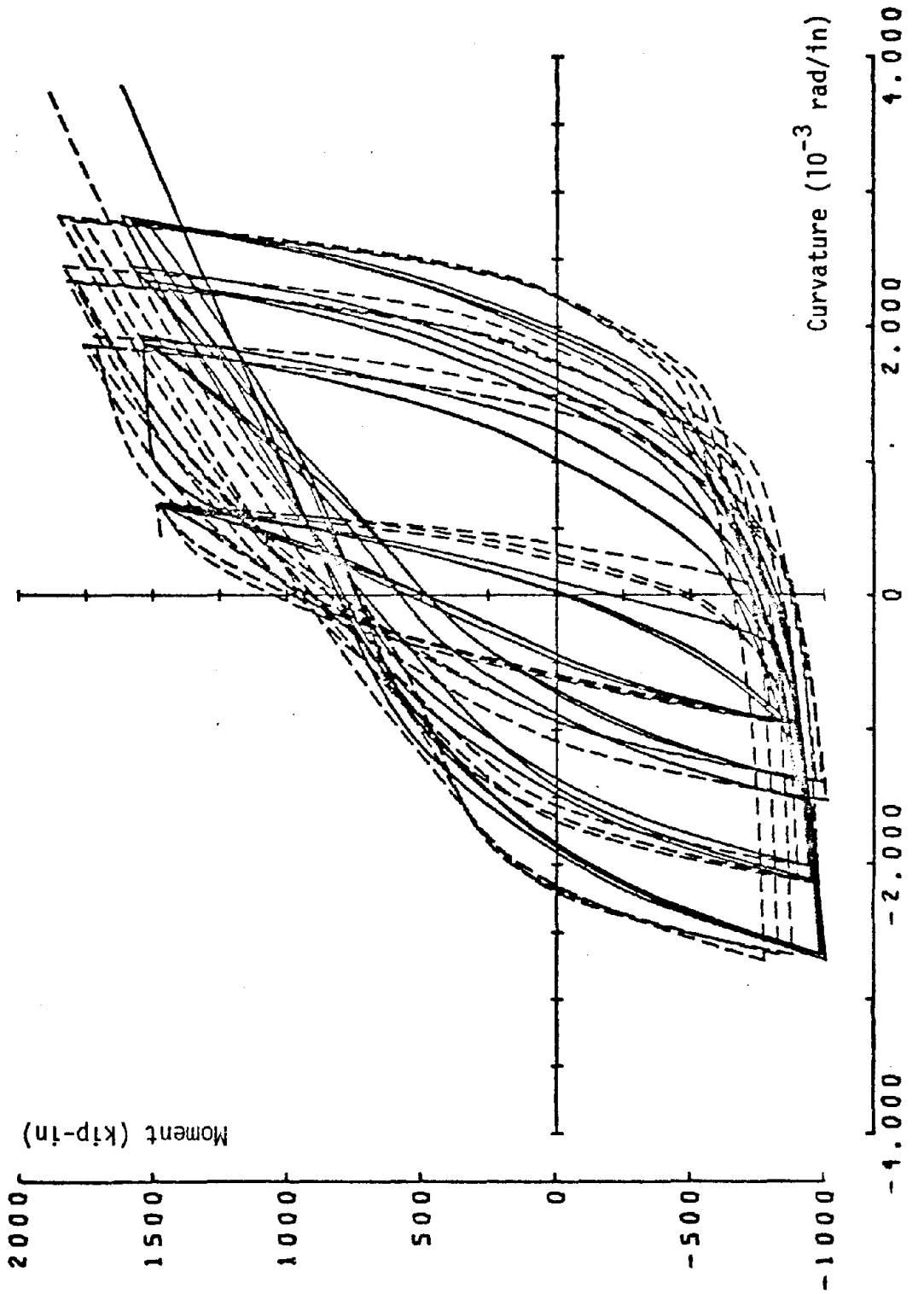

Fig. 9.1c

Series B. Moment-Curvature. Beam R3/1

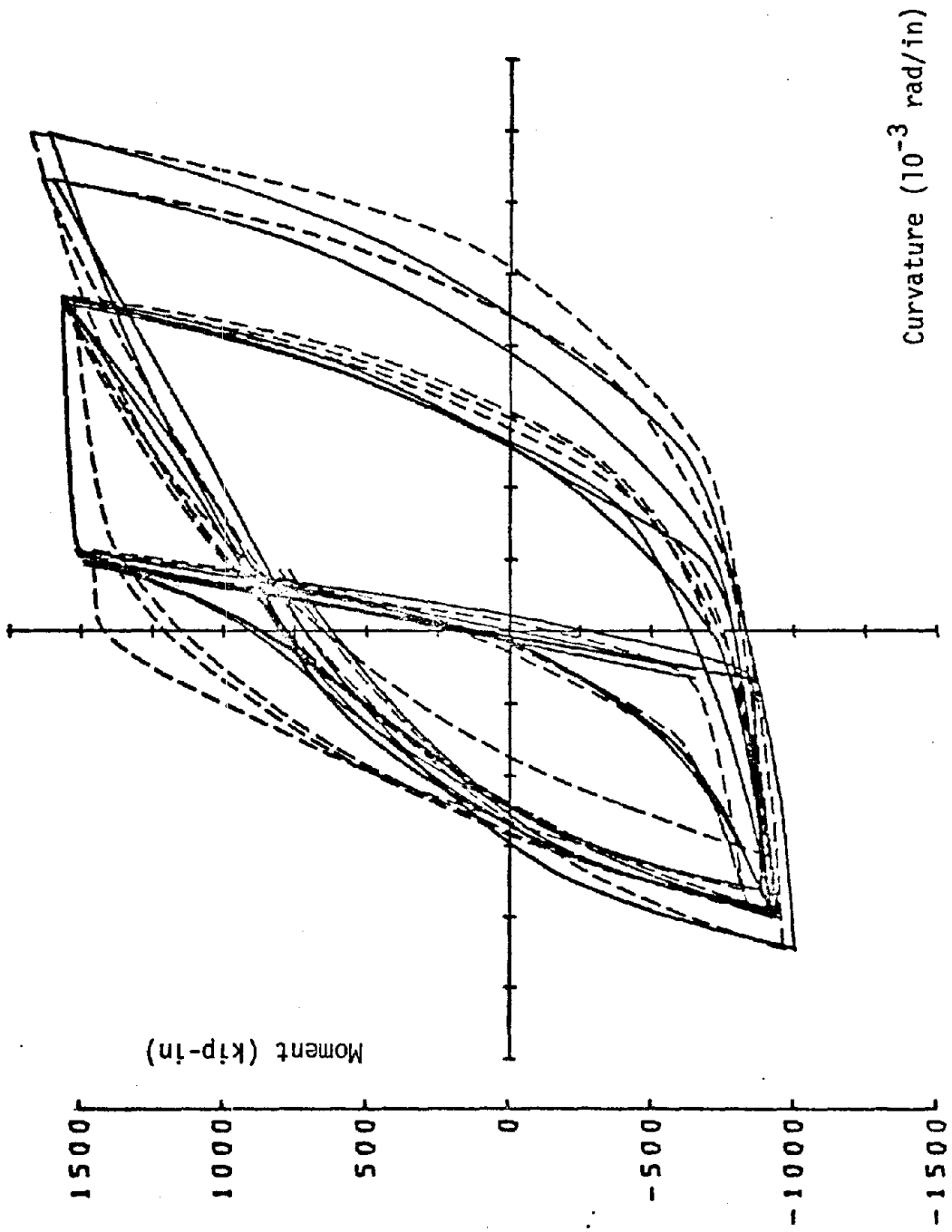

Fig. 9.1d

Series B. Moment-Curvature. Beam R3/2

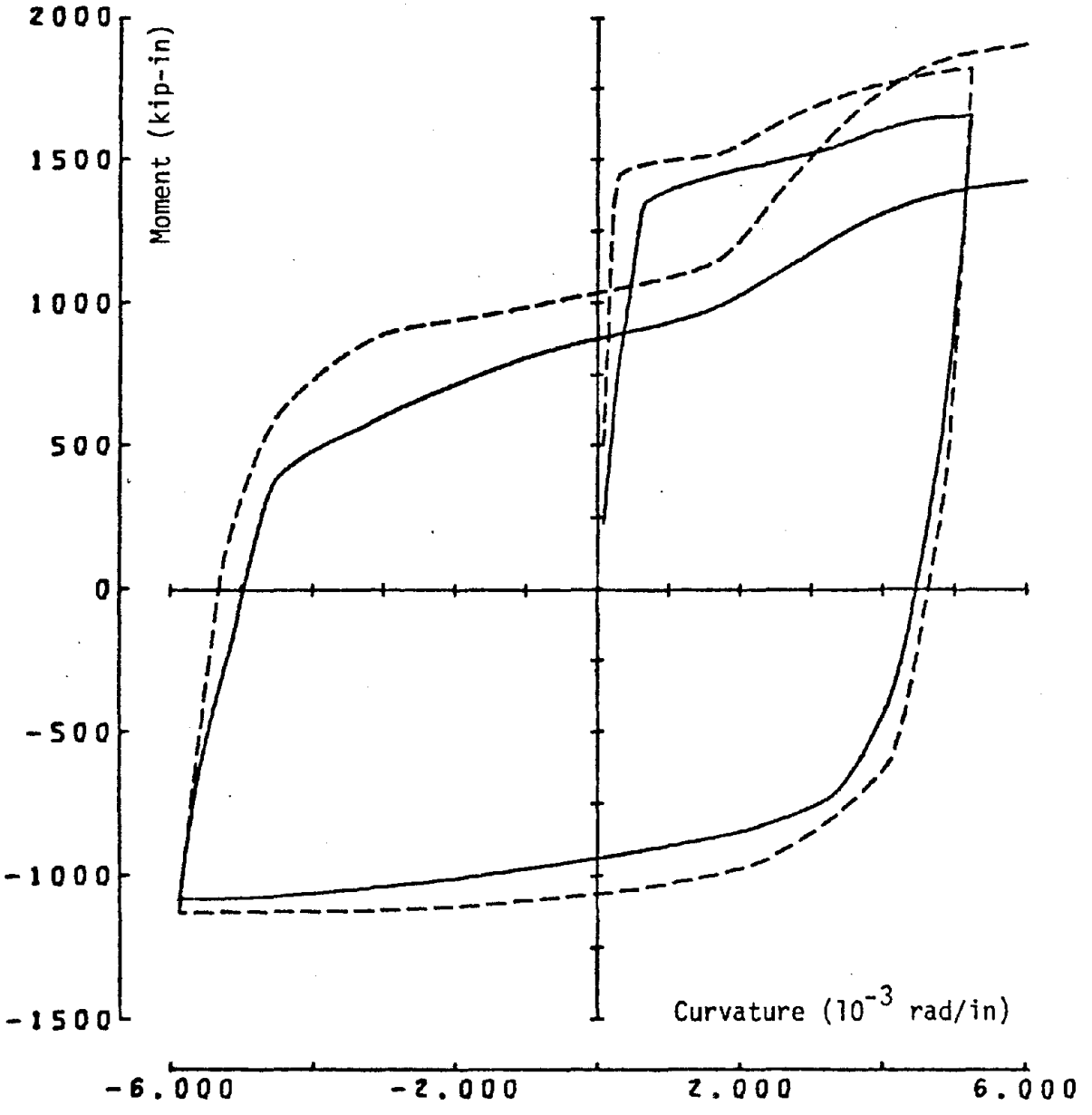

Fig. 9.1e

Series B. Moment-Curvature. Beam R4/1

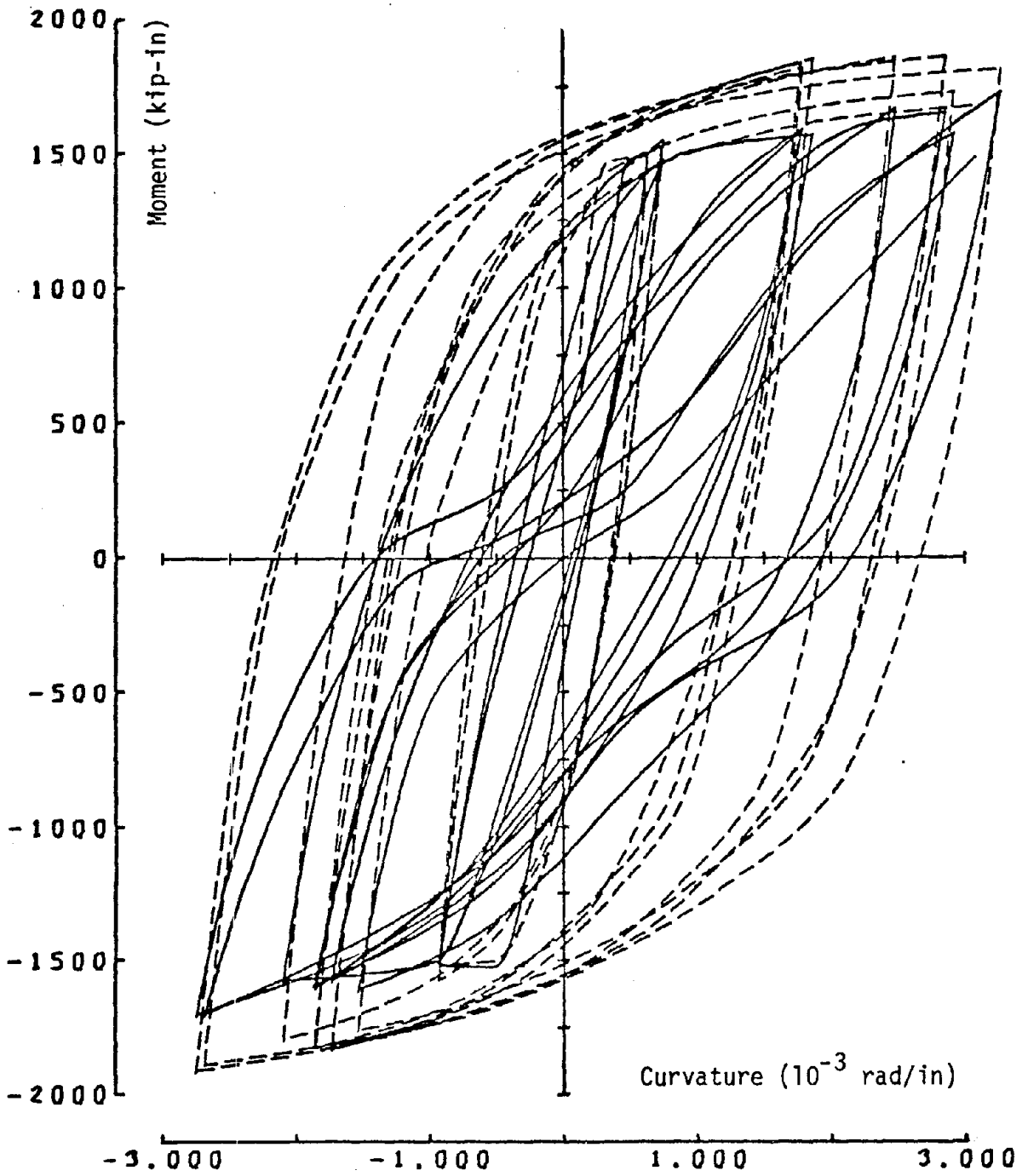

Fig. 9.1f

Series B. Moment-Curvature. Beam R5/1

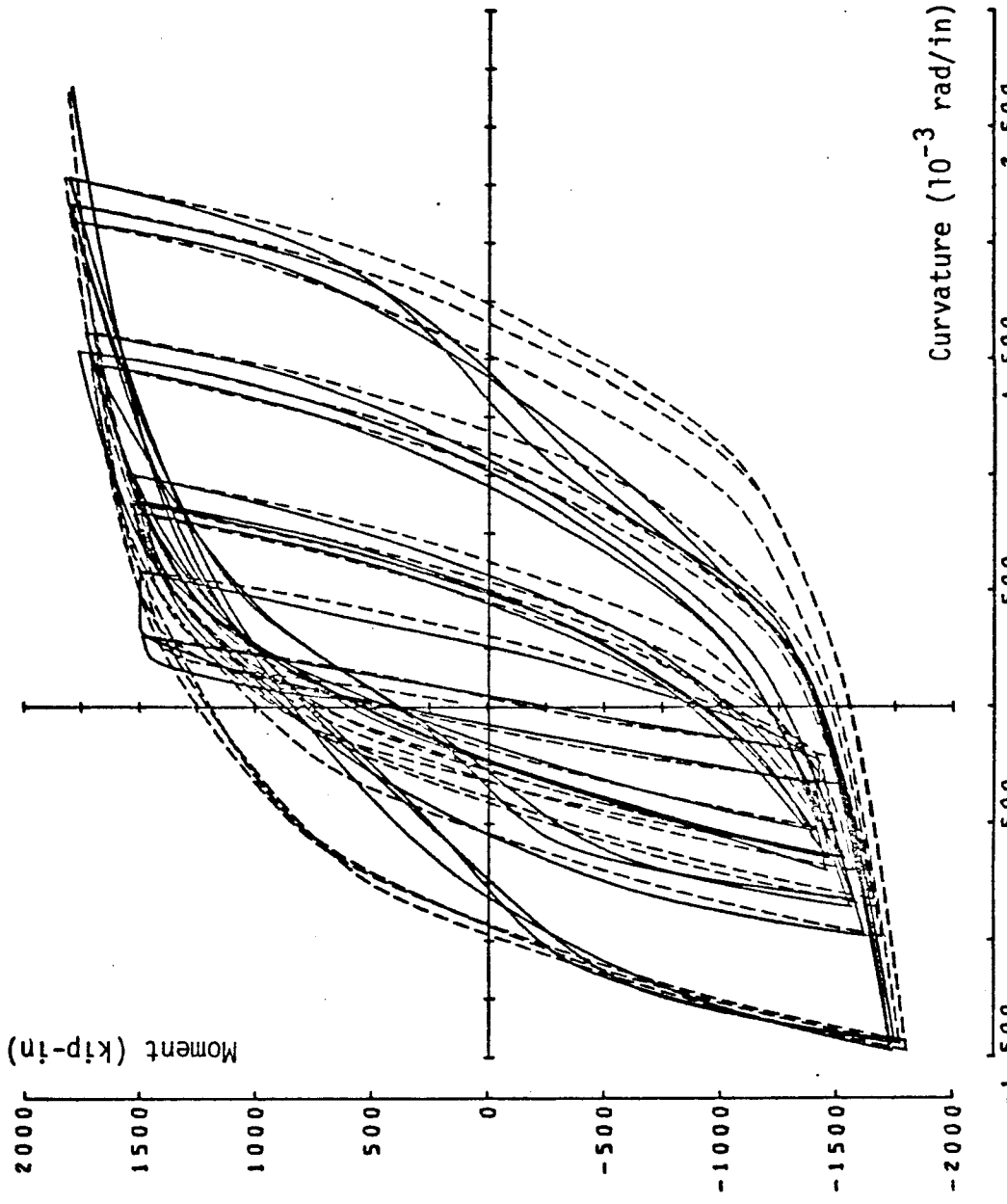

Fig. 9.1g

Series B. Moment-Curvature. Beam R6/1

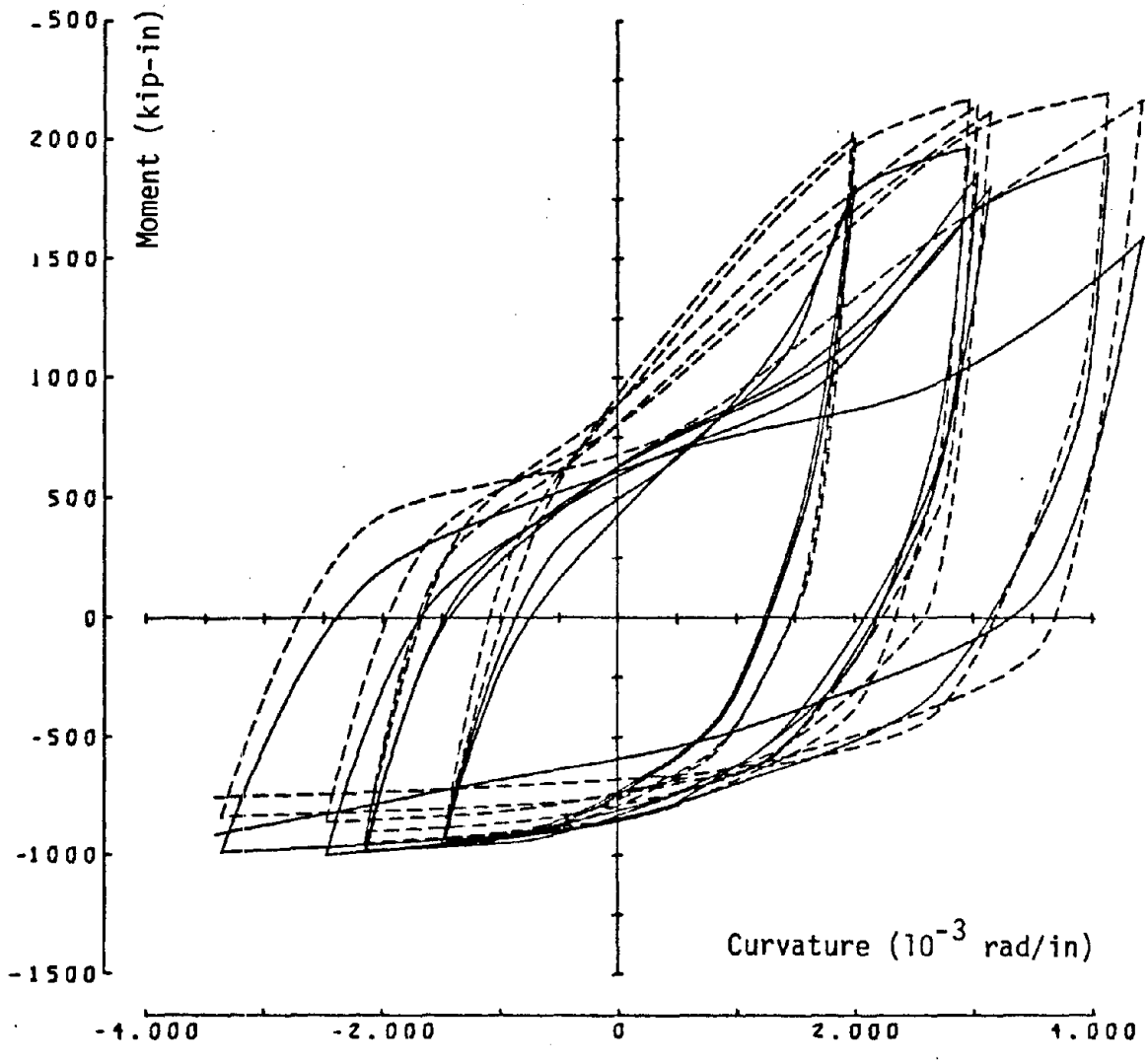

Fig. 9.1h

Series B. Moment-Curvature. Beam T1/1

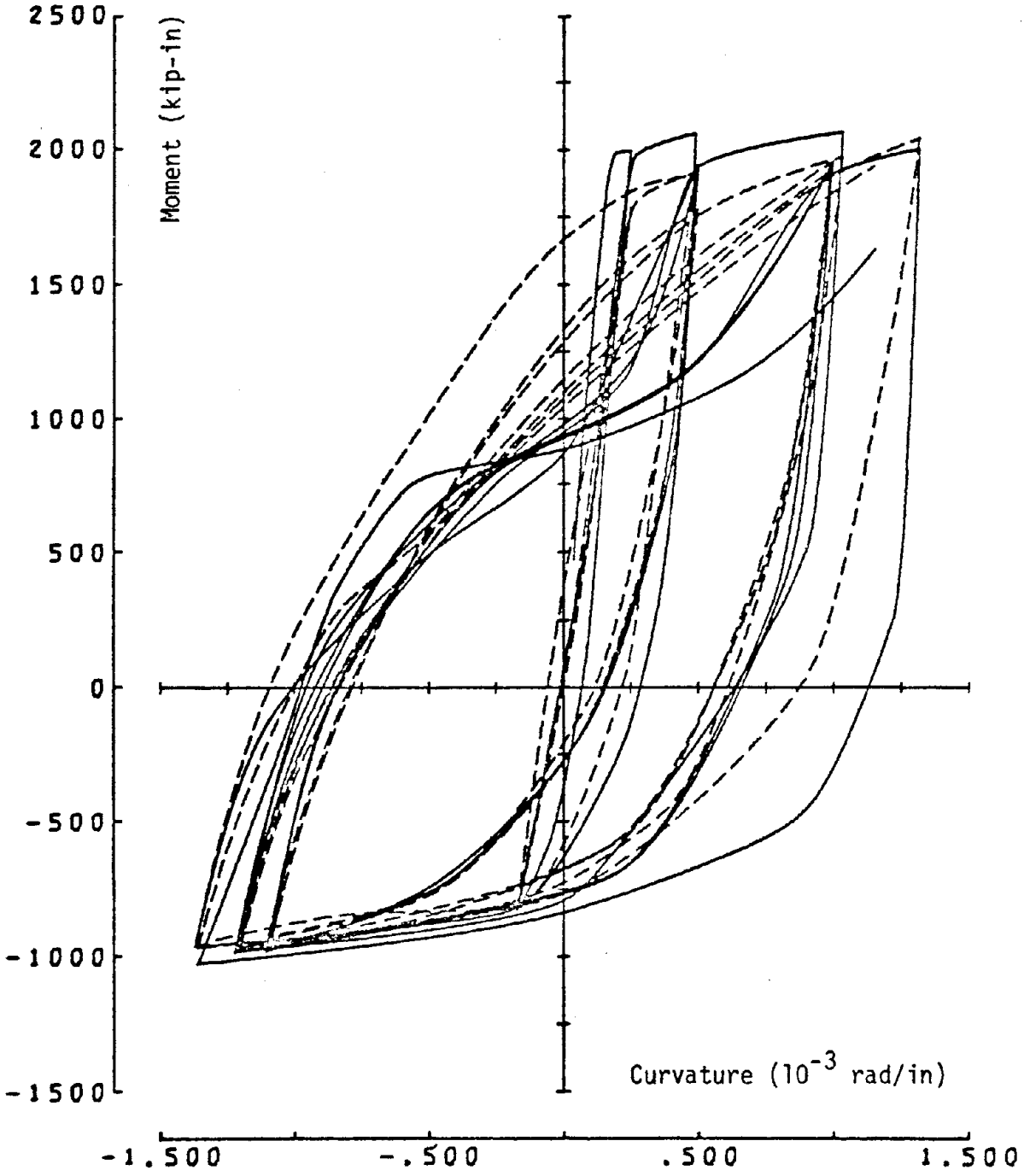

Fig. 9.1i

Series B. Moment-Curvature. Beam T1/2

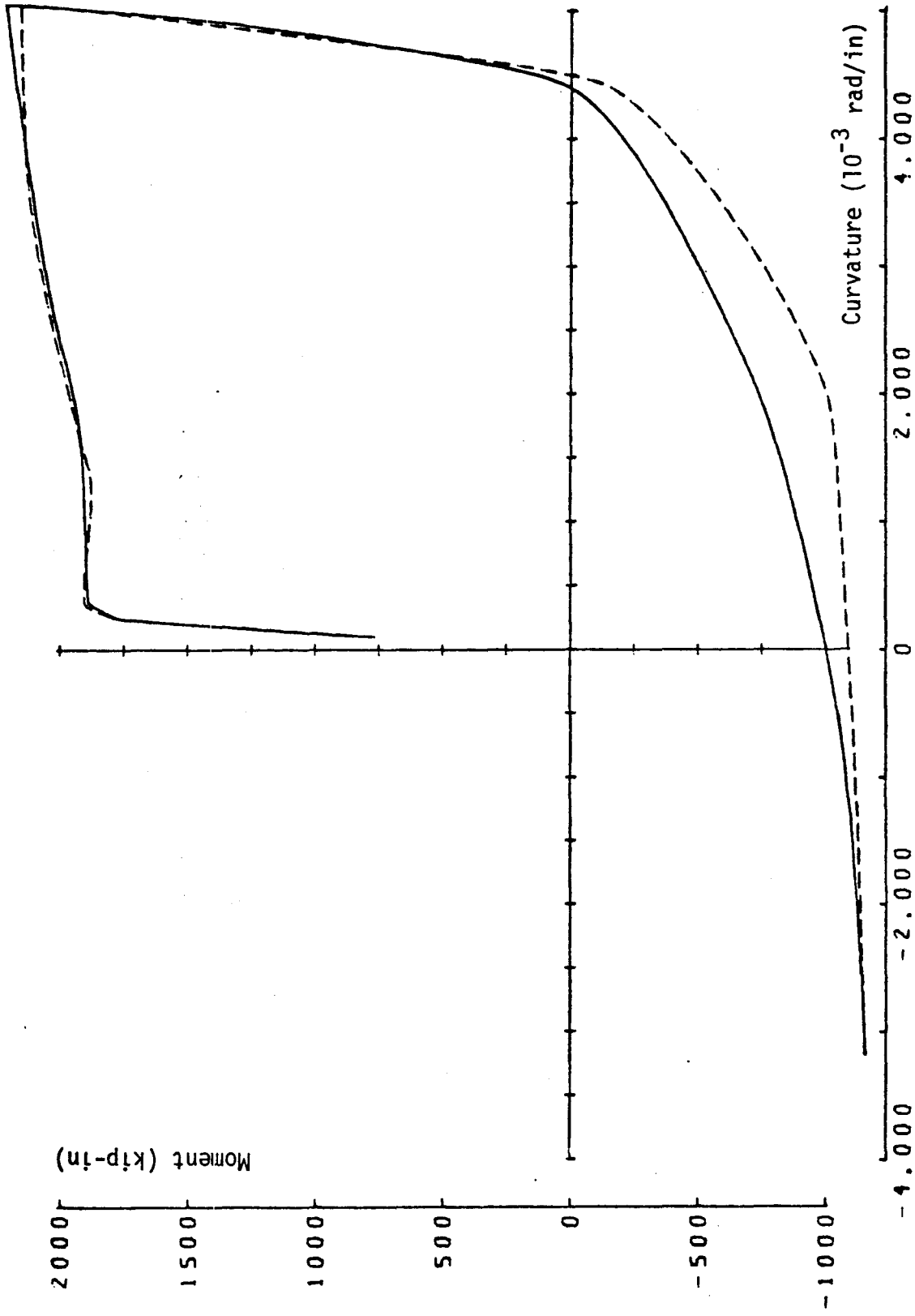

Fig. 9.1j Series B. Moment-Curvature. Beam T2/1

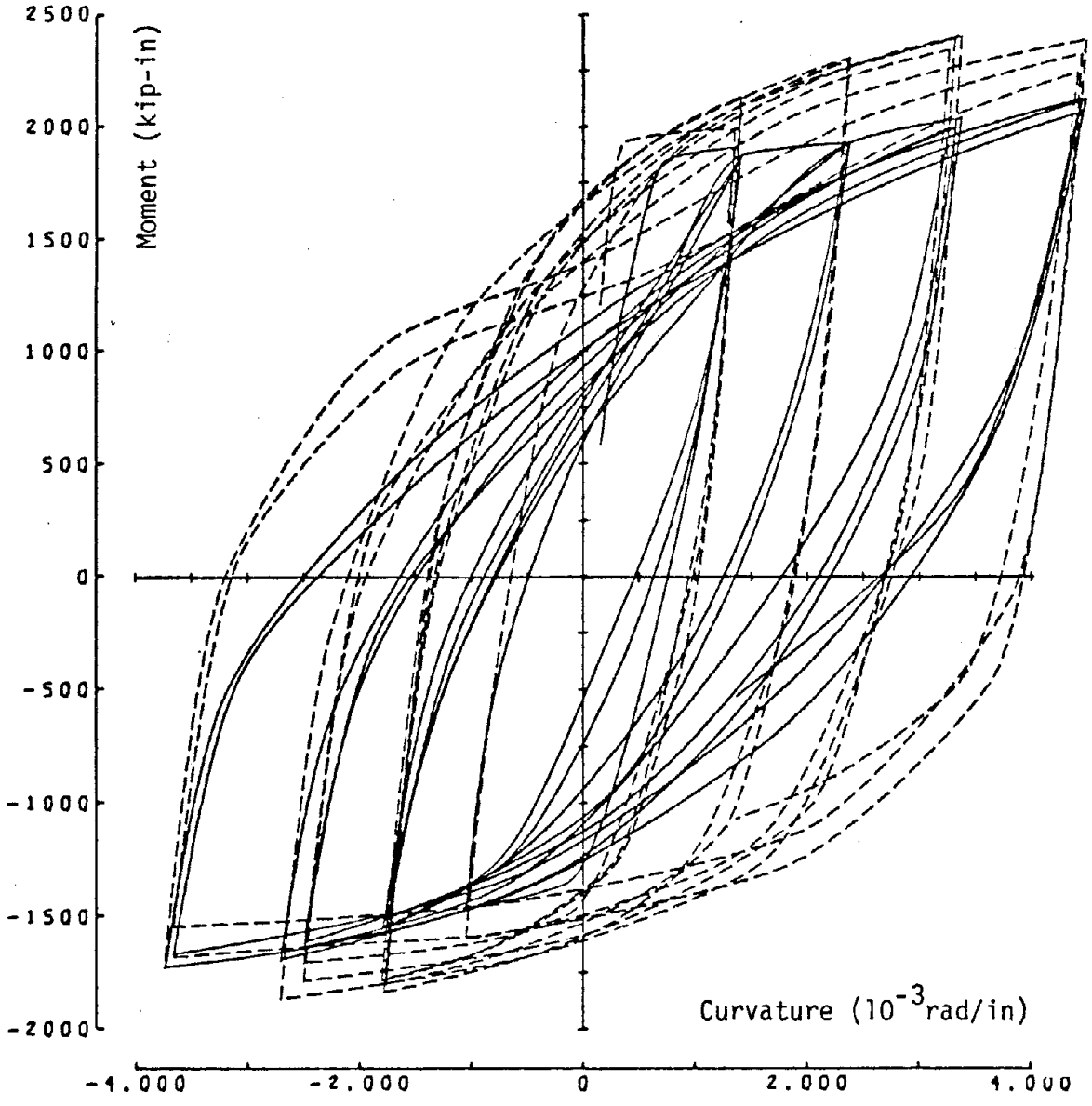

Fig. 9.1k

Series B. Moment-Curvature. Beam T3/1

Beam R3/2 has a smaller r.m.s error than most (for no obvious reason) and beam T2/1 has an even smaller one of only 90. The good result for T2/1 is explained by the fact that the concrete rubble parameter was optimized for this beam and because the beam has such a short load history that the parameters which control the decay of the beam strength are not called into play. The worst errors in T2/1 occur in the second half cycle at a point where the resisting moment is carried by the steel couple alone. A reduction in the parameter R in the steel model would reduce the error.

The error function values obtained for each beam in this Series B study are used as reference values for the subsequent studies.

9.2.3 Test Series C

The Series C tests are intended to find out what improvement can be obtained by optimizing the concrete parameters for each beam. Seven beams were chosen (R1/1, R3/1, R5/1, R6/1, T1/1, T1/2 and T3/1) and in each case the rubble parameter alone was first optimized. In two cases (R5/1 and R6/1) the optimum value established was negative, and so the moments were calculated using a value of 0.0, and no further optimization was done. The results are given in Table 9.4, and the calculated moment-curvative relations are plotted with the experimental ones in Figs. 9.2 a-g. In each beam the error function was reduced to between 45% and 95% of the Series B value. In most cases the shape of the predicted moment-curvature is noticeably closer to the experimental one in the Series C study than in the Series A one, particularly at the end of a half loop where the cracks close and the concrete starts to carry load again. Of the parameters which are identified, only ε_a shows a consistent trend, namely a reduction to approximately -10×10^{-3} from the value of

Beam	R1/1	R3/1	R5/1	R6/1	T1/1	T1/2	T3/1
Parameters							
ε_o	- 2.05	- 2.05	- 2.05	- 2.05	- 2.05	- 2.05	- 2.05
ε_a	-10.0	-10.95	-23.23	-23.23	- 7.64	-23.23	-23.23
a	0	0.15	0.15	0.15	.20327	0.15	0.15
cmx	50	50	50	50	50	50	50
r	0.218	0.263	0.0	0.0	0.189	0.240	0.0
$\frac{\partial k}{\partial \varepsilon}$	0.0	0.0	0.0	0.0	0.05	0.05	0.05
ε_{lim}	-18.0	-18.0	-18.0	-18.0	-18.0	-18.0	-18.0
f'_c	5.07	4.58	4.58	4.58	4.79	4.47	4.47
$\varepsilon_a/\varepsilon_o$	1.5	1.5	1.5	1.5	1.5	1.5	1.5
Error Function	1.96 E6	5.37 E6	28.71 E6	7.96 E6	3.87 E6	3.90 E6	13.89 E6
RMS Error	156	222	539	258	205	227	389
Max. Error	404 (3)	610 (7)	1099 (74)	882 (104)	627 (3)	1026 (67)	943 (25)
Series C/B	.46	0.70	0.75	0.95	0.45	0.67	0.47

TABLE 9.4 - SERIES C RESULTS. OPTIMIZATION OF CONCRETE PARAMETERS FOR EACH BEAM

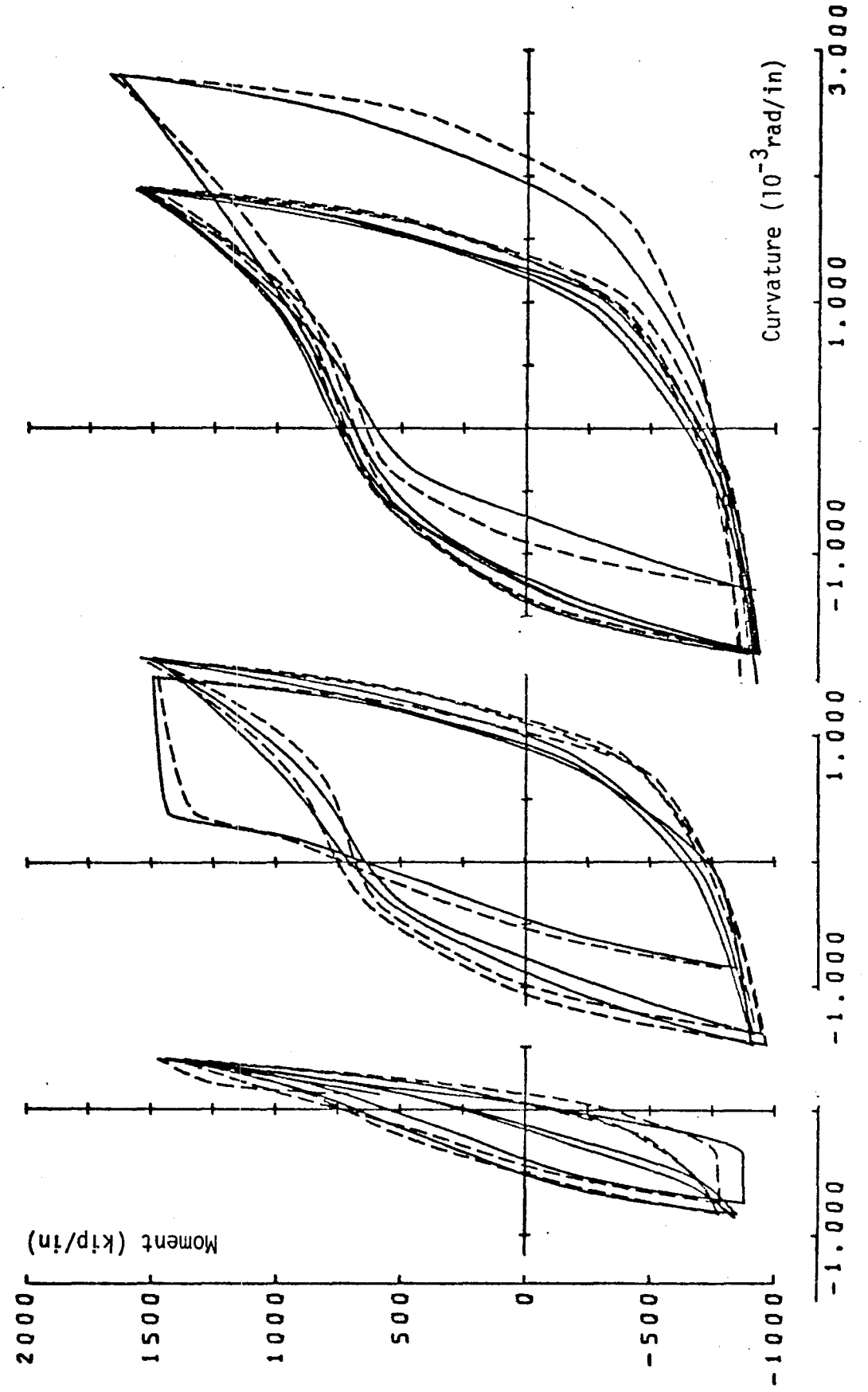

Fig. 9.2a

Series C. Moment-Curvature. Beam R1/1

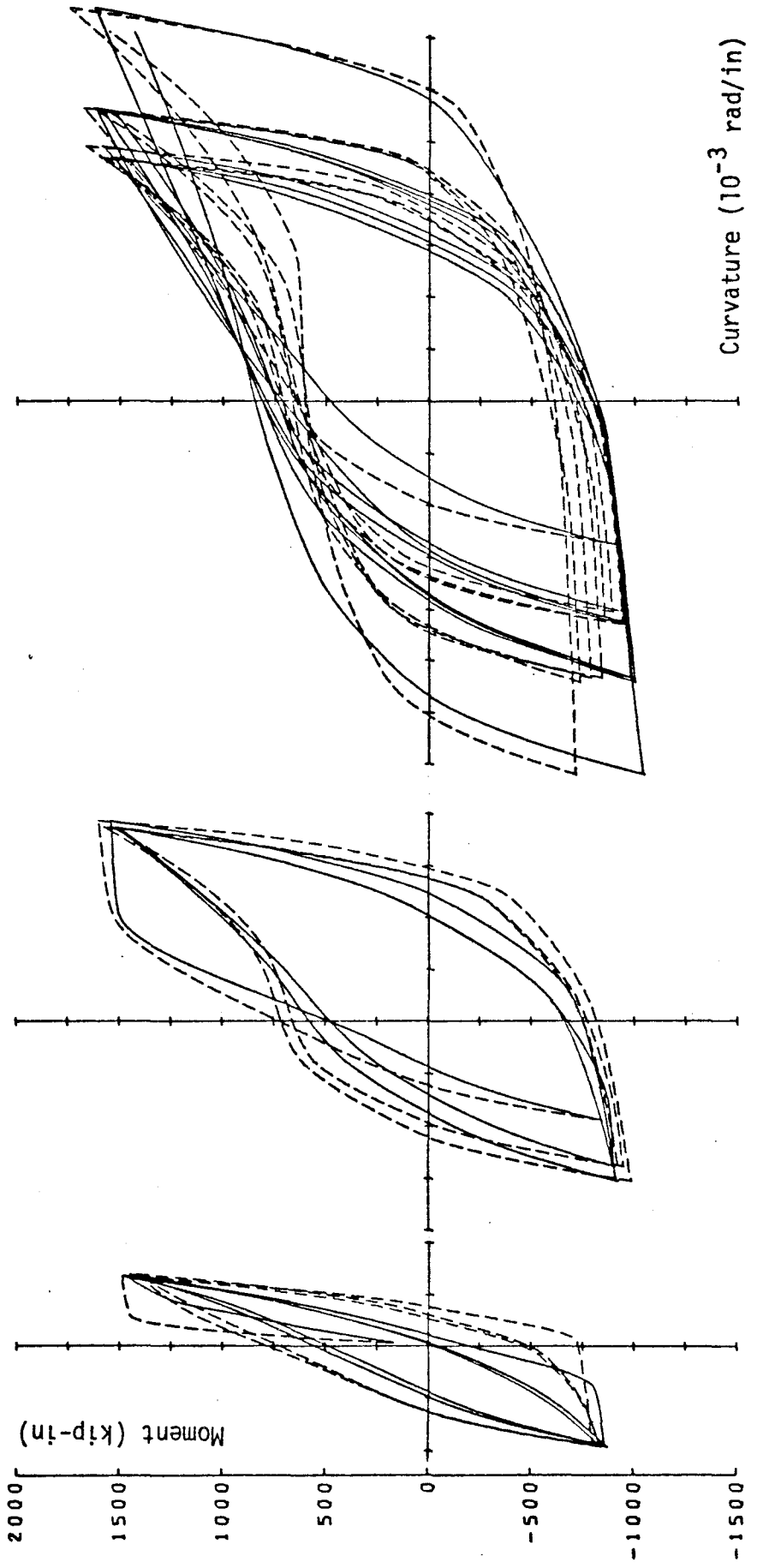

Fig. 9.2b

Series C. Moment-Curvature. Beam R3/1

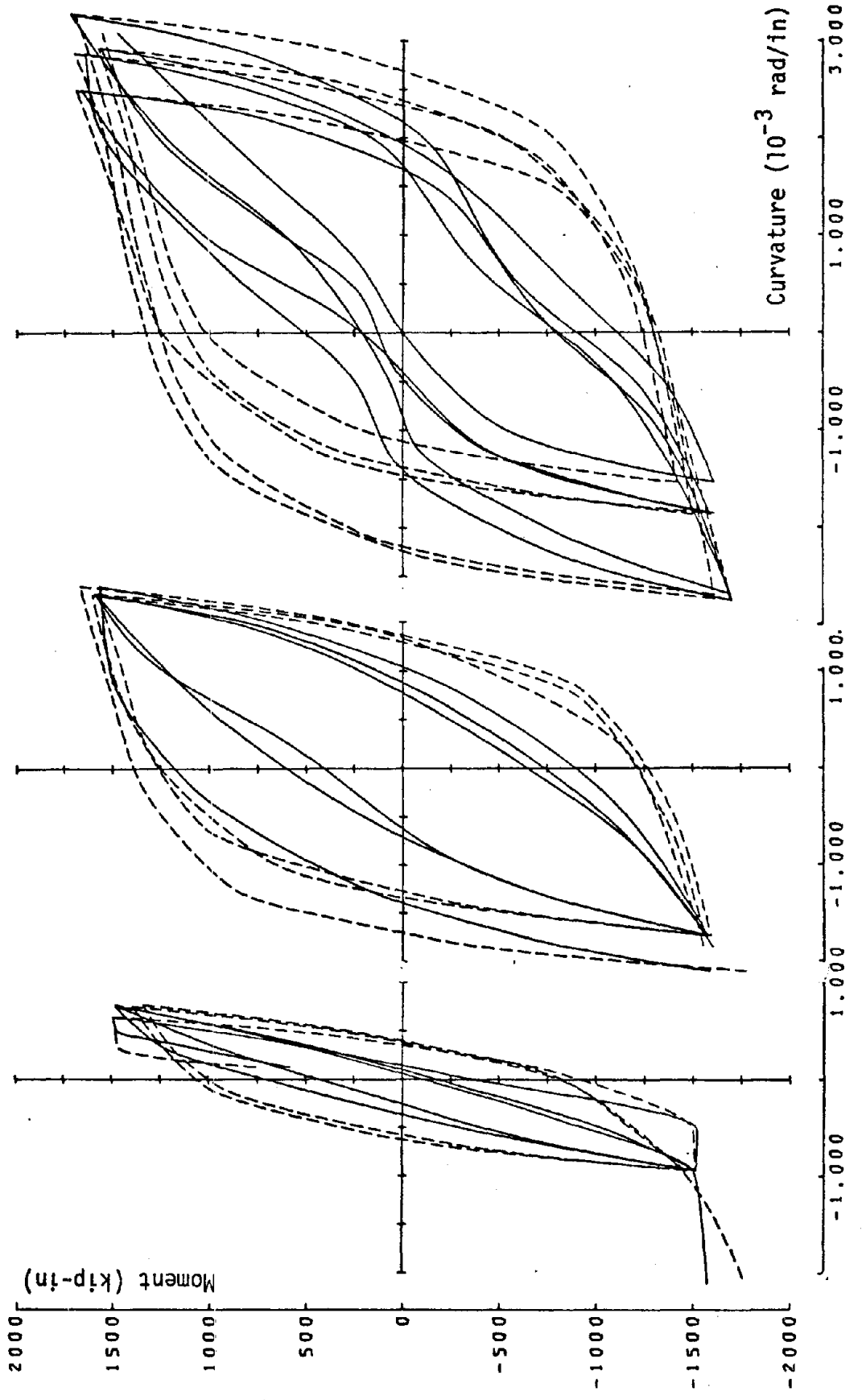

Fig. 9.2c

Series C. Moment-Curvature. Beam R5/1

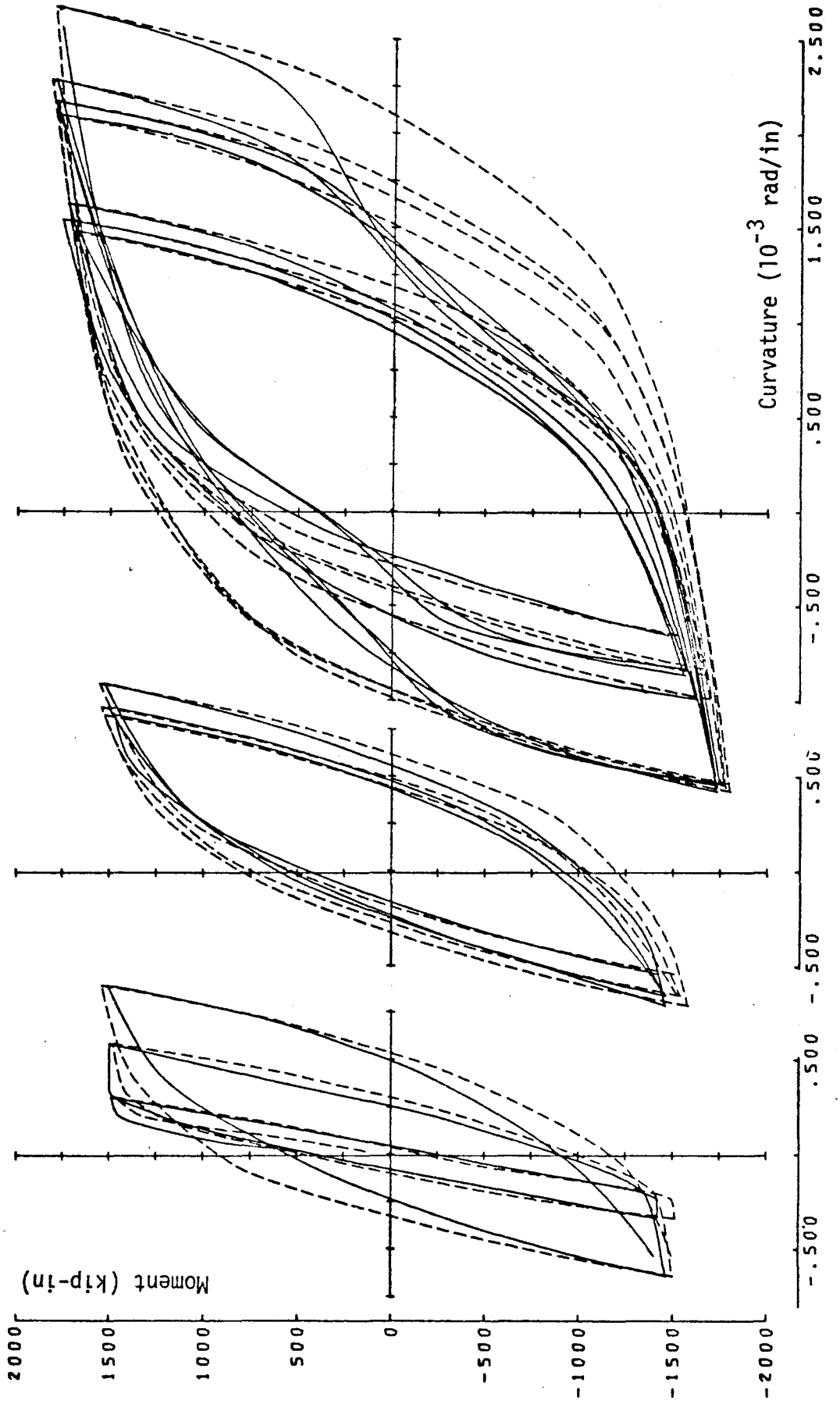

Fig. 9.2d

Series C. Moment-Curvature. Beam R6/1

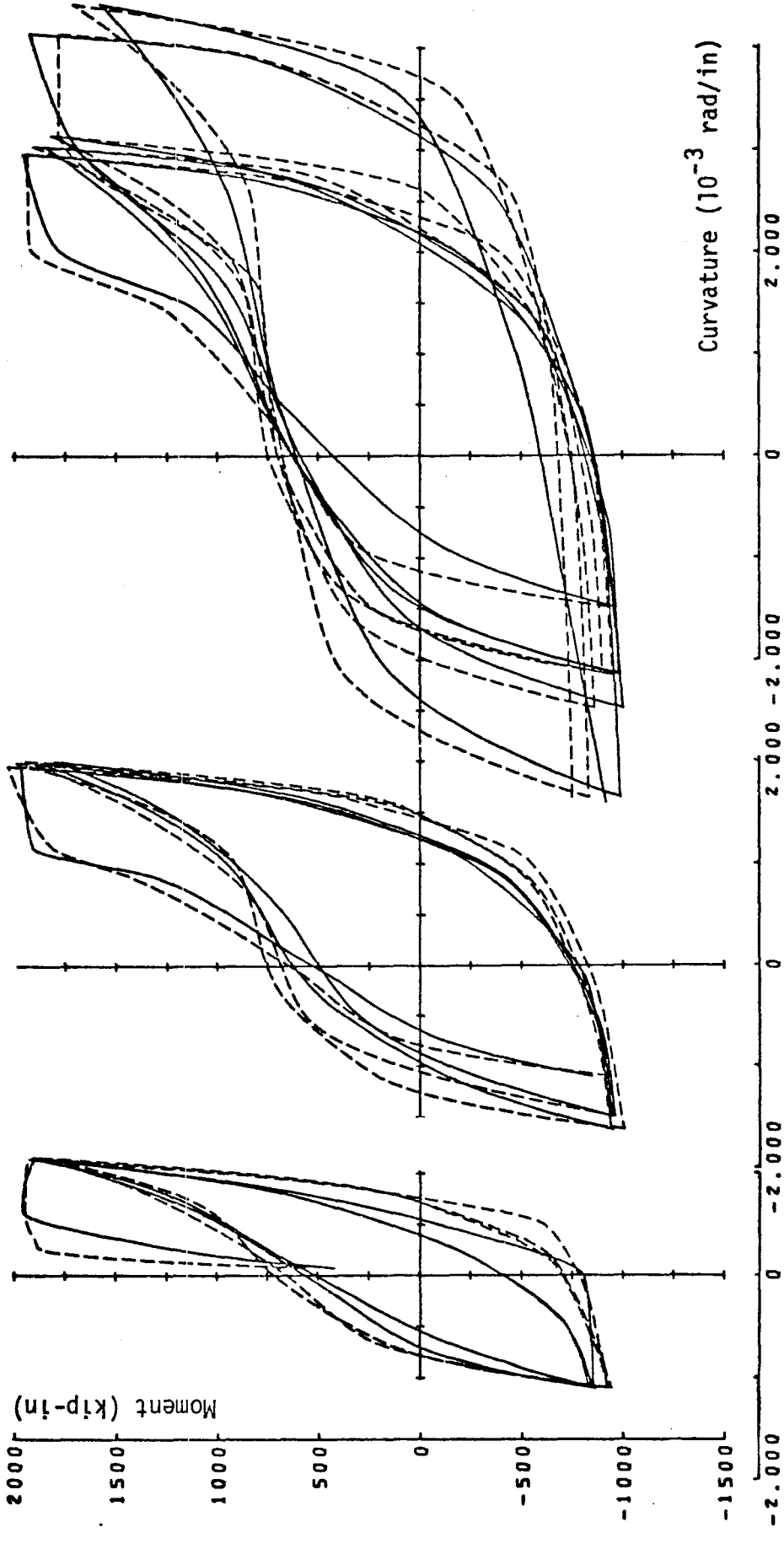

Fig. 9.2e

Series C. Moment Curvature. Beam T1/1

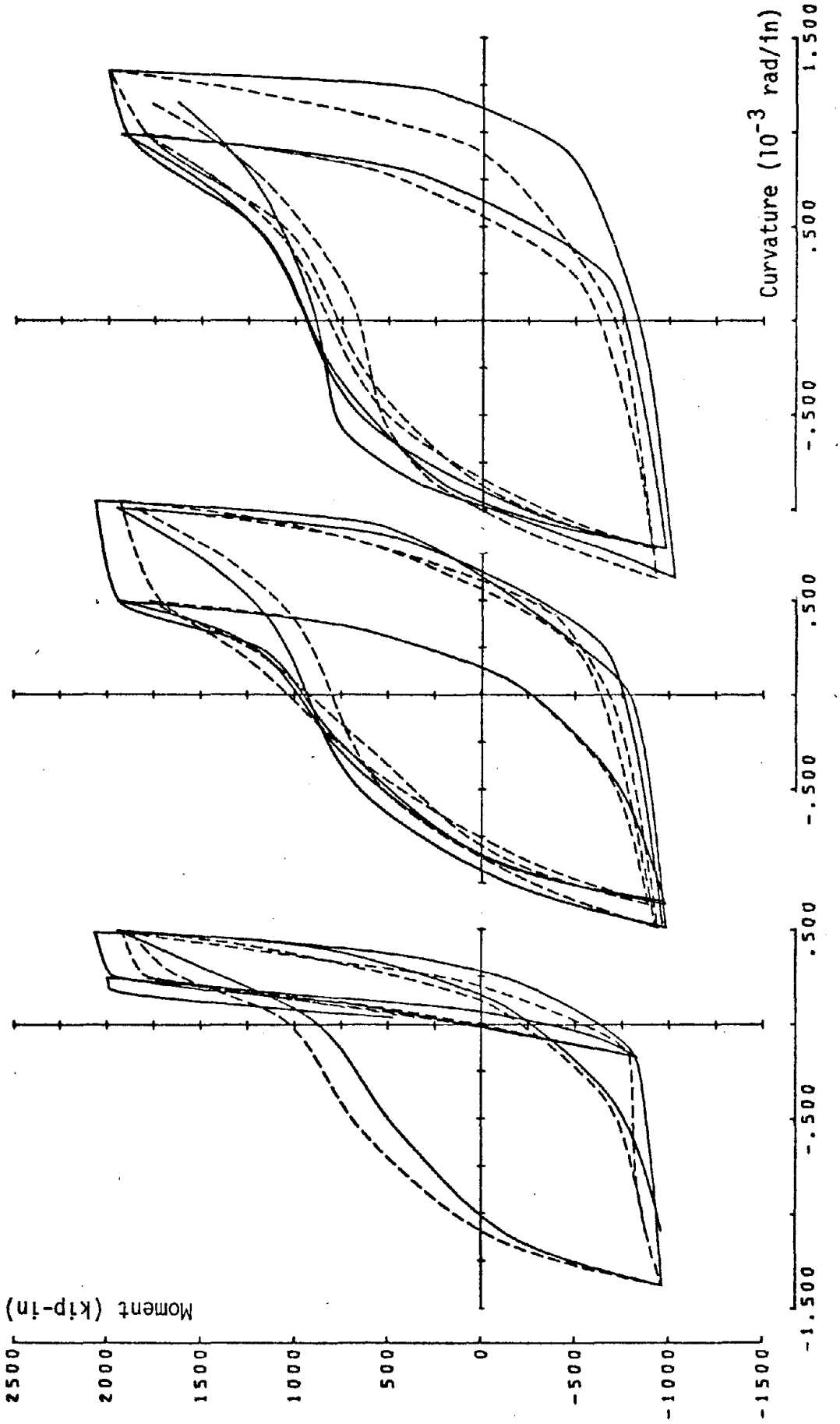

Fig. 9.2f

Series C. Moment-Curvature. Beam T1/2

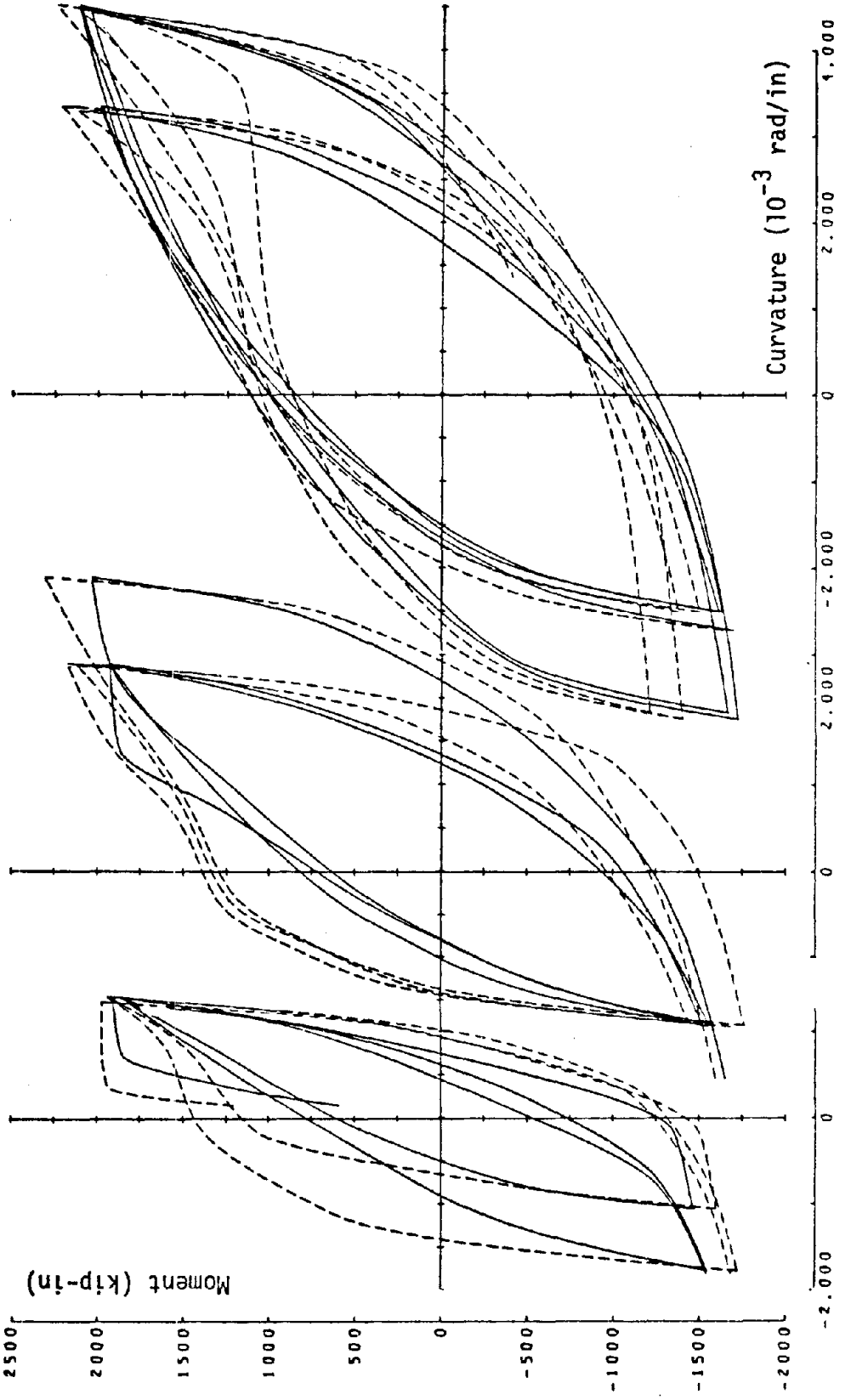

Fig. 9.2g

Series C. Moment Curvature. Beam T3/1

-23.23×10^{-3} obtained from Park's formula. The rubble parameter has a value of approximately 0.2 in all beams in which it is positive except one. In beam T2 the optimum value was 0.7.

Because ε_a had shown a reasonably consistent trend, a test was carried out on the corresponding value for the cover element (ε_c). Using the moment-curvature history of beam T1/1 the value was identified as 1.84 ε_o, comparing reasonably well with the assumed value of 1.5 ε_o.

9.2.4 Test Series D

The objective of the Series D tests was to investigate the effect of introducing the bond-slip mechanism. Preliminary tests had shown that one effect was to increase the cost of calculation by a factor of two to two and a half, so only a few beams were tested.

The early tests on beam R4 indicated that the analytical model was both stronger and stiffer than the test specimen, and the bond-slip model was developed in order to rectify the discrepancy. Therefore beam R4 was one of those chosen to include bond-slip. The others were:

T2/1 because it has a short load history

R5/1 in the hopes of improving the poor fit

R6/1 because it contains only one bar size and so should be simpler to identify.

The first trial runs were performed with beam T2. The bond-slip parameters found by identification from Viwathanatepa's tests on a #6 bar are:

$x_1 = PF = 5.0$	$x_5 = E_{\infty o} = 3.84$	$x_9 = R/P_o = 0.05$
$x_2 = P_{\infty oT} = 46.92$	$x_6 = d_2/dam = 0.267$	$x_{10} = E_{oo} = 39.0$
$x_3 = P_{\infty oc} = 43.62$	$x_7 = E_{\infty a} = 0.14$	$x_{11} = E_{oa} = 0.136$
$x_4 = E_{uo} = 39.3$	$x_8 = P_{\infty a} = 0.037$	

Beam T2 contains #2, #5, and #6 bars, but for want of better information the values given above were used as initial estimates for the parameters in all the bars. Variations of all thirty-three of them (eleven for each of three bar sizes) is too time-consuming a task to be practicable, so four parameters ($P_{\infty oT}$, $E_{\infty o}$, E_{oo} and R/P_o) for each bar were selected for variation. Experiments with the bond-slip model itself (Chapter 6) had shown that, besides the four parameters above, d_2 is also important, but it was not used here because T2 and R4 have such short load histories that the value of d_2 has no influence on the error function. A predicted moment history was calculated for beam T2/1 using these initial parametric values, and the error function was exactly twice as large as it was when perfect bond is assumed. The parameters were then varied one by one to determine which had the greatest influence on the response. Only variations in E_{oo} and $P_{\infty oT}$ in the top bars (#6) made any appreciable difference. Next, the four parameters in each bar size were taken as a group, and in three separate runs the error function was minimized with respect to each group. This was done with the intention of finding good initial estimates for the parameters before attempting to minimize all twelve at once. Finally, all twelve parameters were set free to be adjusted and their optimum values found. The complete set of bond-slip parameters at the approximate minimum is given in Table 9.5. The resulting curve is plotted in Fig. 9.3a and the associated errors are:-

	Error Function	R.M.S. Error	Worst Error	At Point
Without Bond-Slip (Series B)	122209	90.262	267.0	13
With Optimal Bond-Slip Parameters (Series D)	126831	91.995	188.5	3

Parameters	#5 bars (bottom)	#6 bars (top)	#2 bars (slab)
x_1	5.0	5.0	5.0
x_2	16.9	200	388
x_3	67.0	60.0	58.0
x_4	500	500	500
x_5	3.85	4.106	3.88
x_6	0.3	0.3	0.3
x_7	0.15	0.15	0.15
x_8	0.04	0.04	0.04
x_9	0.0227	0.0628	0.0428
x_{10}	105.2	183.6	100
x_{11}	0.136	0.136	0.136

TABLE 9.5

SERIES D RESULTS

OPTIMUM BOND-SLIP PARAMETERS FOR BEAM T2/1

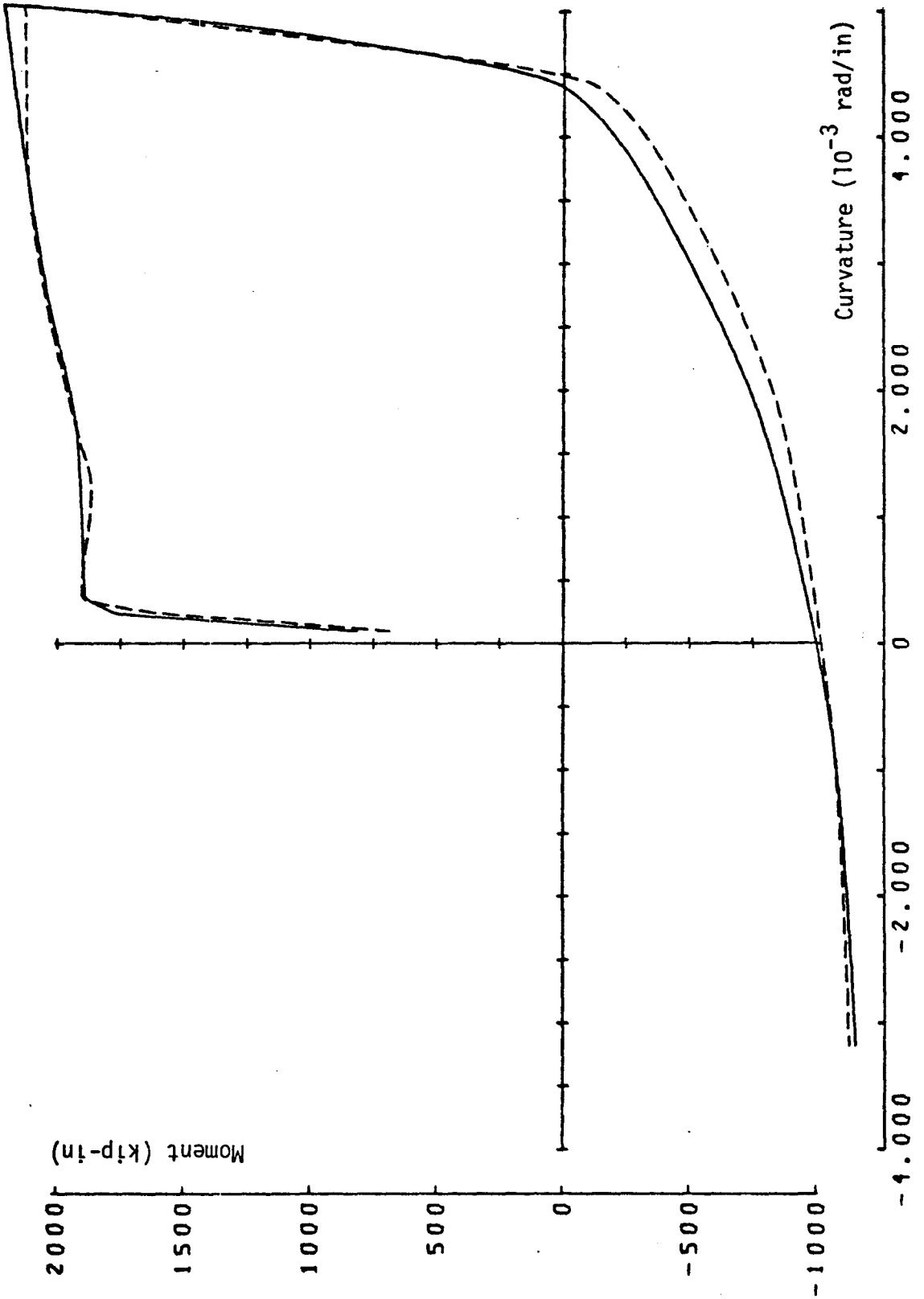

Fig. 9.3 a

Series D. Moment-Curvature. Beam T2/1

Thus the error function has a value 2% larger than it has when perfect bond is assumed, but the worst error is reduced by 30%. So, with the least square error function chosen, the best policy is to assume perfect bond, but if instead we were to use for the criterion the maximum absolute error, just the opposite would be true. The curve which includes bond-slip appears in the plots to lie closer to the experimental results than does the one which assumes perfect bond. The reason is that in the former case the maximum error lies at point 3, on the initial elastic section of the curve, where it is less visually apparent than if it lay on the inelastic segment.

These experiments with the bond-slip model were particularly tedious to perform because the computer runs frequently stopped. Problems were caused by the occasional failure to converge of the iteration procedure which divides the total strain at the bars into a steel strain component and a slip component. Some failures were caused by internal inconsistencies in the bond-slip model, which did not operate as originally intended when two load reversals succeeded each other so rapidly that the load did not fall to zero between them. The computer code is sufficiently complicated that the cause of the errors was not easy to locate. The iteration also failed to converge in the limiting number of cycles if the minimization algorithm assigned to one of the bond-slip stiffness parameters a value which differed radically from the bar stiffness. Under these circumstances the iterative calculation converges slowly and may not meet the tolerance before reaching the iteration limit.

The optimal bond-slip parameters found in the T2/1 tests were applied to beam R4/1, in which both the error function and the maximum error were reduced in comparison with the value calculated in Series A. The values are:

	Function Value	R.M.S.	Worst	At Point
Series B	2,896,180	296	714	4
Series D	2,316,340	265	641	5

Fig. 9.3b shows a comparison of the experimental response and that calculated including bond-slip. The fit is improved by including bond-slip, but the predicted strength in positive bending (when the top bars are in tension) is still 33% too great. The error is probably caused by buckling of the bottom #5 bars since, in the predicted analysis, the strain in them changes from +93.24 to -0.53×10^{-3} in/in. in the last half cycle of load.

The global model including bond-slip was then applied to beams R5/1 and R6/1, both of which contain only one bar size (#6). In beam R5/1 the principal discrepancy between the Series B predictions and the experimental results lies in the stiffness directly after a load reversal. Thus the three parameters E_{uo}, E_{oo}, and d_2/dam were selected for adjustment. The other parameters were assigned values which would cause the bond-slip model to affect only the elastic unloading part of the curve. E_o, E_∞ and P_∞ were kept constant throughout the load history by setting E_{oa}, $E_{\infty a}$ and $P_{\infty a}$ equal to zero. The resulting predictions are shown in Fig. 9.3c. The value of the error function with and without bond-slip is:

	Function Value	R.M.S.	Worst	At Point
Without Bond-Slip (Series B)	38,190,900	621.00	1316	74
With Bond-Slip (Series D)	8,137,590	286.70	796.4	74

and the optimizing parameters are

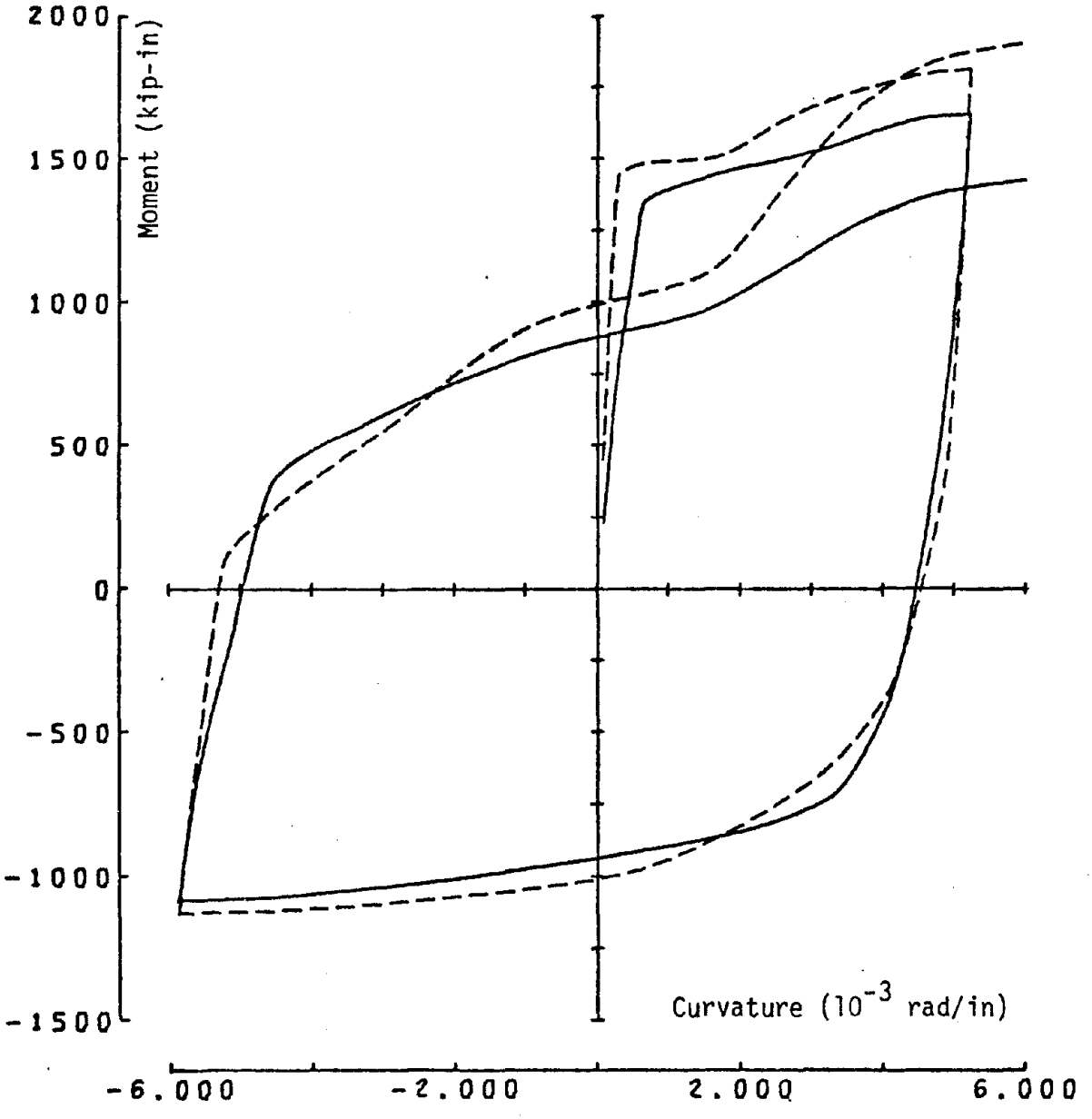

Fig. 9.3b

Series D. Moment-Curvature. Beam R4/1

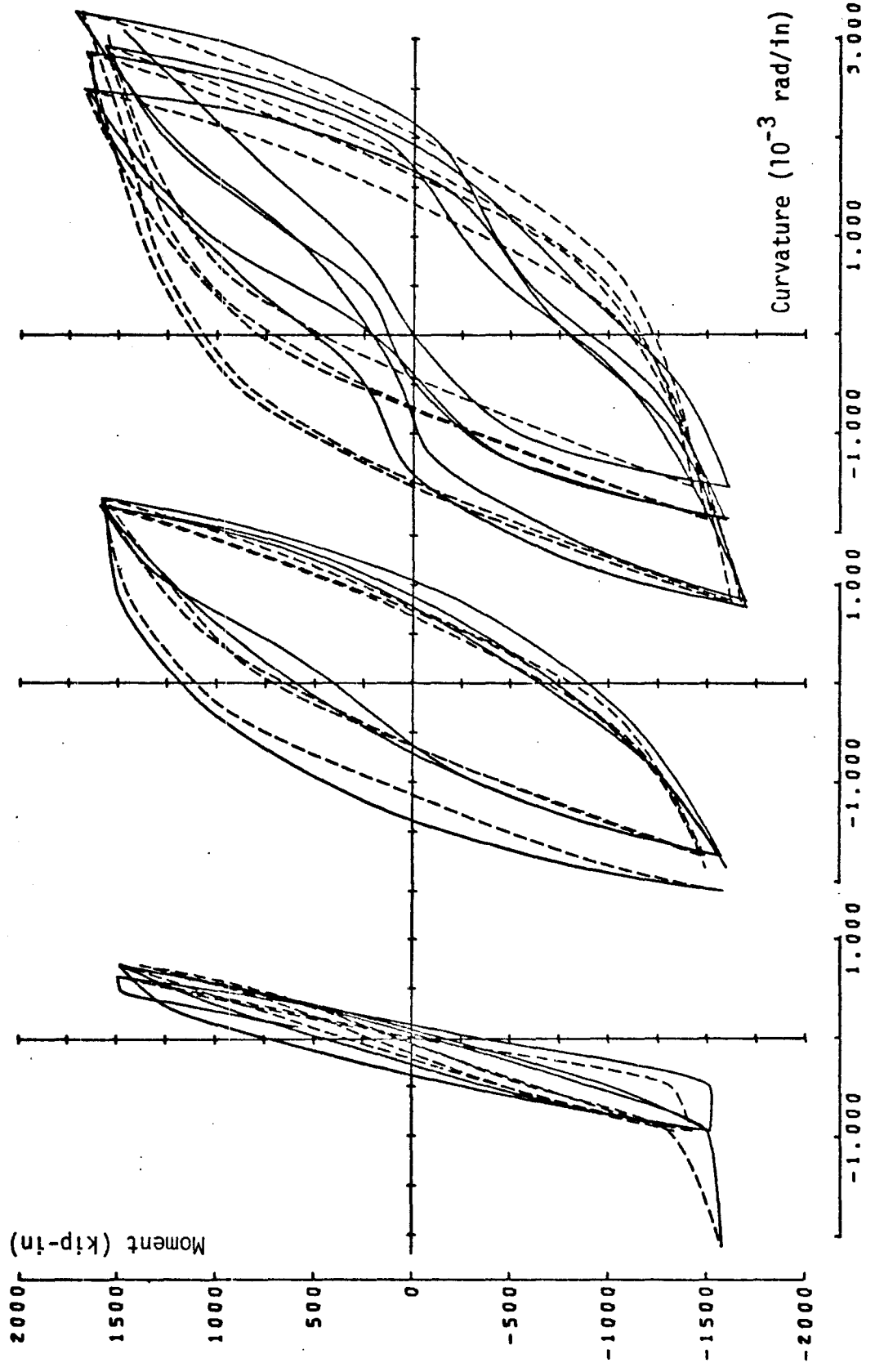

Fig. 9.3c

Series D. Moment-Curvature. Beam R5/1

$x_1 = 20$	$x_5 = 5$	$x_9 = .06$
$x_2 = 100$	$x_6 = .01$	$x_{10} = 15$
$x_3 = 100$	$x_7 = 0.0$	$x_{11} = 0.0$
$x_4 = 15$	$x_8 = 0.0$	

Fig. 9.3 c shows a comparison between the predicted and experimental results. The fit between them is improved by the bond-slip model but it is still poor, so we conclude that the influence of shear is the prime cause of the poor prediction.

A similar exercise was carried out on beam R6/1. In the Series B tests, the ratio of the maximum to the r.m.s. error for beam R6/1 is 3.83. This value is greater than or equal to the ratio in any other beam, indicating that the errors in the predicted moment history for beam R6/1 are very unevenly distributed. In the interests of economy (because R6 has a long load history) and in order to omit the worst point, the bond-slip parameters in R6/1 were optimized using only the first half of the curvature history. The optimizing parameters so established were then applied to the beam with the full curvature history. The values of the parameters and the error function are:-

$x_1 = 15.312$	$x_5 = 10.0$	$x_9 = .0206$
$x_2 = 74.31$	$x_6 = 0.0$	$x_{10} = 155.3$
$x_3 = 74.31$	$x_7 = 0.0$	$x_{11} = 0.0$
$x_4 = 155.3$	$x_8 = 0.0$	

	Function Value	R.M.S. Error	Worst Error	At Point
Series B	8,399,090	265	1016	104
Series D	5,723,440	218	953	113

The results are shown in Fig. 9.3c. $P_{\infty oT}$ and $P_{\infty oC}$ were purposely set equal, and in separate trial runs the error function proved insensitive to their value provided it was greater than 74. E_{uo} and E_{oo} were also set equal.

9.2.5 Test Series E

Series E contained a study of only one beam, namely T1/1. The results of the studies in Series A-D indicate that the steel model, even in combination with the bond-slip model, is unable to predict perfectly the response of the bars in the beam. Since it matches the results of the axial bar tests extremely well, we conclude that the bars in the beam behave differently from the steel test specimens. Inspection of the plotted moment-curvature results reveals three major types of discrepancy. The analytical model is too stiff after a reversal point, it shows too sharp a knee in the middle portion of the half-cycles of load, and the predicted strength of the beam decays too rapidly with cycling. The Series E study is an attempt to improve the match achieved by the global model without going to the expense of introducing bond-slip. The concrete parameters are fixed at their Series C optimal values, perfect bond is assumed, the eleven steel parameters retain their values, and the steel model is then modified by introducing six new parameters. They are:

E_{max}	assumed maximum value for Young's modulus (used to be 30.0 at $\varepsilon_r = 0$)
E_{min}	assumed minimum value for Young's modulus (was 22.0)
σ_{LT}, σ_{LC}	limits to envelope stress shift (tension and compression)
R_{FT}, R_{FC}	modification factor by which previously calculated R value is multiplied (tension and compression)

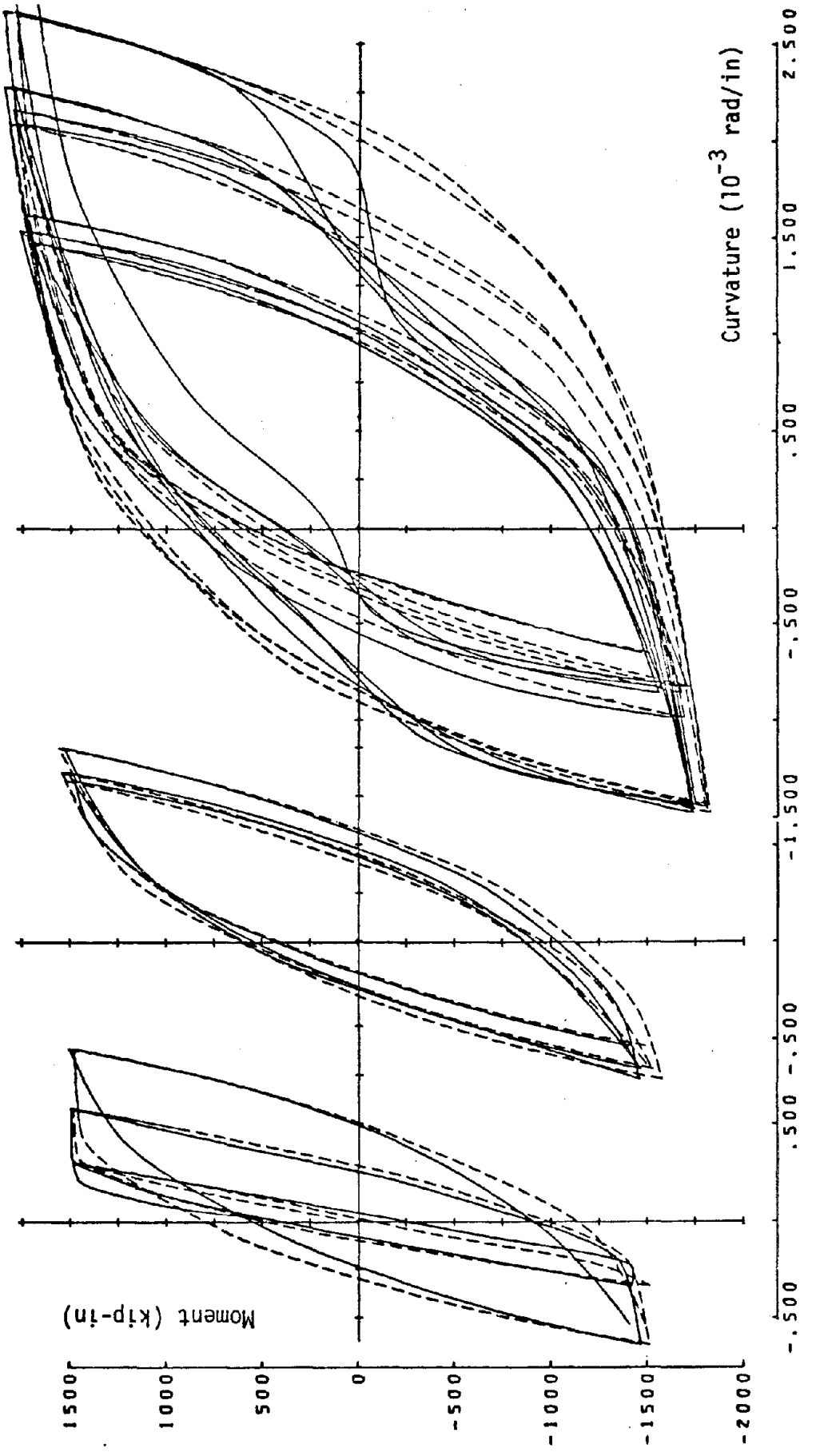

Fig. 9.3d

Series D. Moment Curvature. Beam R6/1

All other parameters were held constant, and these six were identified. Their values and that of the error function are:-

E_{max} = 19 $\quad \sigma_{LT}$ = -10 $\quad R_{FT}$ = 0.486

E_{min} = 19 $\quad \sigma_{LC}$ = -15 $\quad R_{FC}$ = 0.720

	Function Value	R.M.S. Error	Worst Error	At Point
Series B	3,873,120	205	627	(3)
Series E	1,460,870	126	626	(9)

A comparison of the Series B results (Fig. 9.1h) with the Series E results (Fig. 9.4) shows a marked improvement in the fit.

9.3 Discussion of Results

Figs. 9.1a to 9.4, which compare measured and predicted moment-curvature relations, show that in the majority of cases the form of the model is adequate to achieve its objective. Even when the values of the parameters are not the optimal ones, the predicted response has the correct shape, implying that a good model form is at least as important as optimizing the parametric values. This point is further emphasized by the fact that the optimum values for the parameters depend to some extent on the number and location of the digital points chosen to represent the continuous curve. In the present study we used about four points per half loop, located so as to pick up the salient features of the curve. More points would have given rise to parameters less sensitive to the exact location of the points but would have increased the computer time used.

The model performed worst in beams R5 (which was subjected to high

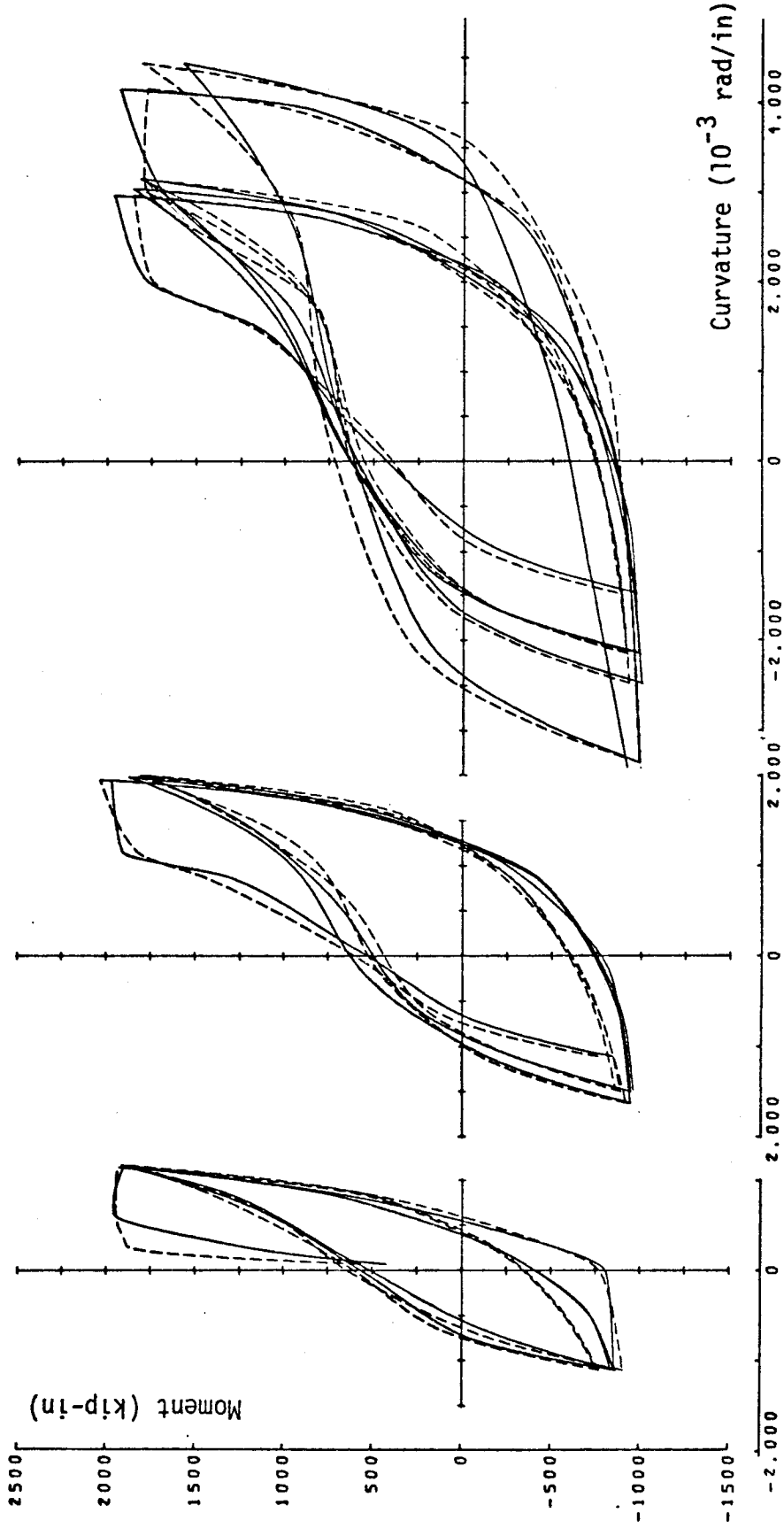

Fig. 9.4

Series E. Moment-Curvature. Beam T1/1

shear), R4 (in which the bars almost certainly buckled), and T3 (in which the beam strength was overestimated for reasons which are not clear). However, even in beam R5 the maximum moments are quite well predicted.

Most of the discrepancies between the predicted and measured moments appear to be due to inadequacies in the steel model because they occur at points in the load cycle at which the concrete is unstressed. This must call into question the assumption made in Chapter 2 that the steel in the beam behaves in exactly the same way as the steel in the test specimens. Three explanations for the differences appear plausible. One is that the bars in the beam display a modest amount of buckling and so are more flexible than those in the steel tests. The second possibility is that the machining of the steel specimens influenced the shape of the branch curves. Because Ma only performed cyclic load tests on machined specimens, the parameters which control the branch curves were of necessity established from their response. The behavior of the unmachined reinforcement was then predicted using the same branch curve parameters but the envelope appropriate to unmachined bars. The last possibility is that the bars were slipping through the concrete in a way which the proposed bond-slip relation was not able to mimic successfully.

Of the concrete parameters, the most important were the rubble parameter and ε_a, the strain at which the concrete strength becomes constant. The value of ε_a which gives the best results is about -10.0×10^{-3} (approximately half that suggested by Park's formula). However, minor alterations in the steel model could change this value significantly.

The rubble parameter showed a variation from less than 0% (which makes no sense physically) to a maximum of 70%.

The model works best in a situation where decay of the stiffness and strength do not need to be modelled, as in beam T2, provided that the bars do not buckle.

To observe the model's ability to reproduce behavior of beams which are identical but for the size of reinforcing bars, we compare the results of beams R3/1 and R6/1 and of T1/1 and T3/1. In Series B, beams R3/1 and R6/1 both had an r.m.s. error of 265 kip/in., whereas in Series C it decreased to 222 and 258, respectively. For all practical purposes both beams were equally well modelled. Comparing the two T-beams, we find that the response of T1 is much better reproduced than T3 in both the Series B and C tests. T3 was the more heavily reinforced.

The effect of the slab is seen by comparing beams T1/1 to R1/1 or R1/2 to T1/2. In both cases the rectangular beam was modelled better, although the predictions for both were adequate. Ma noted the presence of shear lag in the flange of the T-beams, which the model does not account for and which will detract from its performance. Also, the steel parameters used for the #2 bars in the slab were the same as those used for the #5 and #6 bars because no cyclic axial load tests were carried out on #2 bars. Both effects must detract from the accuracy with which the slab bars are modelled.

Comparison of R5/1 and R6/1 shows that the presence of high shear forces significantly impairs the model's ability to reproduce the moment-curvature relationship. However, the most important aspect (the maximum moment) is still adequately modelled.

The predicted values for only one beam (T2/1) come close to the

desired 5% accuracy without using the bond-slip relation. Results for most of the beams displayed r.m.s. errors which were 10-15% of the beam's strength. Thus there is still room for improvement in the model.

Chapter 10

CONCLUSIONS AND SUGGESTIONS FOR FURTHER RESEARCH

Several conclusions can be drawn from the results of this research program. The most important is that the global model achieves its objective of predicting the moment-curvature relationship of a reinforced concrete beam. It does so best in circumstances which do not violate its underlying assumptions of negligible shear and bars which do not buckle. The root mean square difference between the predicted and measured response for most of the beams is on the order of 10% of the maximum moment. Considering the complications of reproducing the decay in strength and stiffness of each material, we feel that this level of accuracy is acceptable, particularly because the maximum moments are generally predicted with an error smaller than this value. However, the discrepancy is greater than the expected random errors in the data, so there is still some room for improvement in the model.

The model is expensive to use in its present form. To calculate a complete load history of 100 points requires about 8 seconds of CPU time on the CDC 6400 computer at the University of California at Berkeley, and about 20 seconds if bond-slip is included in the formulation. These times would be reduced slightly if coarser tolerances were accepted for some of the iterative calculations, but in most cases convergence is rapid enough that even a 20% saving in computer time could be obtained only by accepting calculations which are an order of magnitude less accurate.

The bond-slip model did not provide an improvement which is worth the extra expense incurred. The pull-out of the bars from the anchor

block had already been allowed for when the experimental M-ϕ curves were constructed, so the bond-slip model was required to reproduce only the slipping of the bars through the concrete in the beam itself, an effect which appears to influence the beam behavior to only a small degree. The pull-out of the bars contributes significantly to the total rotation of the beam and, if it had not been measured independently, the use of a bond-slip model to predict it would have been essential.

The greatest use of system identification lay in appraising the model form so that it could be modified as necessary. Previous authors [40] have used identification more as a process which is important in its own right, but here it is used very much as a tool applied in whatever situation it is needed.

An unexpected dilemma emerged because system identification was used in conjunction with a compound global model which was made up from a number of individual material models. The difficulty lies in deciding whether to satisfy the mathematical criterion of minimizing the error function or the practical criterion of retaining the physical significance of each parameter. The question does not arise in the modelling of a single homogeneous material, but in the present case it must be considered.

Certain aspects of the calculation strategy proved to be very successful. First, an enormous amount of effort was saved by using a minimization routine which does not require analytical expressions for the derivatives of the error function. The model form was changed so many times during its development that the use of a true gradient minimization method would have required a much greater programming effort.

Another feature which increased the program's flexibility of use was the ability to select, when the data for a particular run was input, which of the potential parameters were to be assigned fixed values and which were to be treated as truly adjustable parameters.

There are several developments which would add to the usefulness of the model.

(a) Increase the efficiency of the computer program. For example, integration across the cross section with, say, the trapezoidal rule or Simpson's rule might permit a significant reduction in the number of concrete layers needed.

(b) Test the steel model against more experimental data. We need to know if the branch curves for machined and unmachined steel differ, and if the model can be applied successfully to other types of steel with a knowledge only of their monotonic stress-strain curves.

APPENDIX A

Proof of the Orthogonality of the Search Directions in Powell's Minimization Method

The objective of this appendix is to show that the procedure outlined in section 8.4.2 does indeed generate the set of A-conjugate search directions which are crucial to the success of Powell's minimization method.

The proof requires the use of two theorems, which are presented first.

Theorem 1

Let $f(x) = \underset{\sim}{x}^T \underline{A} \underset{\sim}{x} - 2\underset{\sim}{b}^T \underset{\sim}{x} + c$ (A1)

where $\underline{A}$ is an n x n symmetric positive definite matrix.

Let $\underset{\sim}{u}_j$, $j = 1, m$ $(m \leq n)$ be a set of non-zero A-orthogonal directions such that

$$\underset{\sim}{u}_i^T \underline{A} \underset{\sim}{u}_j = 0 \qquad i \neq j \tag{A2}$$

Then the minimum of $f(x)$ in the m-dimensional space defined by $\underset{\sim}{u}_j$ $j = 1, m$ can be found by performing one line search in each of the m directions.

Proof

Let $\underset{\sim}{x}$ be an arbitrary starting vector.

$\underset{\sim}{u}_j$, $j = 1, m$ are non-zero and A-orthogonal, and so are linearly independent. Thus they form a basis, and any vector $\underset{\sim}{y}$ in the m-dimensional subspace can be expressed as

$$\underset{\sim}{y} = \sum_{\ell=1}^{m} a_\ell \underset{\sim}{u}_\ell \tag{A3}$$

Consider $$f(\underset{\sim}{x} + \underset{\sim}{y}) = f(\underset{\sim}{x} + \sum_{\ell=1}^{m} a_\ell \underset{\sim}{u}_\ell) \tag{A4}$$

where the a_ℓ are arbitrary.

Now if a_k^* is the value of a_k which minimizes $f(\underset{\sim}{x} + \underset{\sim}{y})$ in the direction $\underset{\sim}{u}_k$

$$\frac{\partial}{\partial a_k} \left[f(\underset{\sim}{x} + \sum_{\substack{\ell=1 \\ \ell \neq k}}^{m} a_\ell \underset{\sim}{u}_\ell + a_k \underset{\sim}{u}_k) \right] \Big|_{a_k = a^*_k} = 0 \tag{A5}$$

$$\therefore \quad (\underset{\sim}{x} + \sum_{\substack{\ell=1 \\ \ell \neq k}}^{m} a_\ell \underset{\sim}{u}_\ell)^T \underline{\underline{A}} \underset{\sim}{u}_k + a_k^* \underset{\sim}{u}_k^T \underline{\underline{A}} \underset{\sim}{u}_k - a_k^* \underset{\sim}{b}^T \underset{\sim}{u}_k = 0 \tag{A6}$$

but eq^n(A2)

leads to $$(\sum_{\substack{\ell=1 \\ \ell \neq k}}^{m} a_\ell \underset{\sim}{u}_\ell)^T \underline{\underline{A}} \underset{\sim}{u}_k = 0 \tag{A7}$$

$$\therefore \quad \underset{\sim}{x}^T \underline{\underline{A}} \underset{\sim}{u}_k + a_k^* (\underset{\sim}{u}_k^T \underline{\underline{A}} \underset{\sim}{u}_k - \underset{\sim}{b}^T \underset{\sim}{u}_k) = 0$$

and the value of a_k^* is independent of the a_ℓ, $\ell \neq k$.

So if we minimize f in the direction $\underset{\sim}{u}_k$, and

then add to $(\underset{\sim}{x} + a_k^* \underset{\sim}{u}_k)$ any vector of the form

$$\underset{\sim}{z} = \sum_{\substack{\ell=1 \\ \ell \neq k}}^{m} a_\ell \underset{\sim}{u}_\ell \qquad a_\ell \text{ arbitrary}$$

the resulting vector $(\underset{\sim}{x} + a_k^* \underset{\sim}{u}_k + \underset{\sim}{z})$ will still minimize f in the direction $\underset{\sim}{u}_k$. Thus the minimum of f in the m-dimensional subspace spanned by $\underset{\sim}{u}_j$, $j = 1, m$ can be located by one line search in each of the m directions.

Q.E.D.

Theorem 2

Let $f(x)$ be defined by equation (A1)

Let $\underset{\sim}{x}_1^*$ and $\underset{\sim}{x}_2^*$ minimize f in direction $\underset{\sim}{u}$ (arbitrary),

starting from $\underset{\sim}{x}_1$ and $\underset{\sim}{x}_2$ respectively.

Then $\underset{\sim}{w} = (\underset{\sim}{x}_2^* - \underset{\sim}{x}_1^*)$ is A-orthogonal to $\underset{\sim}{u}$.

Proof

$\underset{\sim}{x}_1^*$ and $\underset{\sim}{x}_2^*$ minimize f in direction $\underset{\sim}{u}$,

$$\therefore \quad \frac{\partial}{\partial a_i} [f(\underset{\sim}{x}_i^* + a_i \underset{\sim}{u})] \Big|_{a_i = 0} = 0 \quad i = 1, 2$$

$$\therefore \quad 2\, \underset{\sim}{u}^T (\underline{A}\, \underset{\sim}{x}_i^* - \underset{\sim}{b}) = 0 \quad i = 1, 2$$

$$\therefore \quad \underset{\sim}{u}^T \underline{A} (\underset{\sim}{x}_2^* - \underset{\sim}{x}_1^*) = \underset{\sim}{u}^T \underline{A} \underset{\sim}{w} = 0$$

Q.E.D.

Theorem 1, with $m = n$, offers an alternative proof to the one given in section 8.4.2 of why the global minimum of a quadratic function can be located in n line searches, if n non-zero A-orthogonal search directions are available.

We also need to show that $\underset{\sim}{w}^k$, the new search direction given by $\underset{\sim}{x}_n^k - \underset{\sim}{x}_0^k$ in the k th subcycle of Powell's method, is A-orthogonal to $\underset{\sim}{u}_i^k$, $(i = n - k + 1, n)$. Theorem 1 shows that $\underset{\sim}{x}_n^k$ minimizes f in directions $\underset{\sim}{u}_i^k$ $(i = n - k + 1, n)$, because they are mutually A-orthogonal and the line searches along them are performed <u>after</u> those in the non-orthogonal directions $\underset{\sim}{u}_i$, $(i = 1, n - k)$. But $\underset{\sim}{x}_0^k$ also minimizes f in the same k directions $\underset{\sim}{u}_i^k$ $(i = n - k + 1, n)$, (although the minimization starts

and ends at different points in the full n-dimensional space), because, during subcycle k-1, line searches were carried out in these same directions, which were at the time called $\underset{\sim}{u}_i^{k-1}$, $(i = n - k + 2, n)$ and $\underset{\sim}{w}^{k-1}$. Thus, by Theorem 2, $\underset{\sim}{w}^{k}$ is A-orthogonal to the k vectors $\underset{\sim}{u}_i^{k}$, $(i = n - k + 1, n)$. This is the desired result.

APPENDIX B

B-1 General

Appendix B contains details of the computer program which was written to identify the parameters in the global model. In Section B-2 an outline of the whole program is presented, and Sections B-3 and B-4 give details of some of the numerical techniques used.

B-2 Program Outline

The layout of the program is most easily understood through flow charts. Fig. B.1 shows the outline of the whole program. The most important initial calculation is the processing of the data for the steel monotonic stress-strain curves, which is described in Section B-4. The scrambling of the parameters is the procedure by which the parameters to be adjusted are selected from the pool of (53) potential parameters and is described in Section B-3. Subprogram POWBRE is described in Section 8.4 and is a function minimization routine. It makes frequent calls on the function evaluation routine to which it transmits a set of parameters and from which it receives the corresponding error function value. The parameter adjustment occurs within POWBRE and is performed separately from the evaluation of the error function.

Fig. B.2 shows how the error function is calculated. First, variables (such as the accumulated plastic strain in the steel bars) must be reset. Then the parameters must be unscrambled so that they are compatible with the global model. At each point in the curvature history, the predicted moment is calculated, and the square of the difference between it and the measured moment is added to the error function value. The parameters are rescrambled before returning to POWBRE.

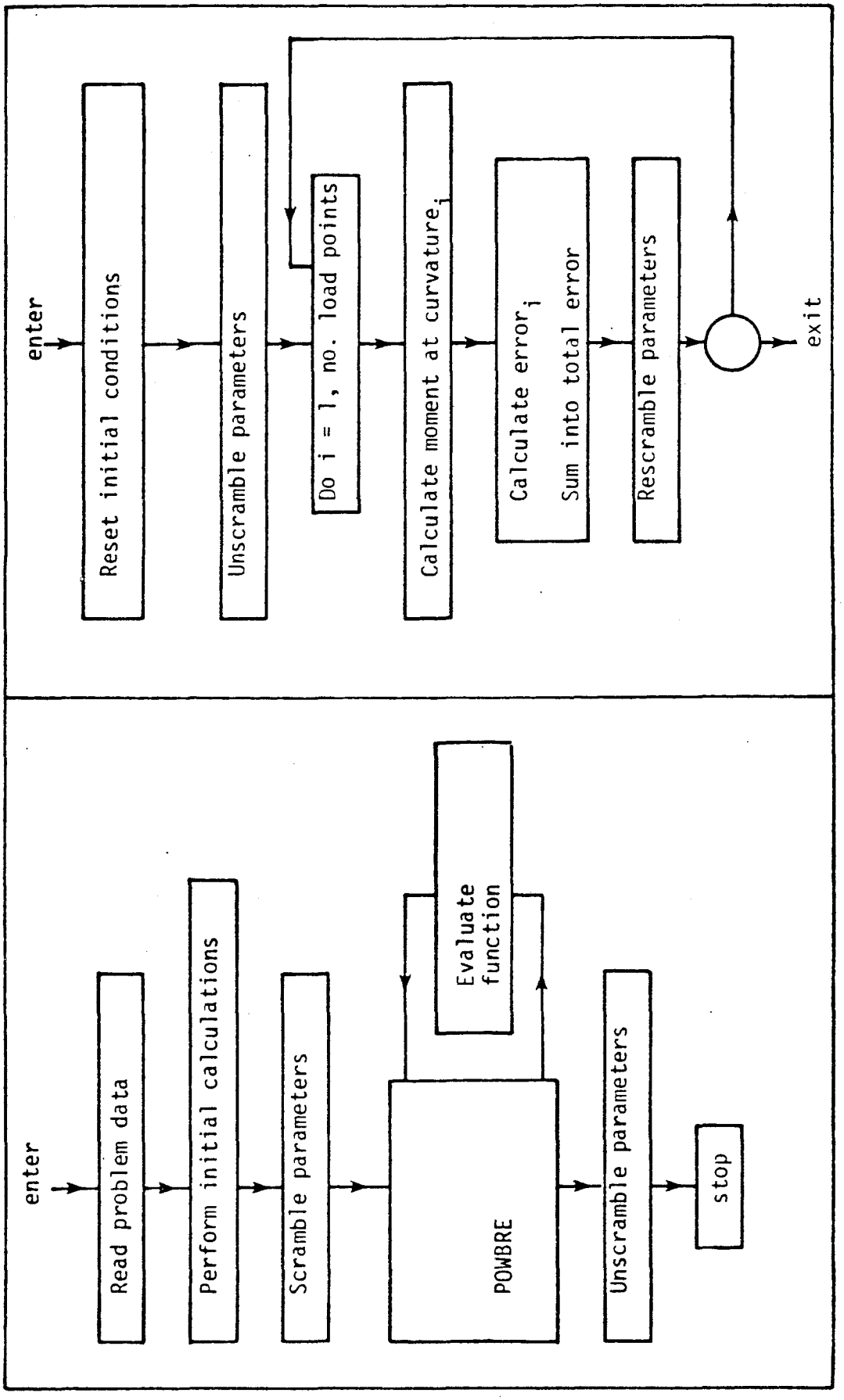

FIG. B.1 - FLOW CHART FOR OVERALL PROGRAM

FIG. B.2 - FLOW CHART FOR FUNCTION EVALUATION

The calculation of the moment at any given curvature is shown in Fig. B.3. We seek the strain distribution which satisfies axial force equilibrium, and find it by varying only the centroidal strain in the manner described in Chapter 7. The slope of the strain distribution is given, and is equal to the curvature. The axial force and bending moment are evaluated at each trial centroidal strain.

Fig. B.4 illustrates the calculation of the axial force and bending moment for a given strain distribution. The contribution of the concrete elements to the axial force and bending moment are calculated first. Strain at the layer center is obtained from the strain field, then the routine which contains the concrete model is called to compute the stress.. The contributions from the steel are calculated similarly, except that the steel strains are obtained from the bond-slip relation, rather than directly from the concrete strain field.

None of the calculations are in themselves very time consuming, but the flow charts show clearly how they are nested inside each other, causing the innermost ones (calculation of material stresses) to be performed a very large number of times.

B-3 Selection of Adjustable Parameters From Potential Parameters

The parameters to be adjusted by subprogram POWBRE are transmitted to it in vector form through the argument list. The length, N, of the vector must also be supplied. However, all of the 53 potential parameters are needed by the function evaluation routine each time it is called by POWBRE. We thus need to rearrange the parameters before they enter POWBRE so that the ones to be adjusted occupy the first N locations

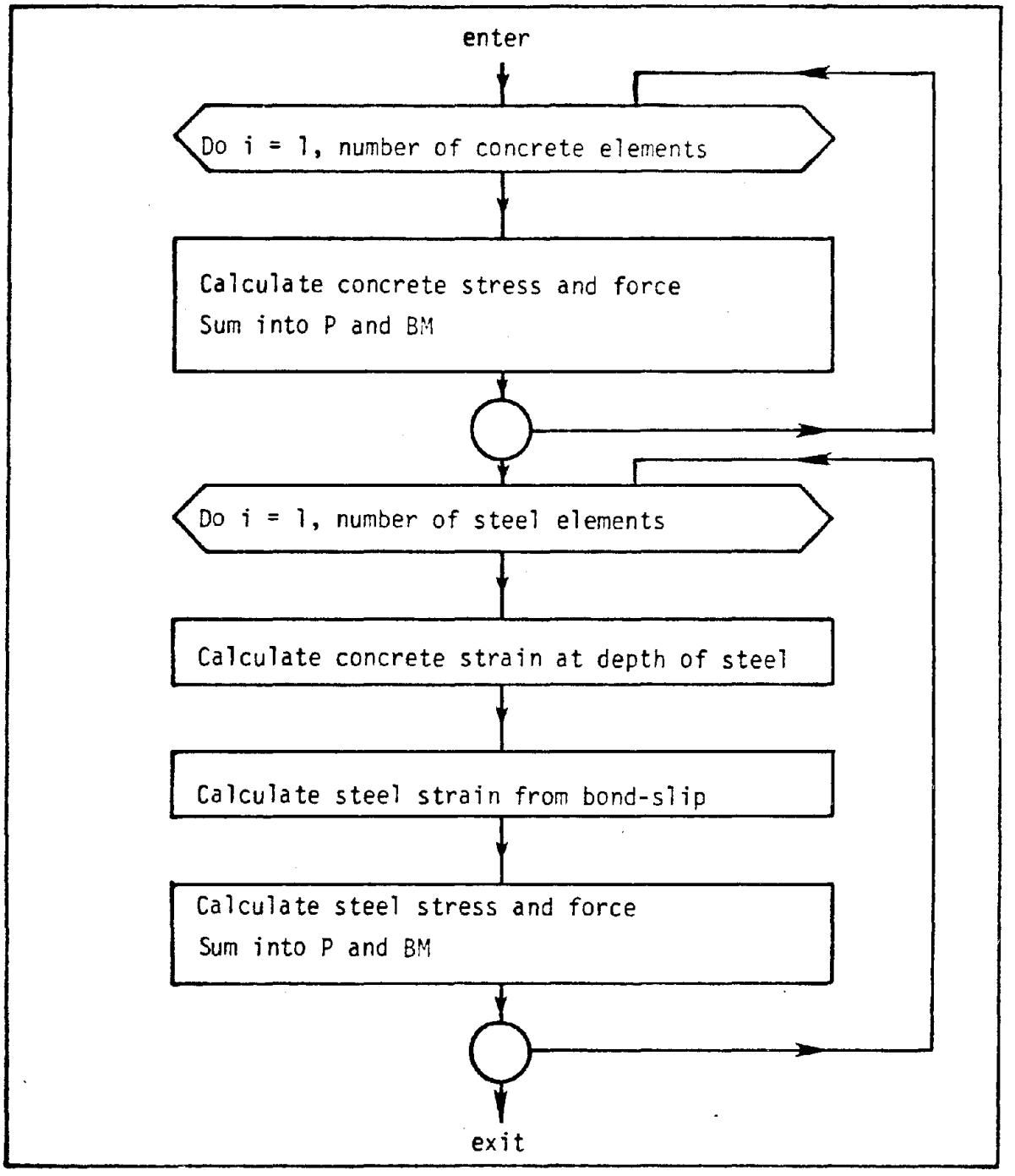

FIG. B.3 - FLOW CHART FOR ESTABLISHING STRAIN DISTRIBUTION AT A GIVEN CURVATURE

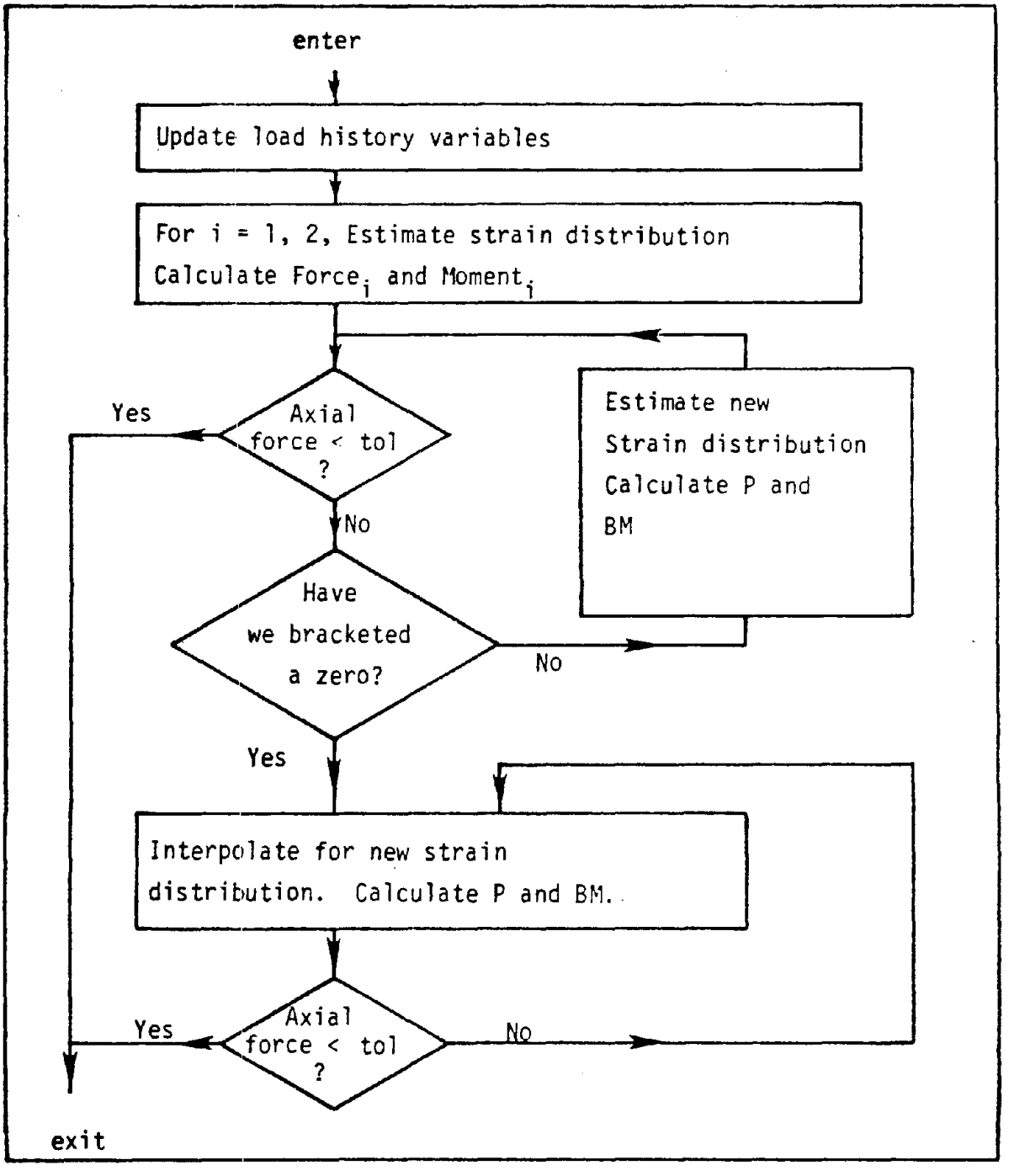

FIG. B.4 - FLOW CHART FOR CALCULATING AXIAL FORCE AND BENDING MOMENT FOR A GIVEN STRAIN DISTRIBUTION

of the vector. This is achieved by reading in to the main program in a fixed order the initial values of all 53 potential parameters. A code number of 0 or 1 is read in for each, depending on whether or not the parameter is to be adjusted. The parameters are then reordered accordingly, and their new order is recorded in another vector. The true parameters are also scaled so that they all have a value of 1.0 on first entry to POWBRE. This is done because the position of the first point in any line search is chosen on the basis of an estimated distance to the global minimum. If the parameter values vary widely, this strategy could cause the small ones to change so radically that they enter the infeasible region. Scaling the parameters prevented this from happening. Thus the process of scrambling the parameters shown in Figs. B.1 and B.2 consists of ordering them and then dividing the N true parameters by the scale factors. Unscrambling is the reverse, namely multiplying by the scale factors, then reordering the elements of the vector to their original positions.

B-4 Definition of the Steel Stress-Strain Curve

We wish to define the monotonic stress-strain curve for steel in a way which will allow easy calculation of the stress and tangent modulus at any point along it and yet will still permit a completely arbitrary definition of its shape. Both objectives can be fulfilled if the curve is defined by specifying the coordinates of a number of points along it and then fitting cubic splines between them.

A p^{th} order spline function is a curve which is defined by a (different) p^{th} order polynominal between each pair of points, but which maintains continuity of p-1 derivatives over the whole interval. Spline

fitting is often preferable to polynominal interpolation (in which a single $(n-1)^{th}$ order polynominal is fitted between the n points) because the latter tends to give rise to enormous oscillations between the points if n is greater than about 4. The order of the spline, p, is almost always odd, in order to maintain symmetry of the end conditions. Here we use cubic splines, which are fitted as follows.

Given n points (x_i, y_i) $i = 1,\ldots,n$

define $$h_i = x_{i+1} - x_i \quad i = 1,\ldots,n \tag{B-1}$$

$$d_i = \frac{y_{i+1} - y_i}{h_i} \quad i = 1,\ldots,n \tag{B-2}$$

$$k_i = \left(\frac{dy}{dx}\right)_{x = x_i} \quad i = 1,\ldots,n \tag{B-3}$$

(note that the k_i are not yet known).

If $$t = \frac{x - y_i}{h_i} \tag{B-4}$$

then

$$q_i(x) = ty_{i+1} + (1-t)y_i + h_i\, t(1-t)\{(k_i - d_i)(1-t) - (k_{i+1} - d_i)t\}$$

$$i = 1,\ldots,n-1 \tag{B-5}$$

are the required interpolating cubics.

This is so because

$$q_i(x_{i+1}) = y_{i+1} = q_{i+1}(x_{i+1}) \quad i=1,\ldots,n-2$$

which shows that y is continuous over the interval $[x_1, x_n]$.

To verify that $\left(\frac{dy}{dx}\right)$ is continuous,

$$\frac{dq_i(x)}{dx} = d_i[6t(1-t)] + k_i[(1-3t)(1-t)] + k_{i+1}[(-t)(2-3t)] \tag{B-6}$$

Setting $t = 0$ in (B-6) gives

$$\frac{dq_i}{dx}(x_i) = k_i \tag{B-7}$$

Substituting $i+1$ for i gives

$$\frac{dq_{i+1}}{dx}(x_{i+1}) = k_{i+1} \tag{B-8}$$

But $t=1$ in (B-6) gives

$$\frac{dq_i}{dx}(x_{i+1}) = k_{i+1} \tag{B-9}$$

$$\frac{dq_i}{dx}(x_{i+1}) = \frac{dq_{i+1}}{dx}(x_{i+1})$$

which shows that $\left(\frac{dy}{dx}\right)$ is continuous on $[x_1,x_n]$.

Now

$$\frac{d^2q_i}{dx^2}(x) = \frac{2}{h_i}\{3d_i(1-2t) - k_i(2-3t) - k_{i+1}(1-3t)\} \tag{B-10}$$

But for y" to be continuous on $[x_1,x_n]$, we require

$$\frac{d^2q_i}{dx^2}(x_{i+1}) = \frac{d^2q_{i+1}}{dx^2}(x_{i+1}) \tag{B-11}$$

or

$$\frac{2}{h_i}\{-3d_i + k_i + 2k_{i+1}\} = \frac{2}{h_{i+1}}\{3d_{i+1} - 2k_{i+1} - k_{i+2}\} \quad i=1,\ldots,n-2 \tag{B-12}$$

These conditions give n-2 equations with which to find the n unknowns k_i. They can be expressed as

$$(h_{i+1})\ k_i + 2(h_i+h_{i+1})\ k_{i+1} + (h_i)\ k_{i+2} = 3(h_i d_{i+1} + h_{i+1} d_i)$$

$$i = 1,\ldots,n-2 \qquad \text{(B-13)}$$

Two more equations are needed, and they are obtained by imposing one condition at each end of the interval. In the program there is a choice of either setting the second derivative of q equal to zero or specifying the value of the first derivative. The former gives rise to

$$2k_1 + k_2 = 3d_i \qquad \text{(B-14a)}$$

$$k_{n-1} + 2k_n = 3d_{n-1} \qquad \text{(B-14b)}$$

and the latter to

$$k_1 = \tilde{k}_1 \qquad \text{(B-15a)}$$

$$k_n = \tilde{k}_n \qquad \text{(B-15b)}$$

where the $\tilde{k}_i$ are the specified values.

We thus have a set of n linear equations in n unknowns. The system is tridiagonal and is particularly easy to solve if pivoting can be avoided. Since the prime objective of pivoting is the prevention of error growth in the solution of a poorly conditioned unsymmetric system, it can be avoided by choosing the h_i to give a well conditioned system. If they are all equal, the system is symmetric and pivoting is unnecessary. If the h_i differ, but not by orders of magnitude, then the system is unsymmetric but well enough conditioned that a solution without pivoting will almost certainly be satisfactory. Large n, large differences in the h_i, or computations carried out to m-digit arithmetic where m is small are the conditions liable to cause problems.

Once the k_i are known, Eqs. B-5 and B-6 can be rewritten as

$$q_i = a_{0i} + a_{1i} t + a_{2i} t^2 + a_{3i} t^3 \tag{B-16}$$

or

$$q_i = a_{0i} + t(a_{1i} + t(a_{2i} + t\, a_{3i})) \tag{B-17}$$

and

$$q'_i = b_{0i} + t(b_{1i} + t\, b_{2i}) \tag{B-18}$$

where

$$\left.\begin{aligned} a_{0i} &= y_i \\ a_{1i} &= h_i k_i \\ a_{2i} &= h_i(3d_i - 2k_i - k_{i+1}) \\ a_{3i} &= h_i(k_i + k_{i+1} - 2d_i) \\ b_{0i} &= k_i \\ b_{1i} &= 2a_{2i}/h_i \\ b_{2i} &= 3a_{3i}/h_i \end{aligned}\right\} \tag{B-19}$$

The a_{ji} and b_{ji} are stored, and then for any x, Eqs. B4, B17 and B18 give q and q' at a cost of six multiplications. This is the desired result.

REFERENCES

1. R. Park, "Theorization of Structural Behavior with a View to Defining Resistance and Ultimate Deformability," Bulletin of the New Zealand Society for Earthquake Engineering, Vol. 6, No. 2, June 1973.

2. A. Veletsos and N. Newmark, "Effect of Inelastic Behavior on the Response of Simple Systems to Earthquake Motions," Second World Conference on Earthquake Engineering, Vol. II, Session II, Japan, p. 895, 1960.

3. H. Aoyama, "Moment Curvature Characteristics of Reinforced Concrete Members Subjected to Axial Load and Reversal of Bending," Proceedings of the International Symposium on Flexural Mechanics of Reinforced Concrete, Miami, Florida, 1964, Published as ACI SP-12.

4. W. Prager and P. G. Hodge, Theory of Perfectly Plastic Solids, Dover, 1968.

5. P. Hidalgo and R. W. Clough, "Earthquake Simulator Study of a Reinforced Concrete Frame," Report No. EERC 74-13, Earthquake Engineering Research Center, University of California, Berkeley, 1974.

6. T. Takeda, M. Sozen, and N. Nielsen, "Reinforced Concrete Response to Simulated Earthquakes," Journal of the Structural Division, ASCE, December 1970.

7. A. Kanaan and G. H. Powell, "DRAIN-2D - A General Purpose Computer Program for Dynamic Analysis of Inelastic Plane Structures," Report No. EERC 73-22, Earthquake Engineering Research Center, University of California, Berkeley, 1973.

8. W. Iwan, "A Model for the Dynamic Analysis of Deteriorating Systems," Proceedings of the Fifth World Conference on Earthquake Engineering, Vol. II, Session 5B, p. 1782.

9. M. B. Atalay and J. Penzien, "The Seismic Behavior of Critical Regions of Reinforced Concrete Components as Influenced by Moment, Shear, and Axial Force," Report No. EERC 75-19, Earthquake Engineering Research Center, University of California, Berkeley, 1975.

10. S. Tani, T. Nagasaka, S. Nomura and A. Hiramatsu, "Study on Restoring Force Characteristics of Reinforced Concrete Structures," Proceedings of Third Japan Earthquake Engineering Symposium, Paper V8, pp. 699-706, 1970.

11. A. Agrawal, L. Tulin and K. Gerstle, "Response of Doubly Reinforced Concrete Beams to Cyclic Loading," ACI Journal, Vol. 63, July 1965.

12. I. D. Karsan and J. O. Jirsa, "Behavior of Concrete Under Varying Strain Gradients," Journal of the Structural Division, ASCE, August 1970.

13. R. Brown and J. O. Jirsa, "Reinforced Concrete Beams Under Load Reversals," ACI Journal, May 1971.

14. N. H. Burns and C. P. Seiss, "Load Deformation Characteristics of Beam-Column Connections in Reinforced Concrete," Structural Research Series No. 234, Civil Engineering Studies, University of Illinois, Urbana, Illinois, January 1962.

15. B. Bresler and V. V. Bertero, "Behavior of Reinforced Concrete Under Repeated Load," Journal of the Structural Division, ASCE, June 1968.

16. S. Viwathanatepa, "Deterioration of Bond in Reinforced Concrete Under Generalized Loading," Ph.D. Dissertation, University of California, Berkeley, California (in preparation).

17. R. Blakeley, "Ductility of Prestressed Concrete Frames Under Seismic Loading," Ph.D. Thesis, University of Canterbury, Christchurch, New Zealand, 1971.

18. D. Kent, "Inelastic Behavior of Reinforced Concrete Members With Cyclic Loading," Ph.D. Thesis, University of Canterbury, Christchurch, New Zealand, 1969.

19. K. Thompson, "Ductility of Concrete Frames Under Seismic Loading," Ph.D. Thesis, University of Canterbury, Christchurch, New Zealand, 1975.

20. D. Kent and R. Park, "Flexural Members With Confined Concrete," Journal of the Structural Division, ASCE, July 1971.

21. R. Park, D. Kent and R. Sampson, "Reinforced Concrete Members With Cyclic Loading," Journal of the Structural Division, ASCE, July 1972.

22. W. Ramberg and W. Osgood, "Description of Stress-Strain Curves by Three Parameters," Technical Note No. 902, NACA, July 1943.

23. E. Hognestad, "A Study of Combined Bending and Axial Load in Reinforced Concrete Members," Bulletin No. 399, University of Illinois Engineering Experimental Station, November 1951.

24. B. Sinha, K. Gerstle and L. Tulin, "Stress-Strain Relations for Concrete Under Cyclic Loading," ACI Journal, February 1964.

25. A. Singh, K. Gerstle and L. Tulin, "The Behavior of Reinforcing Steel Under Reversed Loading," Material Research and Standards, Vol. 5, No. 1, January 1965.

26. B. Sinha, K. Gerstle and L. Tulin, "Response of Singly Reinforced Concrete Beams to Cyclic Loading," ACI Journal, August 1964.

27. G. Agrawal, L. Tulin and K. Gerstle, "Response of Doubly Reinforced Concrete Beams to Cyclic Loading," ACI Journal, July 1965.

28. L. Kriz and S. Lee, "Ultimate Strength of Over-Reinforced Beams," Journal of the Engineering Mechanics Division, ASCE, June 1960.

29. R. Yamishiro and C. P. Seiss, "Moment Relation Characteristics of Reinforced Concrete Members Subjected to Bending, Shear and Axial Load," Structural Research Series No. 260, University of Illinois Civil Engineering Studies, December 1962.

30. A. Aktan, B. Karlsson and M. Sozen, "Stress-Strain Relationships of Reinforcing Bars Subjected to Large Strain Reversals," Structural Research Series No. 397, University of Illinois Civil Engineering Studies, June 1973.

31. N. Burns and C. P. Seiss, "Repeated and Reversed Loading on Reinforced Concrete," Journal of the Structural Division, ASCE, October 1966.

32. M. Menegotto and P. Pinto, "Method of Analysis for Cyclically Loaded Reinforced Concrete Plane Frames Including Changes in Geometry and Nonelastic Behavior of Elements Under Combined Normal Force and Bending," IABSE Symposium on the Resistance and Ultimate Deformability of Structures Acted on by Well-Defined Repeated Loads, Lisbon, 1973.

33. S.Y.M. Ma, V. V. Bertero and E. P. Popov, "Experimental and Analytical Studies on the Hysteretic Behavior of Reinforced Concrete Rectangular and T-Beams," Report No. EERC 76-2, Earthquake Engineering Research Center, University of California, Berkeley, 1976.

34. V. Bertero and B. Bresler, "Seismic Behavior of Reinforced Concrete Framed Structures," Proceedings of Fourth World Conference on Earthquake Engineering, Vol. 1. Santiago, Chile, pp. B2 109-124, 1969.

35. S. Timoshenko, "Strength of Materials," Part II, Advanced Theory and Problems, 3rd Edition, Van Nostrand Reinhold, pp. 413-417.

36. J. Bauschinger, Mitt. Mech-Tech. Lab München, 1886 (in German).

37. J. Morrow and G. Sinclair, "Cyclic Stress Relaxation," ASTM Symposium on Basic Mechanics of Fatigue, ASTM, Special Technical Publication 237, Boston, 1958.

38. J. Morrow, "Cyclic Plastic Strain Energy and Fatigue of Metals," ASTM Symposium on Internal Friction, Damping and Cyclic Plasticity Phenomena in Materials, Annual ASTM Meeting, Chicago, 1964. Published as ASTM Special Technical Publication 378, 1965.

39. R. Smith, M. Hirschberg and S. Manson, "Fatigue Behavior of Materials Under Strain Cycling in Low and Intermediate Life Range," NASA TN D1574, National Aeronautics and Space Administration, 1963.

40. V. C. Matzen and H. D. McNiven, "Investigation of the Inelastic Characteristics of a Single-Story Steel Structure Using System Identification and Shaking Table Experiments," Report No. EERC 76-20, Earthquake Engineering Research Center, University of California, Berkeley, August 1976.

41. V. G. Masing, "Eigenspannungen und Verfestigungen beim Messing," Proceedings of the Second International Conference for Applied Mechanics, Zurich, Switzerland, pp. 332-335, 1962 (in German).

42. Y. Dafalias, "On Cyclic and Anisotropic Plasticity," Thesis in Engineering Science presented to the University of California at Berkeley, 1975.

43. B. Lazan, Damping in Materials and Members in Structural Mechanics, Pergamon Press, pp. 99, 1968.

44. N. Davidenkov, "Energy Dissipation in Vibrations," Journal of Technical Physics, Vol. 8, No. 6, p. 4, 1938.

45. M.T.M. Soliman and C. W. Yu, "The Flexural Stress-Strain Relationship of Concrete Confined by Rectangular Transverse Reinforcement," Magazine of Concrete Research, Vol. 19, No. 61, December 1967.

46. G. M. Sturman, S. P. Shah and G. Winter, "Microcracking and Inelastic Behavior of Reinforced Concrete," International Symposium on the Flexural Mechanics of Reinforced Concrete, Miami, Florida, November 1964. Published as ACI Special Publication No. SP 12.

47. F. E. Richart, A. Brandtzaeg and R. L. Brown, "A Study of the Failure of Concrete Under Combined Compressive Stress," Bulletin No. 185, University of Illinois Experimental Station, p. 104, 1928.

48. ASTM Standard C39-72, "Standard Test Method for Compressive Strength of Concrete Specimens," Annual Book of ASTM Standards, Part 14.

49. H. Rüsch, "Research Towards a General Flexural Theory for Structural Concrete," ACI Journal, July 1960.

50. E. Hognestad, N. W. Hanson and D. McHenry, "Concrete Stress Distribution in Ultimate Strength Design," ACI Journal, December 1955.

51. I. D. Karsan and J. O. Jirsa, "Behavior of Concrete Under Compressive Loadings," Journal of the Structural Division, ASCE, December 1969.

52. P. R. Barnard, Discussion to "Microcracking and Inelastic Behavior of Reinforced Concrete" by G. M. Sturman, S. P. Shah and G. Winter, ACI Special Publication No. SP 12.

53. S. Popovicz, "A Review of Stress-Strain Relationships for Concrete," ACI Journal, March 1970.

54. M.A.F. Ismail and J. O. Jirsa, "Bond Deterioration in Reinforced Concrete Subject to Low Cycle Loads," ACI Journal, June 1972.

55. J. O. Jirsa, "Bond and Anchorage in Reinforced Concrete Frame Joints," U.S.-Japan Seminar on Earthquake Engineering with Special Emphasis on Safety of Reinforced Concrete Structures, Berkeley, California, September 1973.

56. S. Morita and T. Kaku, "Local Bond Stress-Slip Relationship Under Repeated Loading," IABSE Symposium on Resistance and Ultimate Deformability of Structures Acted Upon by Well-Defined Repeated Loads, Lisbon 1973, Preliminary Report, pp. 221-226.

57. F. M. Hassan and N. M. Hawkins, "Effects of Post-Yield Loading Reversals on Bond Between Reinforcing Bars and Concrete," Report SM 73-2, Department of Civil Engineering, University of Washington, Seattle, Washington, March 1973.

58. J. F. Stanton, "An Investigation of the Dowel Action of the Reinforcement of Nuclear Containment Vessels and Their Nonlinear Response to Dynamic Loads," M.S. Thesis, Cornell University, September 1976.

59. E. P. Popov, "Mechanical Characteristics and Bond of Reinforcing Steel Under Seismic Conditions," Workshop on Earthquake-Resistant R/C Construction, University of California, Berkeley, July 1977.

60. R. Brent, Algorithms for Minimization Without Derivatives, Prentice-Hall, 1973.

61. T. J. Dekkev, "Finding a Zero by Means of Successive Linear Interpolation," Constructive Aspects of the Fundamental Theorem of Algebra, B. Dejon and P. Henrici (eds.), Interscience, New York, 1969.

62. Y. Bard, "Comparison of Gradient Methods for the Solution of Nonlinear Parameter Estimation Problems," SIAM Journal of Numerical Analysis, Vol. 7, No. 1, March 1970.

63. T. Straeter and J. E. Hogge, "A Comparison of Gradient Dependent Techniques for the Minimization of an Unconstrained Function of Several Variables," AIAA Journal, Vol. 8, No. 12, December 1970.

64. D. P. Luenberger, "Introduction to Linear and Nonlinear Programming," Addison Wesley, Reading, Mass., 1973.

65. R. Fletcher and M.J.D. Powell, "A Rapidly Convergent Descent Method for Minimization," Computer Journal, Vol. 6, pp. 163-168, 1963.

66. W. C. Davidon, "Variance Algorithm for Minimization," Computer Journal, Vol. 10, No. 4, February 1968.

67. M.J.D. Powell, "An Efficient Method for Finding the Minimum of a Function of Several Variables Without Calculating Derivatives," Computer Journal, Vol. 7, 1964.

EARTHQUAKE ENGINEERING RESEARCH CENTER REPORTS

NOTE: Numbers in parenthesis are Accession Numbers assigned by the National Technical Information Service; these are followed by a price code. Copies of the reports may be ordered from the National Technical Information Service, 5285 Port Royal Road, Springfield, Virginia, 22161. Accession Numbers should be quoted on orders for reports (PB --- ---) and remittance must accompany each order. Reports without this information were not available at time of printing. Upon request, EERC will mail inquirers this information when it becomes available.

EERC 67-1 "Feasibility Study Large-Scale Earthquake Simulator Facility," by J. Penzien, J.G. Bouwkamp, R.W. Clough and D. Rea - 1967 (PB 187 905)A07

EERC 68-1 Unassigned

EERC 68-2 "Inelastic Behavior of Beam-to-Column Subassemblages Under Repeated Loading," by V.V. Bertero - 1968 (PB 184 888)A05

EERC 68-3 "A Graphical Method for Solving the Wave Reflection-Refraction Problem," by H.D. McNiven and Y. Mengi - 1968 (PB 187 943)A03

EERC 68-4 "Dynamic Properties of McKinley School Buildings," by D. Rea, J.G. Bouwkamp and R.W. Clough - 1968 (PB 187 902)A07

EERC 68-5 "Characteristics of Rock Motions During Earthquakes," by H.B. Seed, I.M. Idriss and F.W. Kiefer - 1968 (PB 188 338)A03

EERC 69-1 "Earthquake Engineering Research at Berkeley," - 1969 (PB 187 906)A11

EERC 69-2 "Nonlinear Seismic Response of Earth Structures," by M. Dibaj and J. Penzien - 1969 (PB 187 904)A08

EERC 69-3 "Probabilistic Study of the Behavior of Structures During Earthquakes," by R. Ruiz and J. Penzien - 1969 (PB 187 886)A06

EERC 69-4 "Numerical Solution of Boundary Value Problems in Structural Mechanics by Reduction to an Initial Value Formulation," by N. Distefano and J. Schujman - 1969 (PB 187 942)A02

EERC 69-5 "Dynamic Programming and the Solution of the Biharmonic Equation," by N. Distefano - 1969 (PB 187 941)A03

EERC 69-6 "Stochastic Analysis of Offshore Tower Structures," by A.K. Malhotra and J. Penzien - 1969 (PB 187 903)A08

EERC 69-7 "Rock Motion Accelerograms for High Magnitude Earthquakes," by H.B. Seed and I.M. Idriss - 1969 (PB 187 940)A02

EERC 69-8 "Structural Dynamics Testing Facilities at the University of California, Berkeley," by R.M. Stephen, J.G. Bouwkamp, R.W. Clough and J. Penzien - 1969 (PB 189 111)A04

EERC 69-9 "Seismic Response of Soil Deposits Underlain by Sloping Rock Boundaries," by H. Dezfulian and H.B. Seed 1969 (PB 189 114)A03

EERC 69-10 "Dynamic Stress Analysis of Axisymmetric Structures Under Arbitrary Loading," by S. Ghosh and E.L. Wilson 1969 (PB 189 026)A10

EERC 69-11 "Seismic Behavior of Multistory Frames Designed by Different Philosophies," by J.C. Anderson and V. V. Bertero - 1969 (PB 190 662)A10

EERC 69-12 "Stiffness Degradation of Reinforcing Concrete Members Subjected to Cyclic Flexural Moments," by V.V. Bertero, B. Bresler and H. Ming Liao - 1969 (PB 202 942)A07

EERC 69-13 "Response of Non-Uniform Soil Deposits to Travelling Seismic Waves," by H. Dezfulian and H.B. Seed - 1969 (PB 191 023)A03

EERC 69-14 "Damping Capacity of a Model Steel Structure," by D. Rea, R.W. Clough and J.G. Bouwkamp - 1969 (PB 190 663)A06

EERC 69-15 "Influence of Local Soil Conditions on Building Damage Potential during Earthquakes," by H.B. Seed and I.M. Idriss - 1969 (PB 191 036)A03

EERC 69-16 "The Behavior of Sands Under Seismic Loading Conditions," by M.L. Silver and H.B. Seed - 1969 (AD 714 982)A07

EERC 70-1 "Earthquake Response of Gravity Dams," by A.K. Chopra - 1970 (AD 709 640)A03

EERC 70-2 "Relationships between Soil Conditions and Building Damage in the Caracas Earthquake of July 29, 1967," by H.B. Seed, I.M. Idriss and H. Dezfulian - 1970 (PB 195 762)A05

EERC 70-3 "Cyclic Loading of Full Size Steel Connections," by E.P. Popov and R.M. Stephen - 1970 (PB 213 545)A04

EERC 70-4 "Seismic Analysis of the Charaima Building, Caraballeda, Venezuela," by Subcommittee of the SEAONC Research Committee: V.V. Bertero, P.F. Fratessa, S.A. Mahin, J.H. Sexton, A.C. Scordelis, E.L. Wilson, L.A. Wyllie, H.B. Seed and J. Penzien, Chairman - 1970 (PB 201 455)A06

EERC 70-5 "A Computer Program for Earthquake Analysis of Dams," by A.K. Chopra and P. Chakrabarti - 1970 (AD 723 994)A05

EERC 70-6 "The Propagation of Love Waves Across Non-Horizontally Layered Structures," by J. Lysmer and L.A. Drake 1970 (PB 197 896)A03

EERC 70-7 "Influence of Base Rock Characteristics on Ground Response," by J. Lysmer, H.B. Seed and P.B. Schnabel 1970 (PB 197 897)A03

EERC 70-8 "Applicability of Laboratory Test Procedures for Measuring Soil Liquefaction Characteristics under Cyclic Loading," by H.B. Seed and W.H. Peacock - 1970 (PB 198 016)A03

EERC 70-9 "A Simplified Procedure for Evaluating Soil Liquefaction Potential," by H.B. Seed and I.M. Idriss - 1970 (PB 198 009)A03

EERC 70-10 "Soil Moduli and Damping Factors for Dynamic Response Analysis," by H.B. Seed and I.M. Idriss - 1970 (PB 197 869)A03

EERC 71-1 "Koyna Earthquake of December 11, 1967 and the Performance of Koyna Dam," by A.K. Chopra and P. Chakrabarti 1971 (AD 731 496)A06

EERC 71-2 "Preliminary In-Situ Measurements of Anelastic Absorption in Soils Using a Prototype Earthquake Simulator," by R.D. Borcherdt and P.W. Rodgers - 1971 (PB 201 454)A03

EERC 71-3 "Static and Dynamic Analysis of Inelastic Frame Structures," by F.L. Porter and G.H. Powell - 1971 (PB 210 135)A06

EERC 71-4 "Research Needs in Limit Design of Reinforced Concrete Structures," by V.V. Bertero - 1971 (PB 202 943)A04

EERC 71-5 "Dynamic Behavior of a High-Rise Diagonally Braced Steel Building," by D. Rea, A.A. Shah and J.G. Bouwkamp 1971 (PB 203 584)A06

EERC 71-6 "Dynamic Stress Analysis of Porous Elastic Solids Saturated with Compressible Fluids," by J. Ghaboussi and E. L. Wilson - 1971 (PB 211 396)A06

EERC 71-7 "Inelastic Behavior of Steel Beam-to-Column Subassemblages," by H. Krawinkler, V.V. Bertero and E.P. Popov 1971 (PB 211 335)A14

EERC 71-8 "Modification of Seismograph Records for Effects of Local Soil Conditions," by P. Schnabel, H.B. Seed and J. Lysmer - 1971 (PB 214 450)A03

EERC 72-1 "Static and Earthquake Analysis of Three Dimensional Frame and Shear Wall Buildings," by E.L. Wilson and H.H. Dovey - 1972 (PB 212 904)A05

EERC 72-2 "Accelerations in Rock for Earthquakes in the Western United States," by P.B. Schnabel and H.B. Seed - 1972 (PB 213 100)A03

EERC 72-3 "Elastic-Plastic Earthquake Response of Soil-Building Systems," by T. Minami - 1972 (PB 214 868)A08

EERC 72-4 "Stochastic Inelastic Response of Offshore Towers to Strong Motion Earthquakes," by M.K. Kaul - 1972 (PB 215 713)A05

EERC 72-5 "Cyclic Behavior of Three Reinforced Concrete Flexural Members with High Shear," by E.P. Popov, V.V. Bertero and H. Krawinkler - 1972 (PB 214 555)A05

EERC 72-6 "Earthquake Response of Gravity Dams Including Reservoir Interaction Effects," by P. Chakrabarti and A.K. Chopra - 1972 (AD 762 330)A08

EERC 72-7 "Dynamic Properties of Pine Flat Dam," by D. Rea, C.Y. Liaw and A.K. Chopra - 1972 (AD 763 928)A05

EERC 72-8 "Three Dimensional Analysis of Building Systems," by E.L. Wilson and H.H. Dovey - 1972 (PB 222 438)A06

EERC 72-9 "Rate of Loading Effects on Uncracked and Repaired Reinforced Concrete Members," by S. Mahin, V.V. Bertero, D. Rea and M. Atalay - 1972 (PB 224 520)A08

EERC 72-10 "Computer Program for Static and Dynamic Analysis of Linear Structural Systems," by E.L. Wilson, K.-J. Bathe, J.E. Peterson and H.H.Dovey - 1972 (PB 220 437)A04

EERC 72-11 "Literature Survey - Seismic Effects on Highway Bridges," by T. Iwasaki, J. Penzien and R.W. Clough - 1972 (PB 215 613)A19

EERC 72-12 "SHAKE-A Computer Program for Earthquake Response Analysis of Horizontally Layered Sites," by P.B. Schnabel and J. Lysmer - 1972 (PB 220 207)A06

EERC 73-1 "Optimal Seismic Design of Multistory Frames," by V.V. Bertero and H. Kamil - 1973

EERC 73-2 "Analysis of the Slides in the San Fernando Dams During the Earthquake of February 9, 1971," by H.B. Seed, K.L. Lee, I.M. Idriss and F. Makdisi - 1973 (PB 223 402)A14

EERC 73-3 "Computer Aided Ultimate Load Design of Unbraced Multistory Steel Frames," by M.B. El-Hafez and G.H. Powell 1973 (PB 248 315)A09

EERC 73-4 "Experimental Investigation into the Seismic Behavior of Critical Regions of Reinforced Concrete Components as Influenced by Moment and Shear," by M. Celebi and J. Penzien - 1973 (PB 215 884)A09

EERC 73-5 "Hysteretic Behavior of Epoxy-Repaired Reinforced Concrete Beams," by M. Celebi and J. Penzien - 1973 (PB 239 568)A03

EERC 73-6 "General Purpose Computer Program for Inelastic Dynamic Response of Plane Structures," by A. Kanaan and G.H. Powell - 1973 (PB 221 260)A08

EERC 73-7 "A Computer Program for Earthquake Analysis of Gravity Dams Including Reservoir Interaction," by P. Chakrabarti and A.K. Chopra - 1973 (AD 766 271)A04

EERC 73-8 "Behavior of Reinforced Concrete Deep Beam-Column Subassemblages Under Cyclic Loads," by O. Küstü and J.G. Bouwkamp - 1973 (PB 246 117)A12

EERC 73-9 "Earthquake Analysis of Structure-Foundation Systems," by A.K. Vaish and A.K. Chopra - 1973 (AD 766 272)A07

EERC 73-10 "Deconvolution of Seismic Response for Linear Systems," by R.B. Reimer - 1973 (PB 227 179)A08

EERC 73-11 "SAP IV: A Structural Analysis Program for Static and Dynamic Response of Linear Systems," by K.-J. Bathe, E.L. Wilson and F.E. Peterson - 1973 (PB 221 967)A09

EERC 73-12 "Analytical Investigations of the Seismic Response of Long, Multiple Span Highway Bridges," by W.S. Tseng and J. Penzien - 1973 (PB 227 816)A10

EERC 73-13 "Earthquake Analysis of Multi-Story Buildings Including Foundation Interaction," by A.K. Chopra and J.A. Gutierrez - 1973 (PB 222 970)A03

EERC 73-14 "ADAP: A Computer Program for Static and Dynamic Analysis of Arch Dams," by R.W. Clough, J.M. Raphael and S. Mojtahedi - 1973 (PB 223 763)A09

EERC 73-15 "Cyclic Plastic Analysis of Structural Steel Joints," by R.B. Pinkney and R.W. Clough - 1973 (PB 226 843)A08

EERC 73-16 "QUAD-4: A Computer Program for Evaluating the Seismic Response of Soil Structures by Variable Damping Finite Element Procedures," by I.M. Idriss, J. Lysmer, R. Hwang and H.B. Seed - 1973 (PB 229 424)A05

EERC 73-17 "Dynamic Behavior of a Multi-Story Pyramid Shaped Building," by R.M. Stephen, J.P. Hollings and J.G. Bouwkamp - 1973 (PB 240 718)A06

EERC 73-18 "Effect of Different Types of Reinforcing on Seismic Behavior of Short Concrete Columns," by V.V. Bertero, J. Hollings, O. Küstü, R.M. Stephen and J.G. Bouwkamp - 1973

EERC 73-19 "Olive View Medical Center Materials Studies, Phase I," by B. Bresler and V.V. Bertero - 1973 (PB 235 986)A06

EERC 73-20 "Linear and Nonlinear Seismic Analysis Computer Programs for Long Multiple-Span Highway Bridges," by W.S. Tseng and J. Penzien - 1973

EERC 73-21 "Constitutive Models for Cyclic Plastic Deformation of Engineering Materials," by J.M. Kelly and P.P. Gillis 1973 (PB 226 024)A03

EERC 73-22 "DRAIN - 2D User's Guide," by G.H. Powell - 1973 (PB 227 016)A05

EERC 73-23 "Earthquake Engineering at Berkeley - 1973," (PB 226 033)A11

EERC 73-24 Unassigned

EERC 73-25 "Earthquake Response of Axisymmetric Tower Structures Surrounded by Water," by C.Y. Liaw and A.K. Chopra 1973 (AD 773 052)A09

EERC 73-26 "Investigation of the Failures of the Olive View Stairtowers During the San Fernando Earthquake and Their Implications on Seismic Design," by V.V. Bertero and R.G. Collins - 1973 (PB 235 106)A13

EERC 73-27 "Further Studies on Seismic Behavior of Steel Beam-Column Subassemblages," by V.V. Bertero, H. Krawinkler and E.P. Popov - 1973 (PB 234 172)A06

EERC 74-1 "Seismic Risk Analysis," by C.S. Oliveira - 1974 (PB 235 920)A06

EERC 74-2 "Settlement and Liquefaction of Sands Under Multi-Directional Shaking," by R. Pyke, C.K. Chan and H.B. Seed 1974

EERC 74-3 "Optimum Design of Earthquake Resistant Shear Buildings," by D. Ray, K.S. Pister and A.K. Chopra - 1974 (PB 231 172)A06

EERC 74-4 "LUSH - A Computer Program for Complex Response Analysis of Soil-Structure Systems," by J. Lysmer, T. Udaka, H.B. Seed and R. Hwang - 1974 (PB 236 796)A05

EERC 74-5 "Sensitivity Analysis for Hysteretic Dynamic Systems: Applications to Earthquake Engineering," by D. Ray 1974 (PB 233 213)A06

EERC 74-6 "Soil Structure Interaction Analyses for Evaluating Seismic Response," by H.B. Seed, J. Lysmer and R. Hwang 1974 (PB 236 519)A04

EERC 74-7 Unassigned

EERC 74-8 "Shaking Table Tests of a Steel Frame - A Progress Report," by R.W. Clough and D. Tang - 1974 (PB 240 869)A03

EERC 74-9 "Hysteretic Behavior of Reinforced Concrete Flexural Members with Special Web Reinforcement," by V.V. Bertero, E.P. Popov and T.Y. Wang - 1974 (PB 236 797)A07

EERC 74-10 "Applications of Reliability-Based, Global Cost Optimization to Design of Earthquake Resistant Structures," by E. Vitiello and K.S. Pister - 1974 (PB 237 231)A06

EERC 74-11 "Liquefaction of Gravelly Soils Under Cyclic Loading Conditions," by R.T. Wong, H.B. Seed and C.K. Chan 1974 (PB 242 042)A03

EERC 74-12 "Site-Dependent Spectra for Earthquake-Resistant Design," by H.B. Seed, C. Ugas and J. Lysmer - 1974 (PB 240 953)A03

EERC 74-13 "Earthquake Simulator Study of a Reinforced Concrete Frame," by P. Hidalgo and R.W. Clough - 1974 (PB 241 944)A13

EERC 74-14 "Nonlinear Earthquake Response of Concrete Gravity Dams," by N. Pal - 1974 (AD/A 006 583)A06

EERC 74-15 "Modeling and Identification in Nonlinear Structural Dynamics - I. One Degree of Freedom Models," by N. Distefano and A. Rath - 1974 (PB 241 548)A06

EERC 75-1 "Determination of Seismic Design Criteria for the Dumbarton Bridge Replacement Structure, Vol. I: Description, Theory and Analytical Modeling of Bridge and Parameters," by F. Baron and S.-H. Pang - 1975 (PB 259 407)A15

EERC 75-2 "Determination of Seismic Design Criteria for the Dumbarton Bridge Replacement Structure, Vol. II: Numerical Studies and Establishment of Seismic Design Criteria," by F. Baron and S.-H. Pang - 1975 (PB 259 408)A11 (For set of EERC 75-1 and 75-2 (PB 259 406))

EERC 75-3 "Seismic Risk Analysis for a Site and a Metropolitan Area," by C.S. Oliveira - 1975 (PB 248 134)A09

EERC 75-4 "Analytical Investigations of Seismic Response of Short, Single or Multiple-Span Highway Bridges," by M.-C. Chen and J. Penzien - 1975 (PB 241 454)A09

EERC 75-5 "An Evaluation of Some Methods for Predicting Seismic Behavior of Reinforced Concrete Buildings," by S.A. Mahin and V.V. Bertero - 1975 (PB 246 306)A16

EERC 75-6 "Earthquake Simulator Study of a Steel Frame Structure, Vol. I: Experimental Results," by R.W. Clough and D.T. Tang - 1975 (PB 243 981)A13

EERC 75-7 "Dynamic Properties of San Bernardino Intake Tower," by D. Rea, C.-Y. Liaw and A.K. Chopra - 1975 (AD/A008 406) A05

EERC 75-8 "Seismic Studies of the Articulation for the Dumbarton Bridge Replacement Structure, Vol. I: Description, Theory and Analytical Modeling of Bridge Components," by F. Baron and R.E. Hamati - 1975 (PB 251 539)A07

EERC 75-9 "Seismic Studies of the Articulation for the Dumbarton Bridge Replacement Structure, Vol. 2: Numerical Studies of Steel and Concrete Girder Alternates," by F. Baron and R.E. Hamati - 1975 (PB 251 540)A10

EERC 75-10 "Static and Dynamic Analysis of Nonlinear Structures," by D.P. Mondkar and G.H. Powell - 1975 (PB 242 434)A08

EERC 75-11 "Hysteretic Behavior of Steel Columns," by E.P. Popov, V.V. Bertero and S. Chandramouli - 1975 (PB 252 365)A11

EERC 75-12 "Earthquake Engineering Research Center Library Printed Catalog," - 1975 (PB 243 711)A26

EERC 75-13 "Three Dimensional Analysis of Building Systems (Extended Version)," by E.L. Wilson, J.P. Hollings and H.H. Dovey - 1975 (PB 243 989)A07

EERC 75-14 "Determination of Soil Liquefaction Characteristics by Large-Scale Laboratory Tests," by P. De Alba, C.K. Chan and H.B. Seed - 1975 (NUREG 0027)A08

EERC 75-15 "A Literature Survey - Compressive, Tensile, Bond and Shear Strength of Masonry," by R.L. Mayes and R.W. Clough - 1975 (PB 246 292)A10

EERC 75-16 "Hysteretic Behavior of Ductile Moment Resisting Reinforced Concrete Frame Components," by V.V. Bertero and E.P. Popov - 1975 (PB 246 388)A05

EERC 75-17 "Relationships Between Maximum Acceleration, Maximum Velocity, Distance from Source, Local Site Conditions for Moderately Strong Earthquakes," by H.B. Seed, R. Murarka, J. Lysmer and I.M. Idriss - 1975 (PB 248 172)A03

EERC 75-18 "The Effects of Method of Sample Preparation on the Cyclic Stress-Strain Behavior of Sands," by J. Mulilis, C.K. Chan and H.B. Seed - 1975 (Summarized in EERC 75-28)

EERC 75-19 "The Seismic Behavior of Critical Regions of Reinforced Concrete Components as Influenced by Moment, Shear and Axial Force," by M.B. Atalay and J. Penzien - 1975 (PB 258 842)A11

EERC 75-20 "Dynamic Properties of an Eleven Story Masonry Building," by R.M. Stephen, J.P. Hollings, J.G. Bouwkamp and D. Jurukovski - 1975 (PB 246 945)A04

EERC 75-21 "State-of-the-Art in Seismic Strength of Masonry - An Evaluation and Review," by R.L. Mayes and R.W. Clough 1975 (PB 249 040)A07

EERC 75-22 "Frequency Dependent Stiffness Matrices for Viscoelastic Half-Plane Foundations," by A.K. Chopra, P. Chakrabarti and G. Dasgupta - 1975 (PB 248 121)A07

EERC 75-23 "Hysteretic Behavior of Reinforced Concrete Framed Walls," by T.Y. Wong, V.V. Bertero and E.P. Popov - 1975

EERC 75-24 "Testing Facility for Subassemblages of Frame-Wall Structural Systems," by V.V. Bertero, E.P. Popov and T. Endo - 1975

EERC 75-25 "Influence of Seismic History on the Liquefaction Characteristics of Sands," by H.B. Seed, K. Mori and C.K. Chan - 1975 (Summarized in EERC 75-28)

EERC 75-26 "The Generation and Dissipation of Pore Water Pressures during Soil Liquefaction," by H.B. Seed, P.P. Martin and J. Lysmer - 1975 (PB 252 648)A03

EERC 75-27 "Identification of Research Needs for Improving Aseismic Design of Building Structures," by V.V. Bertero 1975 (PB 248 136)A05

EERC 75-28 "Evaluation of Soil Liquefaction Potential during Earthquakes," by H.B. Seed, I. Arango and C.K. Chan - 1975 (NUREG 0026)A13

EERC 75-29 "Representation of Irregular Stress Time Histories by Equivalent Uniform Stress Series in Liquefaction Analyses," by H.B. Seed, I.M. Idriss, F. Makdisi and N. Banerjee - 1975 (PB 252 635)A03

EERC 75-30 "FLUSH - A Computer Program for Approximate 3-D Analysis of Soil-Structure Interaction Problems," by J. Lysmer, T. Udaka, C.-F. Tsai and H.B. Seed - 1975 (PB 259 332)A07

EERC 75-31 "ALUSH - A Computer Program for Seismic Response Analysis of Axisymmetric Soil-Structure Systems," by E. Berger, J. Lysmer and H.B. Seed - 1975

EERC 75-32 "TRIP and TRAVEL - Computer Programs for Soil-Structure Interaction Analysis with Horizontally Travelling Waves," by T. Udaka, J. Lysmer and H.B. Seed - 1975

EERC 75-33 "Predicting the Performance of Structures in Regions of High Seismicity," by J. Penzien - 1975 (PB 248 130)A03

EERC 75-34 "Efficient Finite Element Analysis of Seismic Structure - Soil - Direction," by J. Lysmer, H.B. Seed, T. Udaka, R.N. Hwang and C.-F. Tsai - 1975 (PB 253 570)A03

EERC 75-35 "The Dynamic Behavior of a First Story Girder of a Three-Story Steel Frame Subjected to Earthquake Loading," by R.W. Clough and L.-Y. Li - 1975 (PB 248 841)A05

EERC 75-36 "Earthquake Simulator Study of a Steel Frame Structure, Volume II - Analytical Results," by D.T. Tang - 1975 (PB 252 926)A10

EERC 75-37 "ANSR-I General Purpose Computer Program for Analysis of Non-Linear Structural Response," by D.P. Mondkar and G.H. Powell - 1975 (PB 252 386)A08

EERC 75-38 "Nonlinear Response Spectra for Probabilistic Seismic Design and Damage Assessment of Reinforced Concrete Structures," by M. Murakami and J. Penzien - 1975 (PB 259 530)A05

EERC 75-39 "Study of a Method of Feasible Directions for Optimal Elastic Design of Frame Structures Subjected to Earthquake Loading," by N.D. Walker and K.S. Pister - 1975 (PB 257 781)A06

EERC 75-40 "An Alternative Representation of the Elastic-Viscoelastic Analogy," by G. Dasgupta and J.L. Sackman - 1975 (PB 252 173)A03

EERC 75-41 "Effect of Multi-Directional Shaking on Liquefaction of Sands," by H.B. Seed, R. Pyke and G.R. Martin - 1975 (PB 258 781)A03

EERC 76-1 "Strength and Ductility Evaluation of Existing Low-Rise Reinforced Concrete Buildings - Screening Method," by T. Okada and B. Bresler - 1976 (PB 257 906)A11

EERC 76-2 "Experimental and Analytical Studies on the Hysteretic Behavior of Reinforced Concrete Rectangular and T-Beams," by S.-Y.M. Ma, E.P. Popov and V.V. Bertero - 1976 (PB 260 843)A12

EERC 76-3 "Dynamic Behavior of a Multistory Triangular-Shaped Building," by J. Petrovski, R.M. Stephen, E. Gartenbaum and J.G. Bouwkamp - 1976

EERC 76-4 "Earthquake Induced Deformations of Earth Dams," by N. Serff and H.B. Seed - 1976

EERC 76-5 "Analysis and Design of Tube-Type Tall Building Structures," by H. de Clercq and G.H. Powell - 1976 (PB 252 220) A10

EERC 76-6 "Time and Frequency Domain Analysis of Three-Dimensional Ground Motions, San Fernando Earthquake," by T. Kubo and J. Penzien (PB 260 556)A11

EERC 76-7 "Expected Performance of Uniform Building Code Design Masonry Structures," by R.L. Mayes, Y. Omote, S.W. Chen and R.W. Clough - 1976

EERC 76-8 "Cyclic Shear Tests on Concrete Masonry Piers," Part I - Test Results," by R.L. Mayes, Y. Omote and R.W. Clough - 1976 (PB 264 424)A06

EERC 76-9 "A Substructure Method for Earthquake Analysis of Structure - Soil Interaction," by J.A. Gutierrez and A.K. Chopra - 1976 (PB 257 783)A08

EERC 76-10 "Stabilization of Potentially Liquefiable Sand Deposits using Gravel Drain Systems," by H.B. Seed and J.R. Booker - 1976 (PB 258 820)A04

EERC 76-11 "Influence of Design and Analysis Assumptions on Computed Inelastic Response of Moderately Tall Frames," by G.H. Powell and D.G. Row - 1976

EERC 76-12 "Sensitivity Analysis for Hysteretic Dynamic Systems: Theory and Applications," by D. Ray, K.S. Pister and E. Polak - 1976 (PB 262 859)A04

EERC 76-13 "Coupled Lateral Torsional Response of Buildings to Ground Shaking," by C.L. Kan and A.K. Chopra - 1976 (PB 257 907)A09

EERC 76-14 "Seismic Analyses of the Banco de America," by V.V. Bertero, S.A. Mahin and J.A. Hollings - 1976

EERC 76-15 "Reinforced Concrete Frame 2: Seismic Testing and Analytical Correlation," by R.W. Clough and J. Gidwani - 1976 (PB 261 323)A08

EERC 76-16 "Cyclic Shear Tests on Masonry Piers, Part II - Analysis of Test Results," by R.L. Mayes, Y. Omote and R.W. Clough - 1976

EERC 76-17 "Structural Steel Bracing Systems: Behavior Under Cyclic Loading," by E.P. Popov, K. Takanashi and C.W. Roeder - 1976 (PB 260 715)A05

EERC 76-18 "Experimental Model Studies on Seismic Response of High Curved Overcrossings," by D. Williams and W.G. Godden - 1976

EERC 76-19 "Effects of Non-Uniform Seismic Disturbances on the Dumbarton Bridge Replacement Structure," by F. Baron and R.E. Hamati - 1976

EERC 76-20 "Investigation of the Inelastic Characteristics of a Single Story Steel Structure Using System Identification and Shaking Table Experiments," by V.C. Matzen and H.D. McNiven - 1976 (PB 258 453)A07

EERC 76-21 "Capacity of Columns with Splice Imperfections," by E.P. Popov, R.M. Stephen and R. Philbrick - 1976 (PB 260 378)A04

EERC 76-22 "Response of the Olive View Hospital Main Building during the San Fernando Earthquake," by S. A. Mahin, R. Collins, A.K. Chopra and V.V. Bertero - 1976

EERC 76-23 "A Study on the Major Factors Influencing the Strength of Masonry Prisms," by N.M. Mostaghel, R.L. Mayes, R. W. Clough and S.W. Chen - 1976

EERC 76-24 "GADFLEA - A Computer Program for the Analysis of Pore Pressure Generation and Dissipation during Cyclic or Earthquake Loading," by J.R. Booker, M.S. Rahman and H.B. Seed - 1976 (PB 263 947)A04

EERC 76-25 "Rehabilitation of an Existing Building: A Case Study," by B. Bresler and J. Axley - 1976

EERC 76-26 "Correlative Investigations on Theoretical and Experimental Dynamic Behavior of a Model Bridge Structure," by K. Kawashima and J. Penzien - 1976 (PB 263 388)A11

EERC 76-27 "Earthquake Response of Coupled Shear Wall Buildings," by T. Srichatrapimuk - 1976 (PB 265 157)A07

EERC 76-28 "Tensile Capacity of Partial Penetration Welds," by E.P. Popov and R.M. Stephen - 1976 (PB 262 899)A03

EERC 76-29 "Analysis and Design of Numerical Integration Methods in Structural Dynamics," by H.M. Hilber - 1976 (PB 264 410)A06

EERC 76-30 "Contribution of a Floor System to the Dynamic Characteristics of Reinforced Concrete Buildings," by L.J. Edgar and V.V. Bertero - 1976

EERC 76-31 "The Effects of Seismic Disturbances on the Golden Gate Bridge," by F. Baron, M. Arikan and R.E. Hamati - 1976

EERC 76-32 "Infilled Frames in Earthquake Resistant Construction," by R.E. Klingner and V.V. Bertero - 1976 (PB 265 892)A13

UCB/EERC-77/01 "PLUSH - A Computer Program for Probabilistic Finite Element Analysis of Seismic Soil-Structure Interaction," by M.P. Romo Organista, J. Lysmer and H.B. Seed - 1977

UCB/EERC-77/02 "Soil-Structure Interaction Effects at the Humboldt Bay Power Plant in the Ferndale Earthquake of June 7, 1975," by J.E. Valera, H.B. Seed, C.F. Tsai and J. Lysmer - 1977 (PB 265 795)A04

UCB/EERC-77/03 "Influence of Sample Disturbance on Sand Response to Cyclic Loading," by K. Mori, H.B. Seed and C.K. Chan - 1977 (PB 267 352)A04

UCB/EERC-77/04 "Seismological Studies of Strong Motion Records," by J. Shoja-Taheri - 1977 (PB 269 655)A10

UCB/EERC-77/05 "Testing Facility for Coupled-Shear Walls," by L. Li-Hyung, V.V. Bertero and E.P. Popov - 1977

UCB/EERC-77/06 "Developing Methodologies for Evaluating the Earthquake Safety of Existing Buildings," by No. 1 - B. Bresler; No. 2 - B. Bresler, T. Okada and D. Zisling; No. 3 - T. Okada and B. Bresler; No. 4 - V.V. Bertero and B. Bresler - 1977 (PB 267 354)A08

UCB/EERC-77/07 "A Literature Survey - Transverse Strength of Masonry Walls," by Y. Omote, R.L. Mayes, S.W. Chen and R.W. Clough - 1977 (PB 277 933)A07

UCB/EERC-77/08 "DRAIN-TABS: A Computer Program for Inelastic Earthquake Response of Three Dimensional Buildings," by R. Guendelman-Israel and G.H. Powell - 1977 (PB 270 693)A07

UCB/EERC-77/09 "SUBWALL: A Special Purpose Finite Element Computer Program for Practical Elastic Analysis and Design of Structural Walls with Substructure Option," by D.Q. Le, H. Peterson and E.P. Popov - 1977 (PB 270 567)A05

UCB/EERC-77/10 "Experimental Evaluation of Seismic Design Methods for Broad Cylindrical Tanks," by D.P. Clough (PB 272 280)A13

UCB/EERC-77/11 "Earthquake Engineering Research at Berkeley - 1976," - 1977 (PB 273 507)A09

UCB/EERC-77/12 "Automated Design of Earthquake Resistant Multistory Steel Building Frames," by N.D. Walker, Jr. - 1977 (PB 276 526)A09

UCB/EERC-77/13 "Concrete Confined by Rectangular Hoops Subjected to Axial Loads," by J. Vallenas, V.V. Bertero and E.P. Popov - 1977 (PB 275 165)A06

UCB/EERC-77/14 "Seismic Strain Induced in the Ground During Earthquakes," by Y. Sugimura - 1977 (PB 284 201)A04

UCB/EERC-77/15 "Bond Deterioration under Generalized Loading," by V.V. Bertero, E.P. Popov and S. Viwathanatepa - 1977

UCB/EERC-77/16 "Computer Aided Optimum Design of Ductile Reinforced Concrete Moment Resisting Frames," by S.W. Zagajeski and V.V. Bertero - 1977 (PB 280 137)A07

UCB/EERC-77/17 "Earthquake Simulation Testing of a Stepping Frame with Energy-Absorbing Devices," by J.M. Kelly and D.F. Tsztoo - 1977 (PB 273 506)A04

UCB/EERC-77/18 "Inelastic Behavior of Eccentrically Braced Steel Frames under Cyclic Loadings," by C.W. Roeder and E.P. Popov - 1977 (PB 275 526)A15

UCB/EERC-77/19 "A Symplified Procedure for Estimating Earthquake-Induced Deformations in Dams and Embankments," by F.I. Makdisi and H.B. Seed - 1977 (PB 276 820) A04

UCB/EERC-77/20 "The Performance of Earth Dams during Earthquakes," by H.B. Seed, F.I. Makdisi and P. de Alba - 1977 (PB 276 821)A04

UCB/EERC-77/21 "Dynamic Plastic Analysis Using Stress Resultant Finite Element Formulation," by P. Lukkunapvasit and J.M. Kelly - 1977 (PB 275 453)A04

UCB/EERC-77/22 "Preliminary Experimental Study of Seismic Uplift of a Steel Frame," by R.W. Clough and A.A. Huckelbridge 1977 (PB 278 769)AC8

UCB/EERC-77/23 "Earthquake Simulator Tests of a Nine-Story Steel Frame with Columns Allowed to Uplift," by A.A. Huckelbridge - 1977 (PB 277 944)A09

UCB/EERC-77/24 "Nonlinear Soil-Structure Interaction of Skew Highway Bridges," by M.-C. Chen and J. Penzien - 1977 (PB 276 176)A07

UCB/EERC-77/25 "Seismic Analysis of an Offshore Structure Supported on Pile Foundations," by D.D.-N. Liou and J. Penzien 1977 (PB 283 180)A06

UCB/EERC-77/26 "Dynamic Stiffness Matrices for Homogeneous Viscoelastic Half-Planes," by G. Dasgupta and A.K. Chopra - 1977 (PB 279 654)A06

UCB/EERC-77/27 "A Practical Soft Story Earthquake Isolation System," by J.M. Kelly and J.M. Eidinger - 1977 (PB 276 814)A07

UCB/EERC-77/28 "Seismic Safety of Existing Buildings and Incentives for Hazard Mitigation in San Francisco: An Exploratory Study," by A.J. Meltsner - 1977 (PB 281 970)A05

UCB/EERC-77/29 "Dynamic Analysis of Electrohydraulic Shaking Tables," by D. Rea, S. Abedi-Hayati and Y. Takahashi 1977 (PB 282 569)A04

UCB/EERC-77/30 "An Approach for Improving Seismic - Resistant Behavior of Reinforced Concrete Interior Joints," by B. Galunic, V.V. Bertero and E.P. Popov - 1977

UCB/EERC-78/01 "The Development of Energy-Absorbing Devices for Aseismic Base Isolation Systems," by J.M. Kelly and D.F. Tsztoo 1978 (PB 284 978)A04

UCB/EERC-78/02 "Effect of Tensile Prestrain on the Cyclic Response of Structural Steel Connections," by J.G. Bouwkamp and A. Mukhopadhyay - 1978

UCB/EERC-78/03 "Experimental Results of an Earthquake Isolation System using Natural Rubber Bearings," by J.M. Eidinger and J.M. Kelly - 1978

UCB/EERC-78/04 "Seismic Behavior of Tall Liquid Storage Tanks," by A. Niwa 1978

UCB/EERC-78/05 "Hysteretic Behavior of Reinforced Concrete Columns Subjected to High Axial and Cyclic Shear Forces," by S.W. Zagajeski, V.V. Bertero and J.G. Bouwkamp - 1978

UCB/EERC-78/06 "Inelastic Beam-Column Elements for the ANSR-I Program," by A. Riahi, D.G. Row and G.H. Powell - 1978

UCB/EERC-78/07 "Studies of Structural Response to Earthquake Ground Motion," by O.A. Lopez and A.K. Chopra - 1978

UCB/EERC-78/08 "A Laboratory Study of the Fluid-Structure Interaction of Submerged Tanks and Caissons in Earthquakes," by R.C. Byrd - 1978 (PB 284 957)A08

UCB/EERC-78/09 "Models for Evaluating Damageability of Structures," by I. Sakamoto and B. Bresler - 1978

UCB/EERC-78/10 "Seismic Performance of Secondary Structural Elements," by I. Sakamoto - 1978

UCB/EERC-78/11 Case Study--Seismic Safety Evaluation of a Reinforced Concrete School Building," by J. Axley and B. Bresler 1978

UCB/EERC-78/12 "Potential Damageability in Existing Buildings," by T. Blejwas and B. Bresler - 1978

UCB/EERC-78/13 "Dynamic Behavior of a Pedestal Base Multistory Building," by R. M. Stephen, E. L. Wilson, J. G. Bouwkamp and M. Button - 1978

UCB/EERC-78/14 "Seismic Response of Bridges - Case Studies," by R.A. Imbsen, V. Nutt and J. Penzien - 1978

UCB/EERC-78/15 "A Substructure Technique for Nonlinear Static and Dynamic Analysis," by D.G. Row and G.H. Powell - 1978

UCB/EERC-78/16 "Seismic Performance of Nonstructural and Secondary Structural Elements," by Isao Sakamoto - 1978

UCB/EERC-78/17 "Model for Evaluating Damageability of Structures," by Isao Sakamoto and B. Bresler - 1978

UCB/EERC-78/18 "Response of K-Braced Steel Frame Models to Lateral Loads," by J.G. Bouwkamp, R.M. Stephen and E.P. Popov - 1978

UCB/EERC-78/19 "Rational Design Methods for Light Equipment in Structures Subjected to Ground Motion," by Jerome L. Sackman and James M. Kelly - 1978

UCB/EERC-78/20 "Testing of a Wind Restraint for Aseismic Base Isolation," by James M. Kelly and Daniel E. Chitty - 1978

UCB/EERC-78/21 "APOLLO A Computer Program for the Analysis of Pore Pressure Generation and Dissipation in Horizontal Sand Layers During Cyclic or Earthquake Loading," by Philippe P. Martin and H. Bolton Seed - 1978

UCB/EERC-78/22 "Optimal Design of an Earthquake Isolation System," by M.A. Bhatti, K.S. Pister and E. Polak - 1978

UCB/EERC-78/23 "MASH A Computer Program for the Non-Linear Analysis of Vertically Propagating Shear Waves in Horizontally Layered Deposits," by Philippe P. Martin and H. Bolton Seed - 1978

UCB/EERC-78/24 "Investigation of the Elastic Characteristics of a Three Story Steel Frame Using System Identification," by Izak Kaya and Hugh D. McNiven - 1978

UCB/EERC-78/25 "Investigation of the Nonlinear Characteristics of a Three-Story Steel Frame Using System Identification," by I. Kaya and H.D. McNiven - 1978

UCB/EERC-78/26 "Studies of Strong Ground Motion in Taiwan," by Y.M. Hsiung, B.A. Bolt and J. Penzien - 1978

UCB/EERC-78/27 "Cyclic Loading Tests of Masonry Single Piers Volume 1 - Height to Width Ratio of 2," by P.A. Hildalgo, R.L. Mayes, H.D. McNiven & R.W. Clough - 1978

UCB/EERC-78/28 "Cyclic Loading Tests of Masonry Single Piers Volume 2 - Height to Width Radio of 1," by S.-W.J.Chen, P.A. Hidalgo, R.L. Mayes, R.W. Clough & H.D. McNiven - 1978

UCB/EERC-78/29 "Analytical Procedures in Soil Dynamics," by J. Lysmer - 1978

UCB/EERC-79/01 "Hysteretic Behavior of Lightweight Reinforced Concrete Beam-Column Subassemblages," by B. Forzani, E.P. Popov, and V.V. Bertero - 1979

UCB/EERC-79/02 "The Development of a Mathematical Model to Predict the Flexural Response of Reinforced Concrete Beams to Cyclic Loads, Using System Identification," by J.F. Stanton and H.D. McNiven - 1979